

AD 351104

AD

USAAVLABS TECHNICAL REPORT 66-87

FLUID STATE HYDRAULIC DAMPER

By

R. V. Burton

D. N. Carlson

R. L. Heinecke

R. R. St. John

February 1967

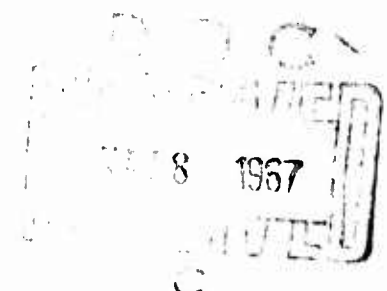
**U. S. ARMY AVIATION MATERIEL LABORATORIES
FORT EUSTIS, VIRGINIA**

**CONTRACT DA 44-177-AMC-294(T)
HONEYWELL AERONAUTICAL DIVISION
MINNEAPOLIS, MINNESOTA**

*Distribution of this
document is unlimited*



ARCHIVE COPY



157

Disclaimers

The findings in this report are not to be construed as an official Department of the Army position unless so designated by other authorized documents.

When Government drawings, specifications, or other data are used for any purpose other than in connection with a definitely related Government procurement operation, the United States Government thereby incurs no responsibility nor any obligation whatsoever; and the fact that the Government may have formulated, furnished, or in any way supplied the said drawings, specifications, or other data is not to be regarded by implication or otherwise as in any manner licensing the holder or any other person or corporation, or conveying any rights or permission, to manufacture, use, or sell any patented invention that may in any way be related thereto.

Trade names cited in this report do not constitute an official endorsement or approval of the use of such commercial hardware or software.

Disposition Instructions

Destroy this report when no longer needed. Do not return it to originator.

RECEIVED BY		
CPSTI	W-115 SECTION	<input checked="" type="checkbox"/>
POC	FOUO SECTION	<input type="checkbox"/>
UNANNOUNCED		<input type="checkbox"/>
JUSTIFICATION <i>Per statement</i>		
<i>on Doc</i>		
BY <i>pm</i>		
DISTRIBUTION AVAILABILITY CODES		
DIST.	AVAIL.	SERIAL
1		



DEPARTMENT OF THE ARMY
U. S. ARMY AVIATION MATERIEL LABORATORIES
FORT EUSTIS, VIRGINIA 23604

This report has been reviewed by the U. S. Army Aviation Materiel Laboratories and is considered to be technically sound. The report is published for the exchange of information and the stimulation of ideas.

Task 1P121401A14186
Contract DA44-177-AMC-294(T)
USAAVLABS Technical Report 66-87
February 1967

FLUID STATE HYDRAULIC DAMPER
Final Report
15-003R

by

R. V. Burton
D. N. Carlson
R. L. Heinecke
R. R. St. John

Prepared by

Honeywell Aeronautical Division
Minneapolis, Minnesota

for

U. S. ARMY AVIATION MATERIEL LABORATORIES
Fort Eustis, Virginia

Distribution of this document is unlimited

SUMMARY

This report covers the developmental work accomplished on a program to demonstrate the feasibility of using fluidic sensing amplification and signal shaping techniques to mechanize a single-axis, rate feedback damper system for V/STOL aircraft. The specific design goal was to increase the yaw axis damping ratio of the UH-1B helicopter from 0.30 unaugmented to 0.60 augmented.

The control problem was analyzed and the damper system mechanization defined through the use of analog and digital computer simulation techniques. The component hardware was designed, fabricated, and bench tested.

Closed-loop system bench testing, using an analog computer to simulate the UH-1B helicopter, showed that the fluidic damper system was feasible for helicopter control system mechanization. The addition of the damper system to the simulated aircraft raised the yaw axis damping ratio from 0.30 unaugmented to 0.60 augmented.

Recommendations for further work are presented.

FOREWORD

This document is the final report on a research and development program authorized by the U. S. Army Aviation Materiel Laboratories under contract No. DA 44-177-AMC-294(T). The objective is to demonstrate the feasibility of developing an automatic control system for V/STOL aircraft using pure fluid (hydraulic oil) sensing, amplification, and signal shaping techniques, by designing, fabricating, and bench testing a functional model of a yaw rate damper system. The program is a part of the continuing effort by the U. S. Army to obtain stabilization systems for V/STOL aircraft that are reliable, lightweight, inexpensive, easily maintained and readily stored. The work presented in this report, representing all of the research and development activity carried out during the program, was initiated on 1 July 1965 and completed on 24 June 1966.

BLANK PAGE

CONTENTS

	<u>Page</u>
SUMMARY	iii
FOREWORD	v
LIST OF ILLUSTRATIONS	viii
LIST OF TABLES	xii
LIST OF SYMBOLS	xiii
CHAPTER 1. INTRODUCTION	1
CHAPTER 2. SYSTEM ANALYSIS	2
CHAPTER 3. MECHANIZATION DESIGN	57
CHAPTER 4. COMPONENT TEST RESULTS	65
CHAPTER 5. SYSTEM TEST RESULTS	98
CHAPTER 6. HYDRAULIC POWER SOURCE SYSTEM STUDY	143
CHAPTER 7. CONCLUSIONS	150
CHAPTER 8. RECOMMENDATIONS	152
APPENDIXES	
I. Fluid State Hydraulic Damper	153
II. System Test Requirements	160
DISTRIBUTION	166

ILLUSTRATIONS

Figure		Page
1	Block Diagram of All-Hydraulic Yaw Damper . . .	4
2	Airframe and Control System Matrix	5
3	Normalized Sensor	7
4	Analytical Block Diagram for UH-1B Yaw Damper Study	10
5	Block Diagram and Equations for Digital Study Matrix	11
6	Nominal Matrix Values - Aircraft Equations . . .	13
7	Aircraft and Control System Matrix	14
8	Analog Simulation of Aircraft Equations	15
9	Analog Simulation of Hydraulic Yaw Damper . . .	16
10	Analog Simulation Potentiometer Settings	17
11	60 Knots - Nominal Performance	19
12	90 Knots - Nominal Performance	21
13	120 Knots - Nominal Performance	23
14	Hover - Nominal Performance	25
15	Hover - Nominal Performance, Augmented Aircraft With 0.46-Degree Linkage Hysteresis	27
16	Root Locus Nominal (Hover)	30
17	Root Locus Nominal (60 Knots)	31
18	Effect of Hi-Pass Time Constant Variation (90 Knots)	32
19	Root Locus Nominal (120 Knots).	33
20	Root Locus Correlation Runs (90 Knots)	35
21	60 Knots - Parametric Study	37
22	90 Knots - Parametric Study	39

Figure		Page
23	120 Knots - Parametric Study	41
24	Overshoot and Response Time Qualitative Trend . .	43
25	Gain Variation in Hi-Pass Mechanization (60 Knots) .	47
26	Gain Variation in Hi-Pass Mechanization (90 Knots) .	49
27	Gain Variation in Hi-Pass Mechanization (120 Knots)	51
28	Parametric Variation - Sensor Logic, Linkage Hysteresis	55
29	Fluid Schematic - Fluid State Hydraulic Damper . .	58
30	Vortex Rate Sensor Flow Fields	60
31	Velocity Components in Vortex Chamber	60
32	Vortex Rate Sensor	66
33	Rate Table Test Setup	67
34	Tilt Table Test Setup	69
35	Rate Sensor Scale Factor	71
36	Fluid Amplifier Test Setup	73
37	Preamplifier Driving Shaping Input Amplifiers . .	75
38	Shaping Input Amplifier No. 1 Driving Shaping Output Amplifier No. 1	76
39	Shaping Input Amplifier No. 2 Driving Shaping Output Amplifier No. 2	77
40	Shaping Output Amplifier No. 1 (Deadhead Load) . .	78
41	Shaping Output Amplifier No. 2 (Deadhead Load) . .	79
42	Straight Cascade (Includes Preamp)	80
43	Lag Cascade Gain (Includes Preamp)	81
44	Schematic - Shaping Network Test Setup	83

Figure		Page
45	Dynamic Response - Low-Pass Filter Section of Shaping Network	85
46	Dynamic Response - Shaping Network (Includes Preamp)	86
47	Transient Response - Shaping Network (Includes Preamp)	88
48	Actuator Displacement Versus Pneumatic Input (S/N 0.001)	90
49	Actuator Displacement Versus Pneumatic Input (S/N 0.002)	91
50	Amplitude Ratio and Phase Lag of Closed Loop Position with Respect to Input Signal	92
51	Phase Lag of Closed Loop Position with Respect to Input Signal	93
52	Actuator Displacement versus ΔP Input	97
53	Open Loop Test Setup	99
54	Damper on Tilt Table	100
55	System on Tilt Table	101
56	Tilt Table	102
57	Output (Noise)	105
58	Straight Cascade Gain	106
59	Lag Cascade Gain	107
60	Hydraulic Schematic - UH-1B Yaw Damper (As Tested Condition)	109
61	Shorted Hi-Pass System Gain	110
62	Shorted Hi-Pass System Gain	111
63	Shorted Hi-Pass System Gain	112
64	Shorted Hi-Pass Open Loop Frequency Response . .	114

Figure		Page
65	Shorted Hi-Pass System Null Shift Versus Fluid Temperature	115
66	Hi-Pass Open Loop Frequency Response	117
67	Hi-Pass System Null Shift Versus Fluid Temperature	119
68	Closed Loop Test Setup	122
69	Analog Computer and Recorders	123
70	Block Diagram of Analog Computer Setup	124
71	Closed Loop Response, Nominal Conditions	127
72	Closed Loop Response, -25° F Flight Day	131
73	Closed Loop Response, 100° F Flight Day	135
74	Measured UH-1B Vibration Levels	138
75	Aircraft Augmented Response With and Without Vibration Compared to Unaugmented Aircraft Response	139
76	Proposed Hydraulic Circuit Yaw Damper System	145
77	Damper System Response	158
78	Open Loop Test Setup	161
79	Closed Loop Test Setup	163

TABLES

Table	Page
I Nominal System Performance.	12
II Reasonable Mechanization Deviations	45
III Rate Sensor Test Results Tabulation	70
IV Amplifier Test Results Tabulation	74
V System Output Noise	103
VI System Output Noise	104
VII Straight-Through Cascade Gain Tabulation	104
VIII Steady-State Gain Results Tabulation	108
IX Shorted High-Pass System Loop Gain	113
X Hi-Pass System Loop Gain.	118
XI Potentiometer Assignment Sheet ADM-1448	125
XII Aircraft Damping Ratio Tabulation	126
XIII Aircraft Damping Ratio Tabulation (-25°F Flight Day at 60 Knots).	133
XIV Aircraft Damping Ratio Tabulation (100°F Flight Day at 60 knots).	137
XV Estimated Component Sizes and Weights Tabulation	148

LIST OF SYMBOLS

r. p. s.	Revolutions per second
V	Velocity - feet per second
β	Side-slip angle - degrees
K_{θ_T}	Loop gain in degrees tail rotor per degree per second
θ_T	Tail rotor angle - degrees
$\theta_{T_{\text{servo}}}$	Augmentation servo position in degrees of tail rotor deflection
ϕ	Roll angle - degrees
$\dot{\phi}$	Roll angle rate of change - degrees per second
ψ	Yaw angle - degrees
$\dot{\psi}$	Yaw angle rate of change - degrees per second
K_{θ_1}	Hi-Pass straight-through gain - psi/psi
K_{θ_2}	Hi-Pass lagged gain - psi/psi
T_H	Hi-Pass time constant - seconds
$\tau_{\%}$	Time to reach and remain within 10% of final solution - seconds
O.S.	Overshoot
ω_s	Frequency response of series servo - rad/sec
ω_g	Frequency response of vortex rate sensor - rad/sec

CHAPTER 1

INTRODUCTION

This report describes the research and development work accomplished to demonstrate the feasibility of using a hydraulic fluidic yaw rate damper to provide helicopter flight control system mechanization. The performance goal was to improve the unaugmented yaw axis damping of the UH-1B helicopter from approximately 0.30 to approximately 0.60 or greater augmented.

The research and development work included system analysis, hardware design, component test results, and system bench test results. Conclusions, problem areas, and recommendations for improvement are presented.

A study of the aircraft hydraulic power source system requirements for the use of the fluidic damper in the UH-1B helicopter is also presented.

CHAPTER 2

SYSTEM ANALYSIS

This section describes the analytical design effort consisting of the Preliminary System Analysis and Final System Analysis. Each area of analytical work is discussed separately.

PRELIMINARY SYSTEM ANALYSIS

SUMMARY

A preliminary yaw damper configuration for the UH-1B helicopter was defined and its linear performance analyzed.

Only the key points of the analysis procedure and significant results are described here. The performance of the final system configuration is described in detail in a later section. The system defined used hi-pass yaw rate with fixed gain to increase the yaw axis damping ratio and to reduce the divergence rates at hover to one-half of their unaugmented value.

DISCUSSION

The objective of the preliminary system analysis was to define mathematically the system block diagram and preliminary parameter values. No performance requirements were specified other than that the system must damp external flight path disturbances during steady maneuvers without opposing the pilot's commands. Self-imposed analysis objectives were to maximize yaw damping with a minimum of system complexity and to deliver this improved damping over the expected range of system developmental tolerances. Stabilization during hover requires more than a simple yaw damper so that substantial reduction in divergence rates is considered satisfactory.

The use of collective pitch and roll crossfeeds was considered and rejected for the following reasons:

1. Airframe data to permit evaluation of a collective crossfeed was not available.
2. Complexity of the system would be increased far beyond that necessary to demonstrate fluid system feasibility.

It was felt that the resulting system described below, had the capability of demonstrating feasibility of an all-hydraulic yaw damper to reduce the pilot workload substantially.

System Description

The preliminary block diagram of the yaw damper is shown in Figure 1. It consisted of a hydraulic yaw rate sensor with the fluid output amplified, hi-passed, and then fed directly to the series augmentation servo. A "trim" was provided to bias out any null offset. The use of hi-pass yaw rate effectively eliminates opposition of the damper to yaw commands by the pilot, and the use of a series servo eliminates feedback of damper commands into the rudder pedals. The hi-pass also will minimize the effects of rate sensor drift.

Data and Assumptions

Lateral equations of motion for four flight conditions were received from Bell Aircraft in matrix form. The matrix with corresponding elements is shown in Figure 2.

A servo with a fluid interface having a natural frequency (90° phase lag) of 10 cps or greater and a damping ratio of 0.7 was specified.

All other system dynamics were assumed to be accounted for in a 50-millisecond double lagged transport lag, $e^{-0.05s}/(1 + 0.05s)^2$ (see Figure 3). Of this, the sensor was to contribute no more amplitude or phase lag below 100 radians per second than is exhibited by the 30-millisecond second order, $1/(1 + 0.03s)^2$.

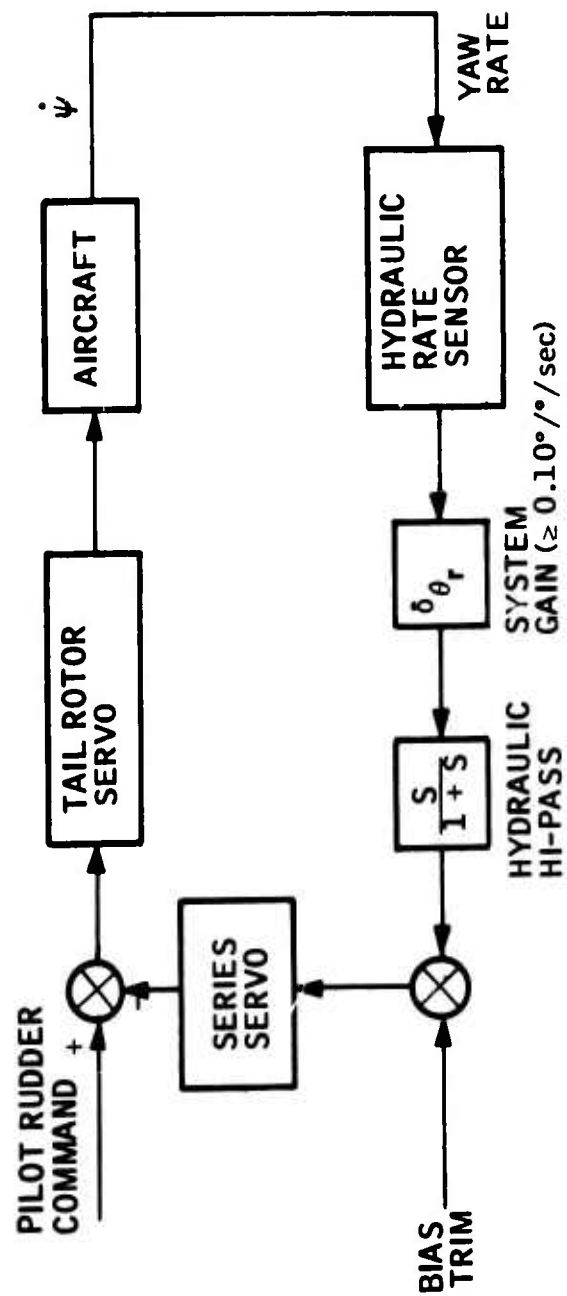
Analysis

Root loci of the augmented yaw axis with unrestrained roll axis were calculated using the Figure 2 matrix.

A second-order Pade approximation of the 50-millisecond time delay was used, $(s^2 - 120s + 4800)/(s^2 + 120s + 4800)$, which is valid for frequencies below 7 cps.

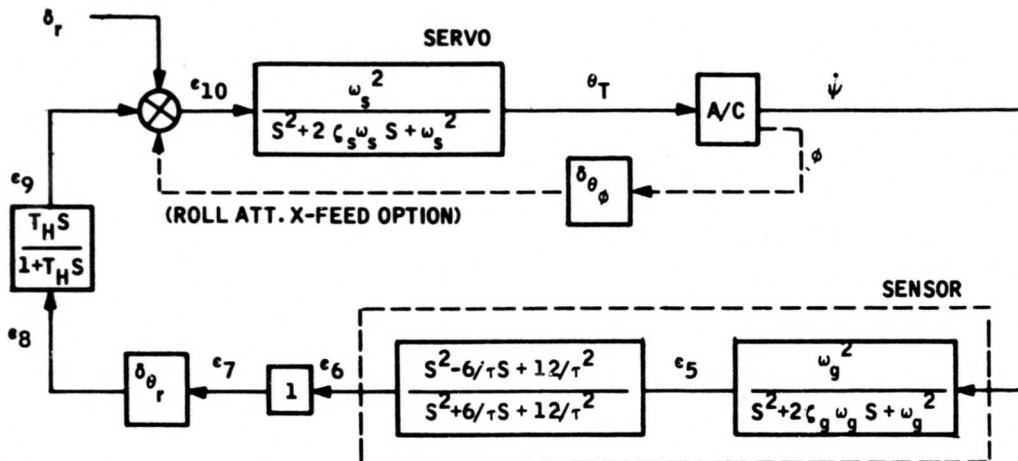
The critical gains and frequencies of the root loci were verified with an analog computer simulation within less than 10 percent.

Optimization of the system was done largely with the analog computer simulation and consisted of observing responses to tail rotor steps and 10 fps side gusts, with and without restraining the roll axis.



NOTE: SERIES SERVO GAIN $\sim 0.19 \text{ IN./PSI}$ to $\pm 0.38 \text{ IN. LIMIT}$
 TAIL ROTOR SERVO GAIN $\sim 6.62^\circ/\text{IN.}$

Figure 1. Block Diagram of All-Hydraulic Yaw Damper



$a_{44} = 1$	
$a_{55} = 1$	
$a_{65} = 1$	$a_{66} = -1$

$b_{11}S$ c_{11}	c_{12}	$b_{13}S$ c_{13}	c_{14}						
$b_{21}S$ c_{21}	$b_{22}S$ c_{22}	$b_{23}S$	c_{24}						
$b_{31}S$ c_{31}	c_{32}	$a_{33}S^2$ $b_{33}S$	c_{34}						
			$a_{44}S^2$ $b_{44}S$ c_{44}						$c_{4,10}$
	c_{52}			$a_{55}S^2$ $b_{55}S$ c_{55}					
				$a_{65}S^2$ $b_{65}S$ c_{65}	$a_{66}S^2$ $b_{66}S$ c_{66}				
					c_{76}	c_{77}			
						c_{87}	c_{88}		
							$b_{98}S$ c_{98}	$b_{99}S$ c_{99}	
		$c_{10,3}$							$c_{10,9}$ $c_{10,10}$

$\beta(v)$
$\dot{\psi}$
ϕ
θ_T
ϵ_5
ϵ_6
ϵ_7
ϵ_8
ϵ_9
ϵ_{10}

Figure 2. Airframe and Control System

CONTROL SYSTEM MATRIX ELEMENTS

$a_{44} = 1$		$b_{44} = 87.8$		$c_{44} = 3960$	$c_{4,10} = -3960$
$a_{55} = 1$		$b_{55} = 40$		$c_{55} = 400$	$c_{52} = -400$
$a_{65} = 1$	$a_{66} = -1$	$b_{65} = -120$	$b_{66} = -120$	$c_{65} = 4800$	$c_{66} = -4800$
				$c_{76} = -1$	$c_{77} = 1$
				$c_{87} = -\delta_{\theta_F}$	$c_{88} = -1$
		$b_{98} = -T_H$	$b_{99} = T_H$	$c_{98} = 0$	$c_{99} = 1$
				$c_{9,10} = 1$	$c_{10,10} = 1$
					$c_{10,3} = -\delta_{\theta_\phi}$

AIRFRAME MATRIX ELEMENTS

	Hover	60 Kn	90 Kn	120 Kn
$b_{11} =$	-205 (v)	-21,038	-31,469	-41,875
$c_{11} =$	-8.25 (v)	-1,509	-3395	-5572
$c_{12} =$	158	-20,762	-31,144	-41,525
$b_{13} =$	-350	-42	-45.7	-44.6
$c_{13} =$	6600	6600	6600	6600
$c_{14} =$	-101,200	-3640	-3880	-4130
$b_{21} =$	0 (v)	7423	8446	9331
$c_{21} =$	158 (v)	33,002	60,850	91,009
$b_{22} =$	-7673	-7268	-7268	-7268
$c_{22} =$	-4974	0	0	0
$b_{23} =$	0	1156	1257.7	1227
$c_{24} =$	23,500	100,176	106,781	113,661
$b_{31} =$	0 (v)	-1316	-1499	-1548
$c_{31} =$	-55.8 (v)	-703	-2908	-3947
$c_{32} =$	1123	0	0	0
$a_{33} =$	-2779	-2545	-2545	-2545
$b_{33} =$	-2470	-226	-246.4	-240.5
$c_{34} =$	3500	19,626	20,920	22,268

Side Force Equations
Yawing Moment Equation
Rolling Moment Equation

β (v)
 ψ
 ϕ
 θ_T
 ϵ_5
 ϵ_6
 ϵ_7
 ϵ_8
 ϵ_9
 ϵ_{10}

= 0

Control System Matrix

B

BLANK PAGE

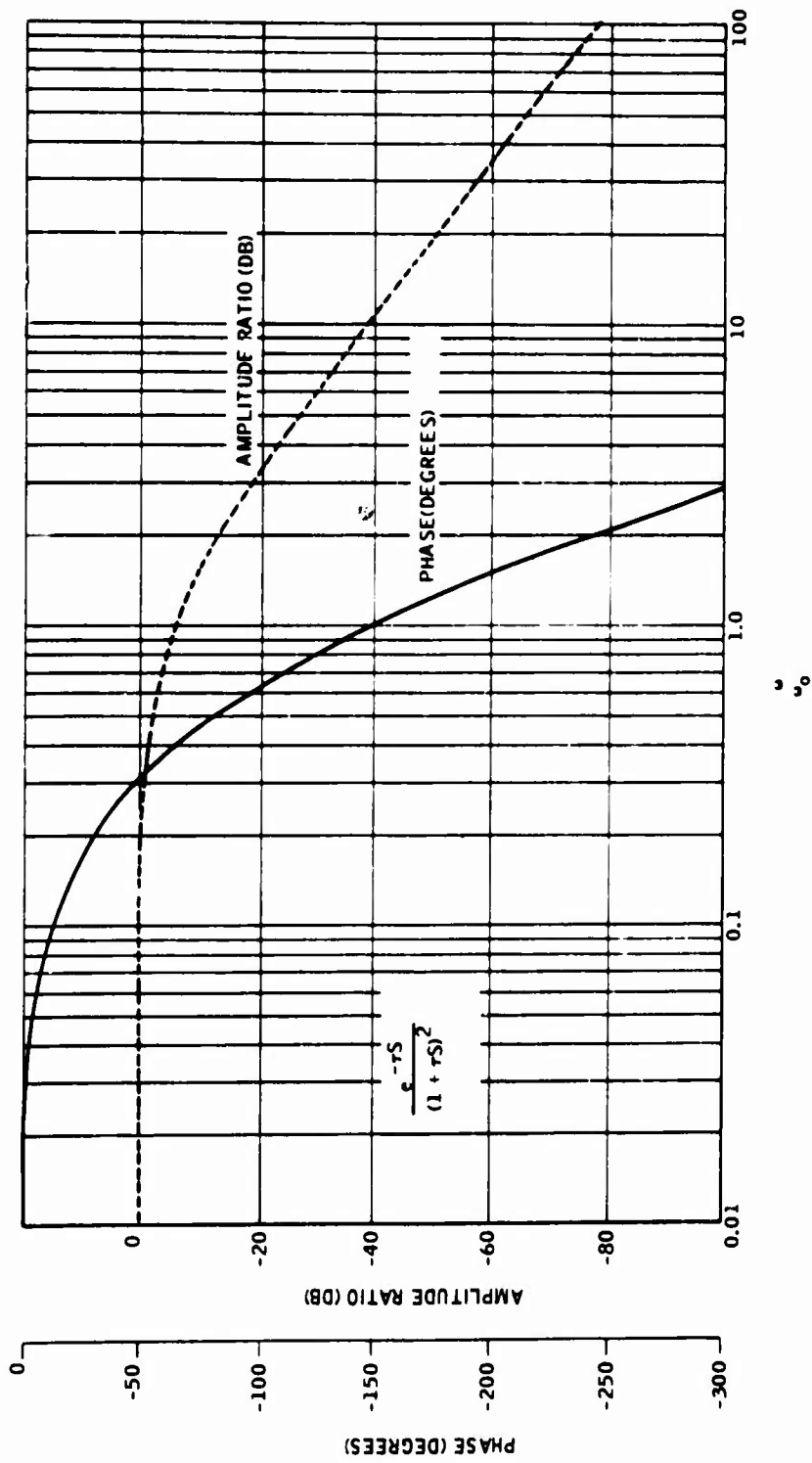


Figure 3. Normalized Sensor

Restraint of the roll axis was accomplished in two ways:

1. Inserting a roll attitude autopilot to simulate "wings level" control by a pilot.
2. Eliminating the rolling moment equation.

Responses to gusts, rudder steps, and roll attitude commands were observed to gain insight into the yaw damper response when the pilot holds the roll attitude fixed.

The control equation for the roll attitude autopilot used is

$A_1 = \left[0.2 \frac{(1+s)^2}{s} \right] \phi$ where A_1 is the cyclic pitch displacement. This control produced a dead-beat roll response to a step roll command with a time to 90 percent of 3 seconds.

Tail boom bending, series servo authority limits, vibration modes, small amplitude linkage non-linearities, etc., were not analyzed. Except for authority limits, insufficient data exists to evaluate the effects of these higher order considerations short of running parametric studies.

RESULTS AND CONCLUSIONS

1. The preliminary analysis indicated that the system would increase the yaw axis damping ratio of the UH-1B from 0.2 unaugmented to 0.6 augmented for all flight conditions but hover. Although unstable in hover, the free vehicle is controllable; and with this damper engaged, the divergence rates should be halved at least, thus substantially reducing the pilot workload.
2. Performance of the yaw damper degrades only slightly with the deviations from nominal gain and/or hi-pass time constant that are expected to occur.
3. Removal of the servo or transport lags had but a slight effect on the major control mode at frequencies below 4 radians per second, implying a degree of tolerance to higher frequency (> 20 rps) unknowns.

FINAL SYSTEM ANALYSIS

SUMMARY

The analog simulation of the UH-1B hydraulic damper system was reiterated when revised aerodynamic data was received from Bell

Helicopter Company. Instabilities associated with the initial definition of the aircraft, including the hover flight condition, were eliminated by the revised data. This resulted in an improved damped response at all flight conditions. It was also determined that a significant improvement in system damping could be realized by increasing the hi-pass time constant. Inclusion of primary control system linkage backlash (not available during the preliminary analysis) required an increase in damper system loop gain. The performance of the yaw damper was found to be strongly tolerant to off-design variations in system component mechanization.

DISCUSSION

The final analytical study was conducted to evaluate the impact of the revised UH-1B aerodynamic and control system data on the initial yaw damper configuration. The objectives of the study were to:

1. Evaluate the effect of the revised data on predicted performance.
2. Revise the system configuration, if necessary, to optimize performance.
3. Determine the effect of primary control system non-linearities (e.g., linkage backlash) on damper system performance.
4. Parametrically investigate the effects of off-design mechanization of the system components to determine range of production tolerances.

Primary emphasis in this study was placed on the dynamic system response to external disturbances as obtained from an analog simulation of the aircraft control system and yaw damper. Stability margins were obtained from the analog and verified by digital root locus techniques. Performance verification and correlation were obtained between digital and analog studies.

System Configuration and Data

An analytical block diagram of the final system configuration is shown in Figure 4. This is essentially the same configuration analyzed during the preliminary study with the addition of the control system non-linearities and a change in the hi-pass time constant. Control system non-linearities were obtained from ECOM Avionics Laboratories.

The control system loop equations used in the root locus analysis are shown in Figure 5. The first four equations represent the aircraft equations of motion with numerical values of the coefficients, a_{ij} , b_{ij} ,

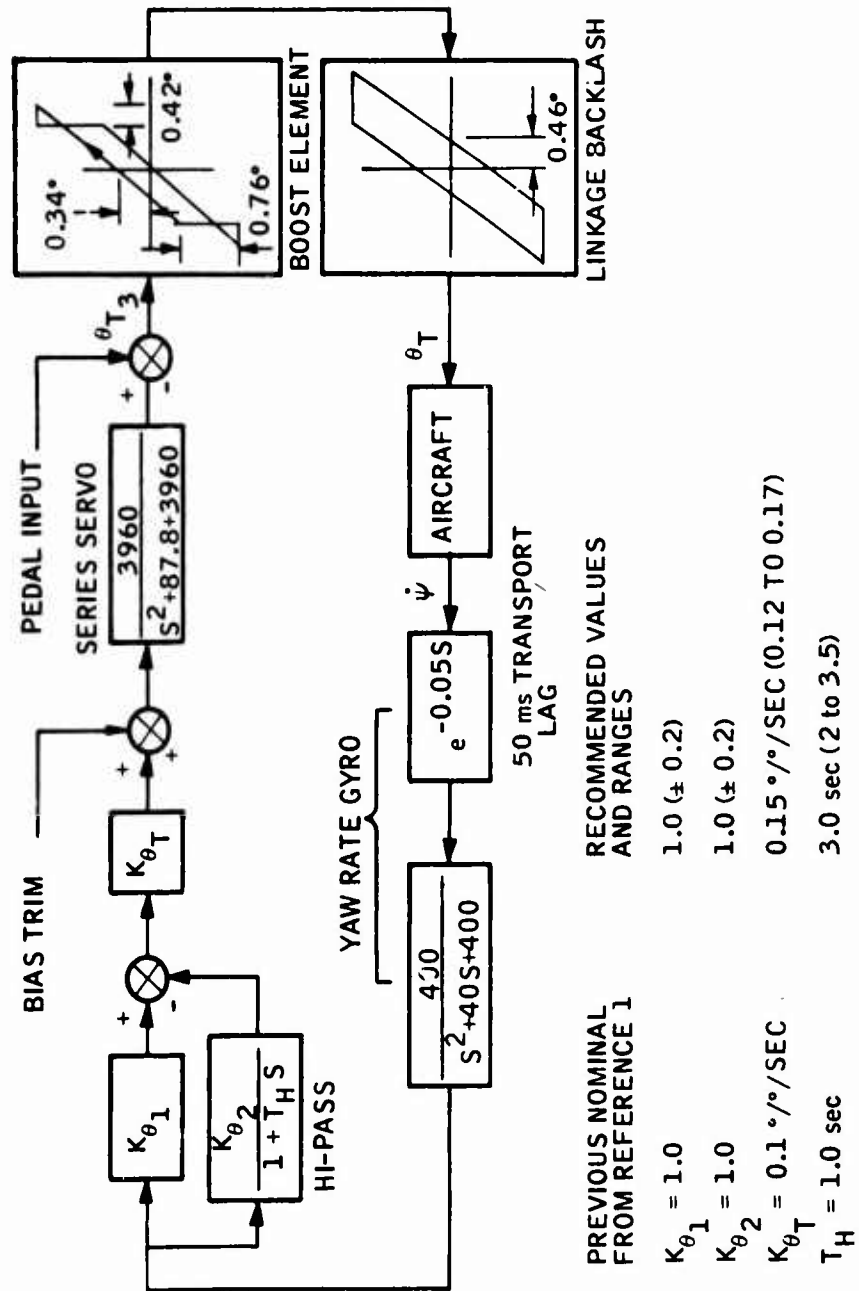
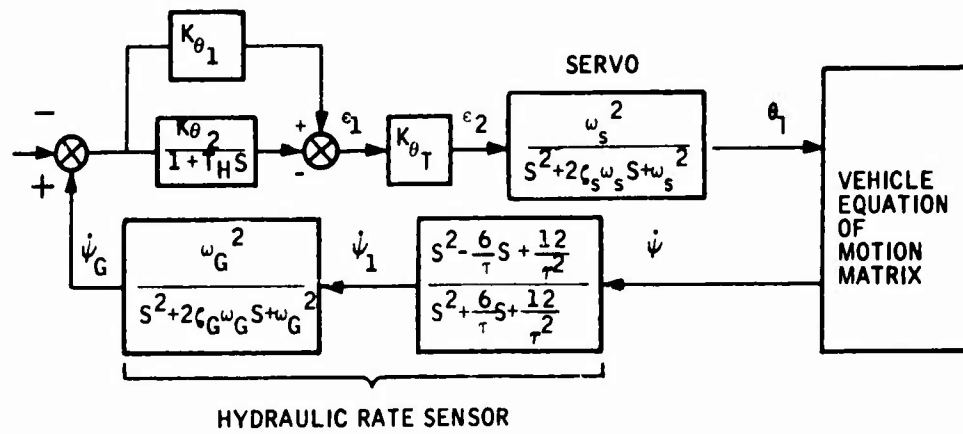


Figure 4. Analytical Block Diagram for UH-1B Yaw Damper Study



1. $b_{11}\dot{\beta} + c_{11}\beta + c_{12}\dot{\psi} + b_{13}\ddot{\phi} + c_{13}\dot{\phi} + b_{14}\ddot{\theta} + c_{14}\dot{\theta} + c_{19}\theta_T = 0$
2. $b_{21}\dot{\beta} + c_{21}\beta + b_{22}\ddot{\psi} + c_{22}\dot{\psi} + c_{29}\theta_T = 0$
3. $b_{31}\dot{\beta} + c_{31}\beta + c_{32}\dot{\psi} + a_{33}\ddot{\phi} + b_{33}\dot{\phi} + b_{34}\ddot{\theta} + c_{34}\dot{\theta} + c_{39}\theta_T = 0$
4. $b_{43}\dot{\phi} + b_{44}\ddot{\theta} + c_{44}\dot{\theta} = 0$

$$\begin{array}{l|l}
 5. \dot{\psi}_1 = \dot{\psi} \left[\frac{s^2 - \frac{6}{\tau}s + \frac{12}{\tau^2}}{s^2 + \frac{6}{\tau}s + \frac{12}{\tau^2}} \right] & \dot{\psi}_1 \left(s^2 + \frac{6}{\tau}s + \frac{12}{\tau^2} \right) - \dot{\psi} \left(s^2 - \frac{6}{\tau}s + \frac{12}{\tau^2} \right) = 0 \\
 6. \dot{\psi}_G = \dot{\psi}_1 \left[\frac{\omega_G^2}{s^2 + 2\zeta_G \omega_G s + \omega_G^2} \right] & \dot{\psi}_G \left(s^2 + 2\zeta_G \omega_G s + \omega_G^2 \right) - \dot{\psi}_1 \omega_G^2 = 0 \\
 7. \epsilon_1 = K_{\theta_1} \dot{\psi}_G - K_{\theta_2} \left(\frac{1}{1+T_H S} \right) \dot{\psi}_G & \epsilon_1 \left(1+T_H S \right) - K_{\theta_1} \left(1+T_H S \right) \dot{\psi}_G + K_{\theta_2} \dot{\psi}_G = 0 \\
 8. \epsilon_2 = K_{\theta_T} \epsilon_1 & \epsilon_2 - K_{\theta_T} \epsilon_1 = 0 \\
 9. \theta_T = \left[\frac{\omega_s^2}{s^2 + 2\zeta_s \omega_s s + \omega_s^2} \right] \epsilon_2 & \theta_T \left(s^2 + 2\zeta_s \omega_s s + \omega_s^2 \right) - \epsilon_2 \omega_s^2 = 0
 \end{array}$$

Figure 5. Block Diagram and Equations for Digital Study Matrix

and c_{ij} given in Figure 6. The complete set of matrix equations is shown in Figure 7.

Study Results

Nominal System Performance

Dynamic responses of the aircraft yaw damper system were obtained with the analog simulation described in Figures 8, 9, and 10. All analog responses include the 0.46-degree linkage backlash of the primary control system. All other parameters are the nominal values defined in the preliminary analysis unless otherwise noted.

The boost servo non-linearity was not simulated but was studied separately.

Figures 11 through 15 are analog traces of the aircraft response at four flight conditions to lateral gusts and step tail rotor commands. Comparisons are made of free aircraft and yaw damper augmented aircraft, both considering the effect of fixing the aircraft roll attitude.

Table I lists the performance quantities of percent overshoot (% O.S.) and solution time (T_{90} - time to reach and remain within 10 percent of the final value). These criteria were obtained from the β trace of the referenced figures. In all cases, the response overshoot was eliminated or substantially reduced with the yaw damper engaged (AUG ON). If one assumes the response to be a second order, this overshoot can be expressed as an increase in effective damping ratio from 0.32 (free aircraft) to better than 0.6 (augmented aircraft).

TABLE I NOMINAL SYSTEM PERFORMANCE										
F. C.	Disturbance		Gust				Step			
	ϕ	Aug	ϕ Free		ϕ Fixed		ϕ Free		ϕ Fixed	
			OFF	ON	OFF	ON	OFF	ON	OFF	ON
60 KTS	ϕ	% O.S.	33.0	0.0	27.0	0.0	36.0	10.0	35.0	5.0
		T_{90}	4.0	1.5	3.6	2.1	3.4	3.0	2.6	1.4
90 KTS	ϕ	% O.S.	33.0	0.0	33.0	0.0	29.0	7.0	25.0	5.0
		T_{90}	3.1	1.0	2.9	1.2	3.0	1.4	1.7	1.0
120 KTS	ϕ	% O.S.	37.0	0.0	33.0	0.0	34.0	10.0	20.0	5.0
		T_{90}	2.6	1.0	2.4	1.0	1.5	1.0	1.8	1.1

FC Element	1. (Hover)	2. V = 60 Knots	3. V = 90 Knots	4. V = 120 Knots
a ₃₃	-2500.	-2500.	-2500.	-2500.
b ₁₁	-217.5	-22373.	-33467.	-40862.
b ₁₂	-350.	-486.	-424.	-335.
b ₁₄	56.	-77.9	-67.9	-53.6
b ₂₁	0.	9982.	11909.	13226.
b ₂₂	-8000.	-8000.	-8000.	-8000.
b ₃₁	0.	-2075.	-2406	-2627.
b ₃₃	-2470.	-3486.	-3074.	-2462.
b ₃₄	-395.	-54.9	-47.9	-37.9
b ₄₃	1.	1.	1.	1.
b ₄₄	1.	1.	1.	1.
c ₁₁	-8.18	-2427.	-4910.	-7044.
c ₁₂	167.5	-22032.	-33060	-40411.
c ₁₃	7000.	7000.	7000.	7000.
c ₁₄	1120.	1133.	1133.	1141.
c ₁₉	3500.	4550.	5060.	5500.
c ₂₁	167.1	27481.	46887.	61620.
c ₂₂	-5440.	0.	0.	0.
c ₂₉	-101200.	-132000.	-146100.	-159000.
c ₃₁	-55.8	-8007.	-14265.	-19435.
c ₃₂	1179.	0.	0.	0.
c ₃₄	7900.	800.	800.	806.
c ₃₉	23500.	30600.	34000.	37000.
c ₄₄	.3	.3	.3	.3

Figure 6. Nominal Matrix Values - Aircraft Equations

$b_{11} S + C_{11}$	C_{12}	$b_{13} S + C_{13}$	$b_{14} S + C_{14}$					C_{19}	β
$b_{21} S + C_{21}$	$b_{22} S + C_{22}$							C_{29}	$\dot{\psi}$
$b_{31} S + C_{31}$	C_{32}	$A_{33} S^2 + b_{33} S$	$b_{34} S + C_{34}$					C_{39}	ϕ
		$b_{43} S$	$b_{44} S + C_{44}$						$\dot{\phi}$
	$-S^2 + \frac{6}{\tau} S - \frac{12}{\tau^2}$			$S^2 + \frac{6}{\tau} S + \frac{12}{\tau^2}$					$\psi_1 = 0$
				$-u_G^2$	$\dot{S}^2 + 2S_G u_G S + u_G^2$				$\dot{\psi}_G$
					$(-K_{\theta 1} + K_{\theta 2}) - K_{\theta 1} T_H S$	$1 + T_H S$			ϵ_1
						$-K_{\theta T}$	1		ϵ_2
							$-u_S^2$	$S^2 + 2\zeta_S u_S S + u_S^2$	θ_T

$$u_S = 62.9285 \text{ rad/sec}$$

$$\zeta_S = 0.7$$

$$u_G = 20.0 \text{ rad/sec}$$

$$\tau = 0.05 \text{ sec}$$

$$K_{\theta 1} = 1$$

$$K_{\theta 2} = 1$$

$$T_H = 1 \text{ sec}$$

Figure 7. Aircraft and Control System Matrix

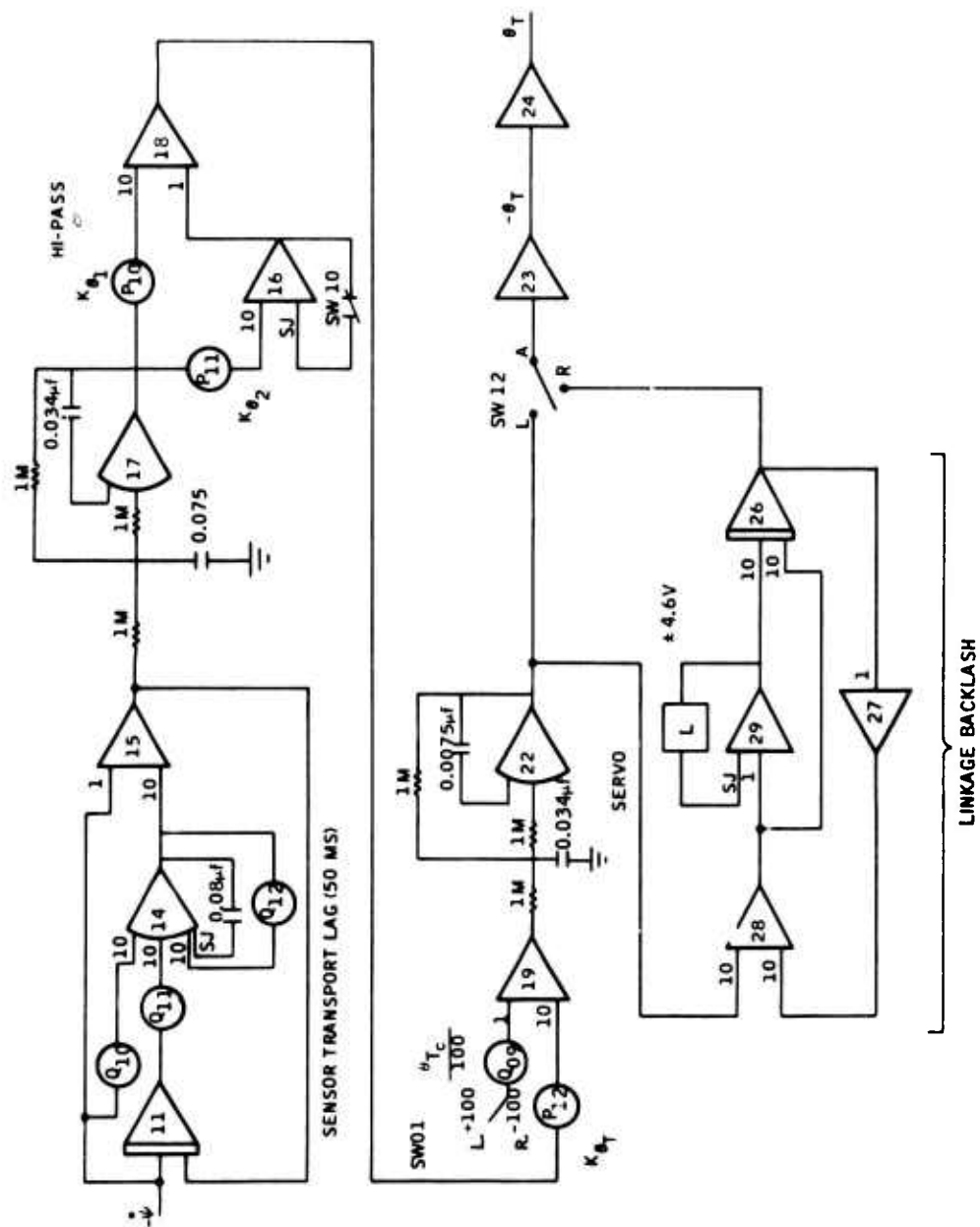


Figure 9. Analog Simulation of Hydraulic Yaw Damper

Pot. No.	Parameter Description	Hover	$u_0 = 60$ Kts	$u_0 = 90$ Kts	$u_0 = 120$ Kts
P 00	$Y \beta$	0376	1085	1047	1729
01	$Y \dot{\psi}$	7710	9890	9900	9930
02	$Y \dot{\phi}^*$	1610 [*]	0218	0127	0083
03	$Y \ddot{\phi}^{**}$	3220 ^{**}	3140	2095	1720
04	$Y \ddot{\phi}$	2580	0035	0020	0013
05	$Y \ddot{\phi}$	9999	0102	0068	0056
06	$Y \theta_T/20$	8050	0102	0076	0068
07	$N \dot{\beta}/10$	0	1250	1490	1660
08	$N \beta/10$	0021	3440	5850	7720
09	$N \dot{\psi}$	6800	0	0	0
10	$K \theta_1/10$	1000	1000	1000	1000
11	$K \theta_2/10$	1000	1000	1000	1000
12	$K \theta_T/10$	0100	0100	0100	0100
13	$K \ddot{\phi}$	3000	3000	3000	3000
Q 00	$N \theta_T/20$	6340	8250	9150	9950
01	$L \dot{\beta}$	0	8300	9620	9999
02	$L \beta/10$	0022	3230	5700	7800
03	$L \dot{\psi}$	4720	0	0	0
04	$L \ddot{\phi}/10$	0990	1395	1228	0985
05	$L \ddot{\phi}$	1580	0220	0192	0152
06	$L \ddot{\phi}/10$	3160	0320	0320	0322
07	$L \theta_T/20$	4765	6110	6800	7400
08	$\beta(\gamma) \ddot{\phi}/100$	1500	1500	1500	1500
09	$\theta_{T_0}/100$	0100	0100	0100	0100
10	$12/1250 \tau$	1920	1920	1920	1920
11	$12/12500 \tau^2$	3840	3840	3840	3840
12	$6/1250 \tau$	9600	9600	9600	9600

* $Y \dot{\phi}/10$

** $Y \ddot{\phi}/100$

Figure 10. Analog Simulation Potentiometer Settings

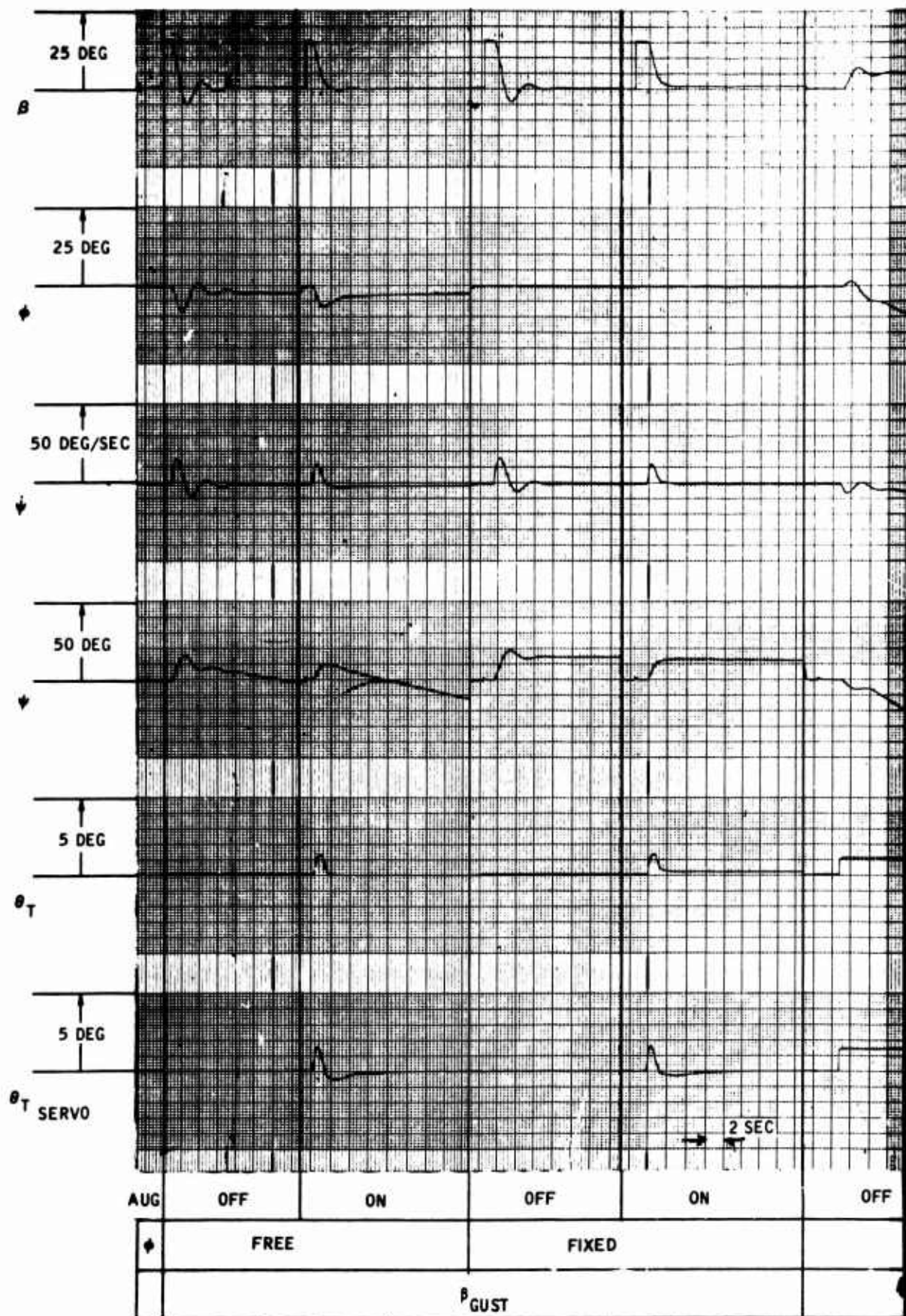
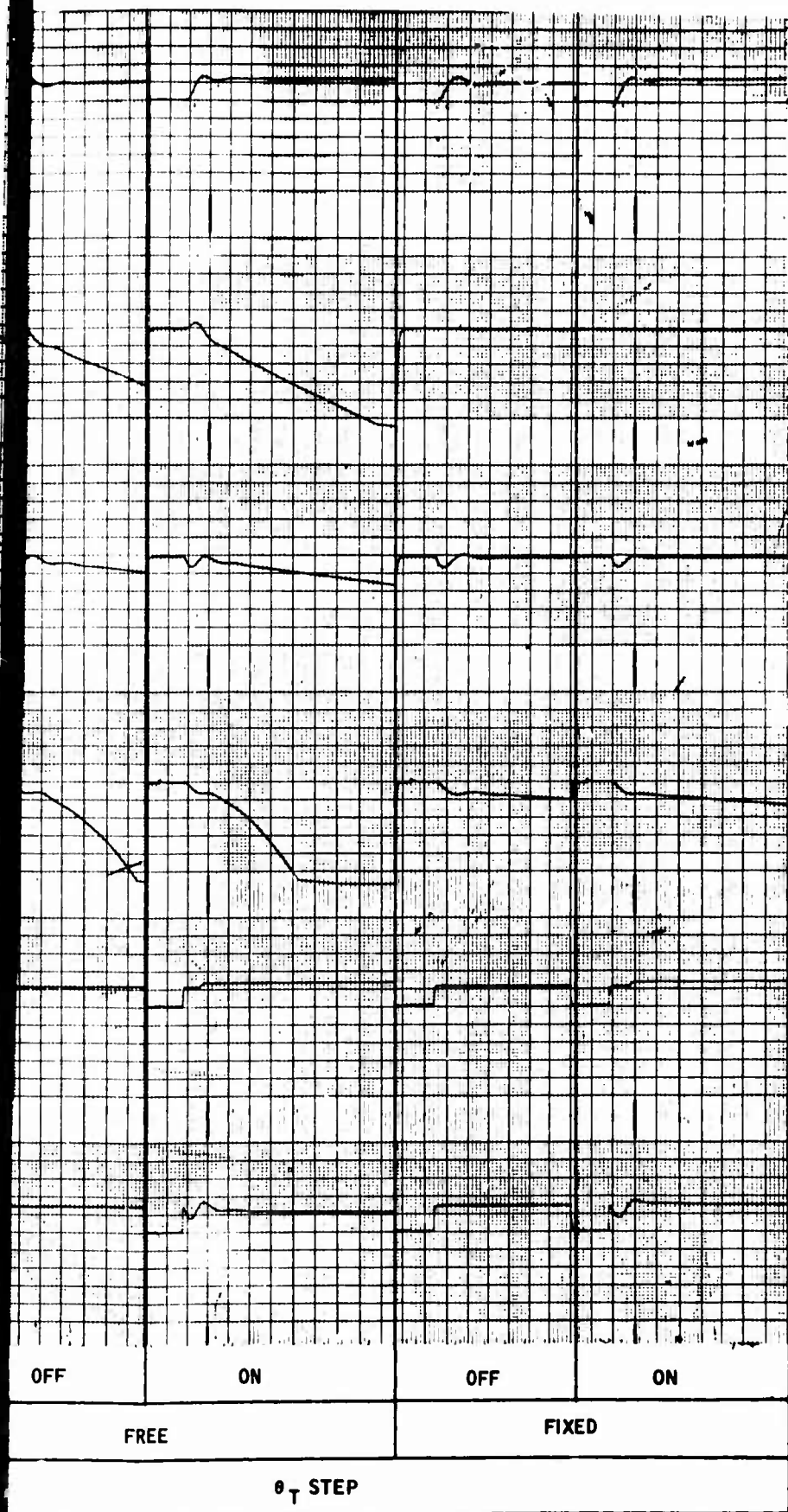


Figure 11. 60 Knots - Nominal Pe



al Performance

(1)

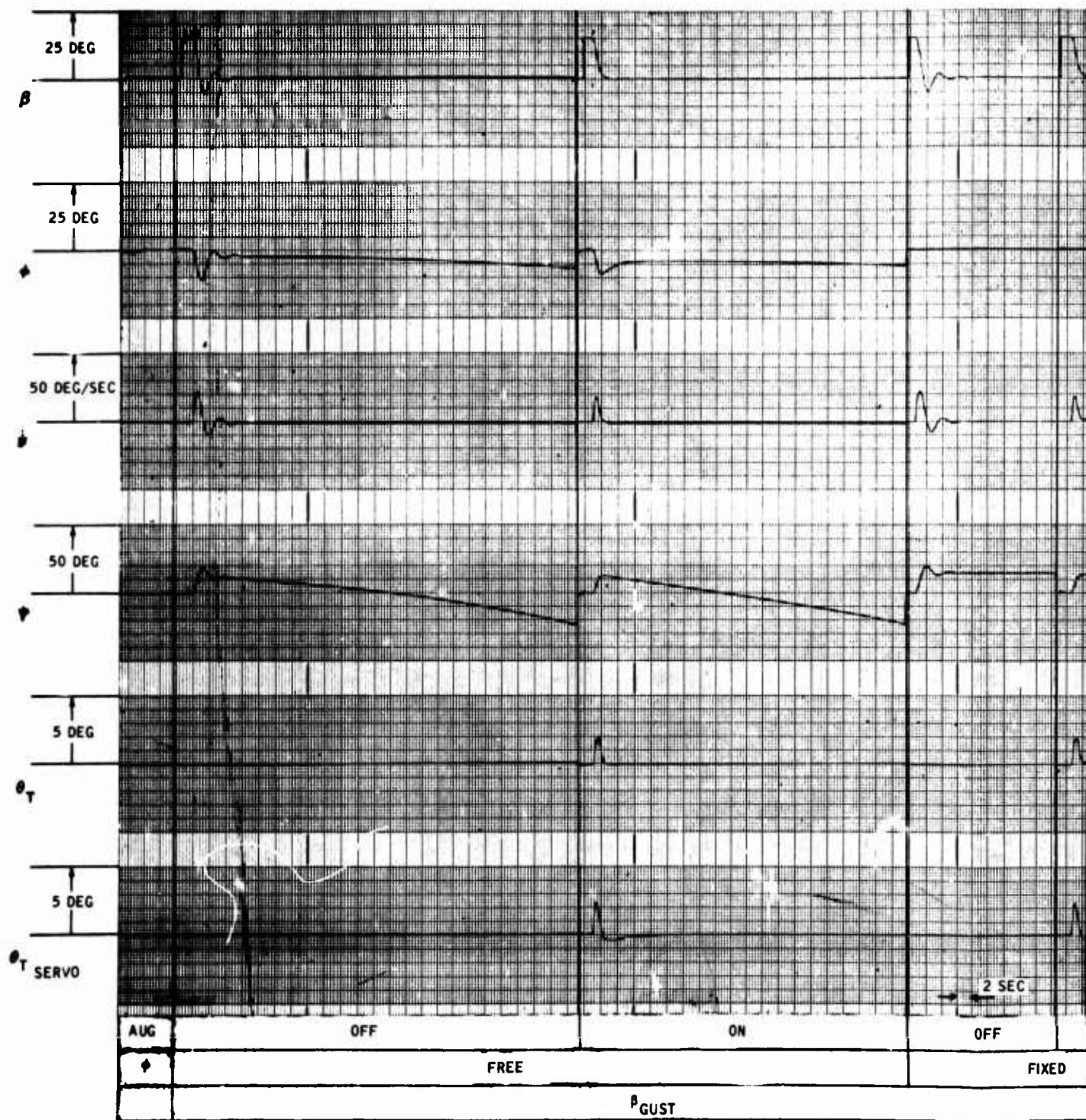
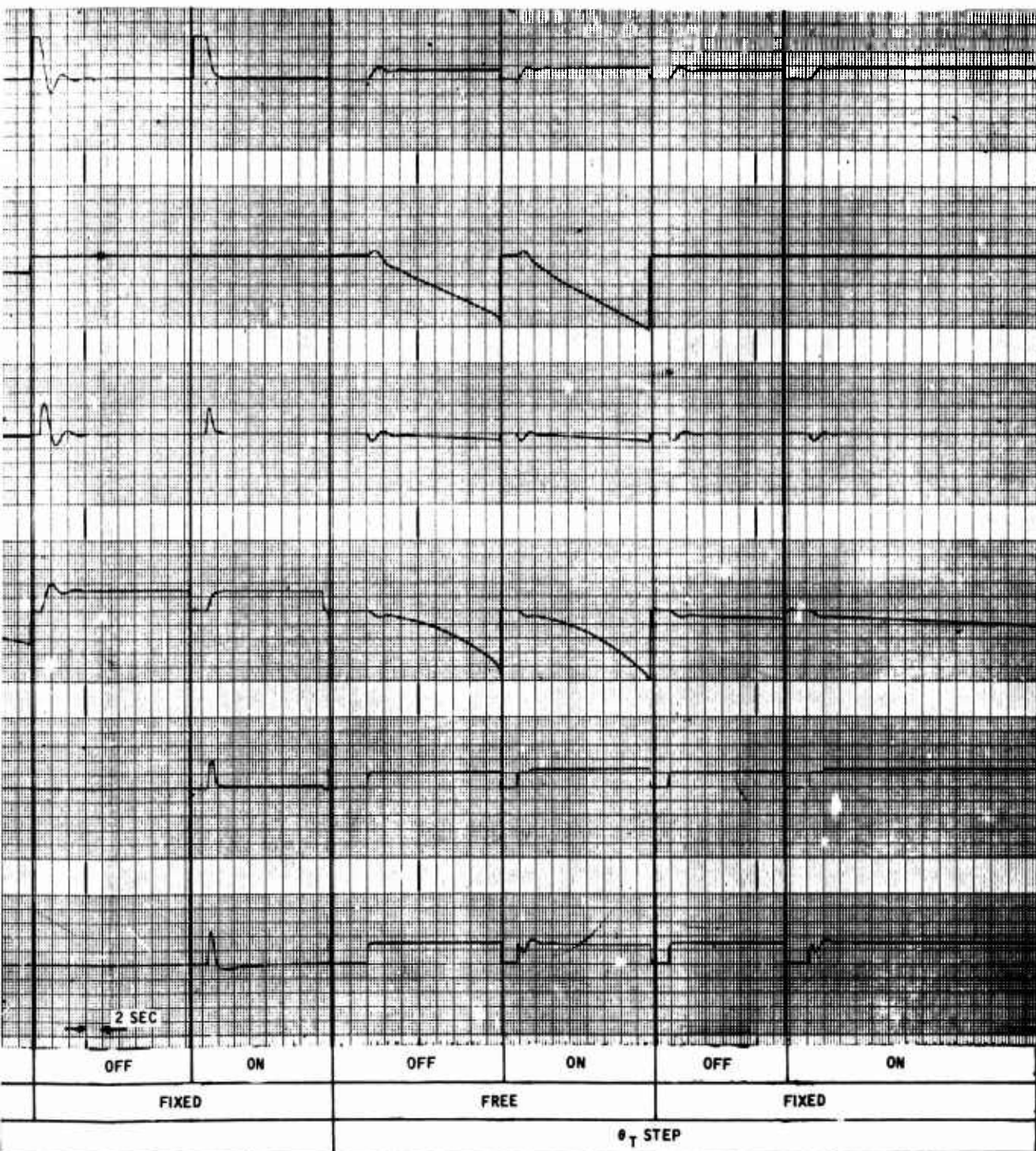


Figure 12. 90 Knots - Nominal Pe

A



Knots - Nominal Performance

B

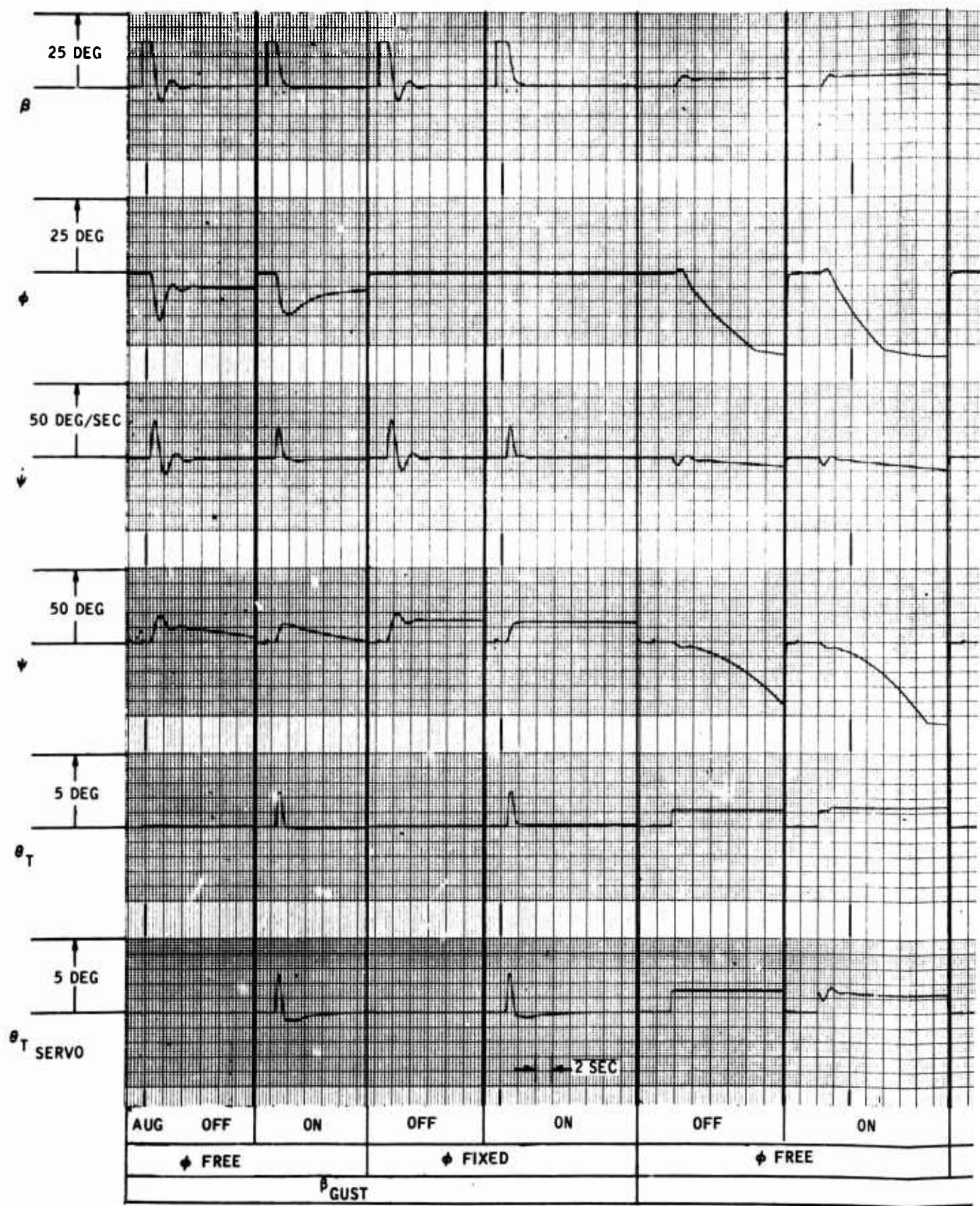
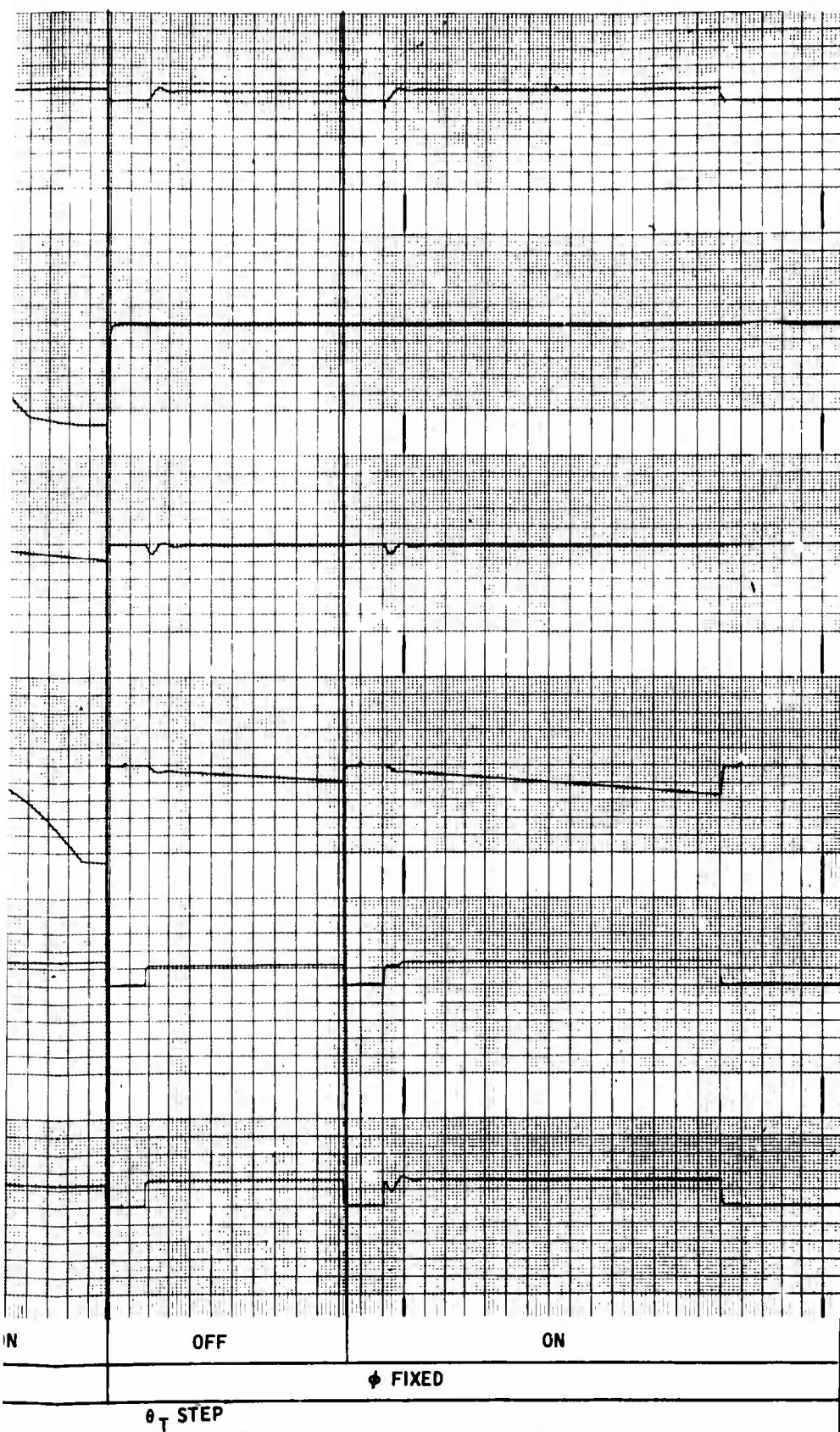


Figure 13. 120 Knots - Nominal Perfor



nal Performance

B

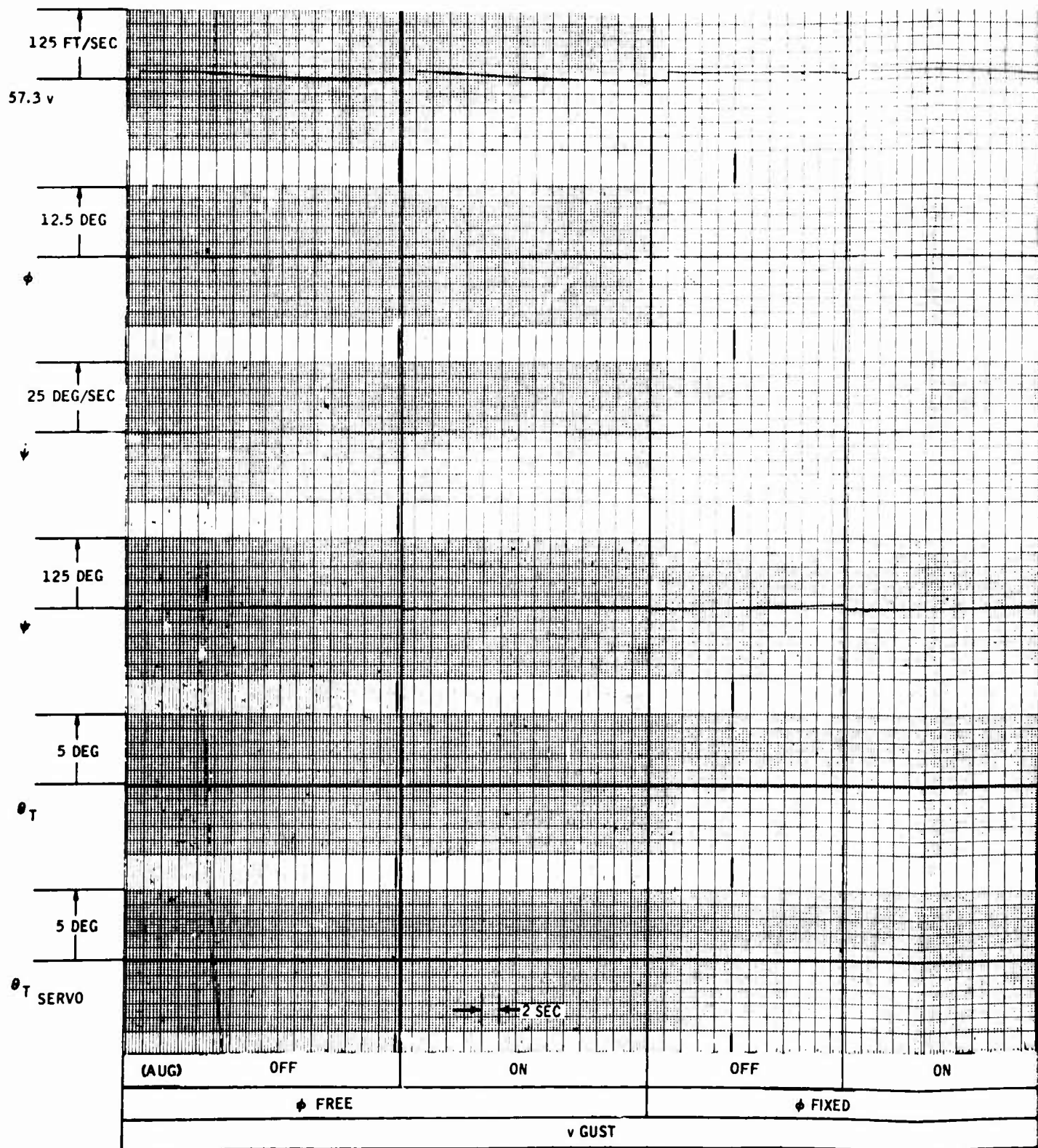
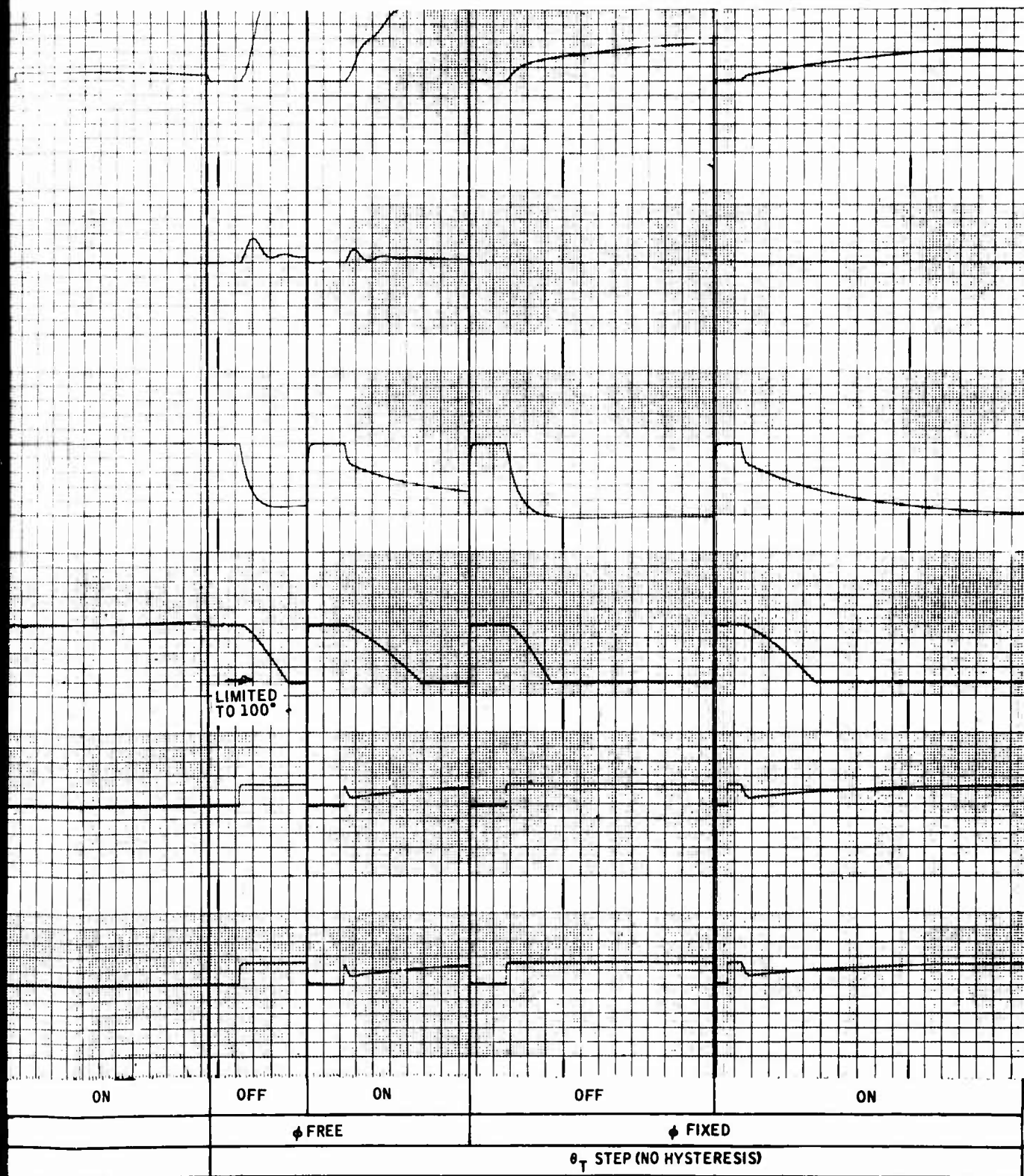


Figure 14. Hover - Nominal P



Plover - Nominal Performance

B

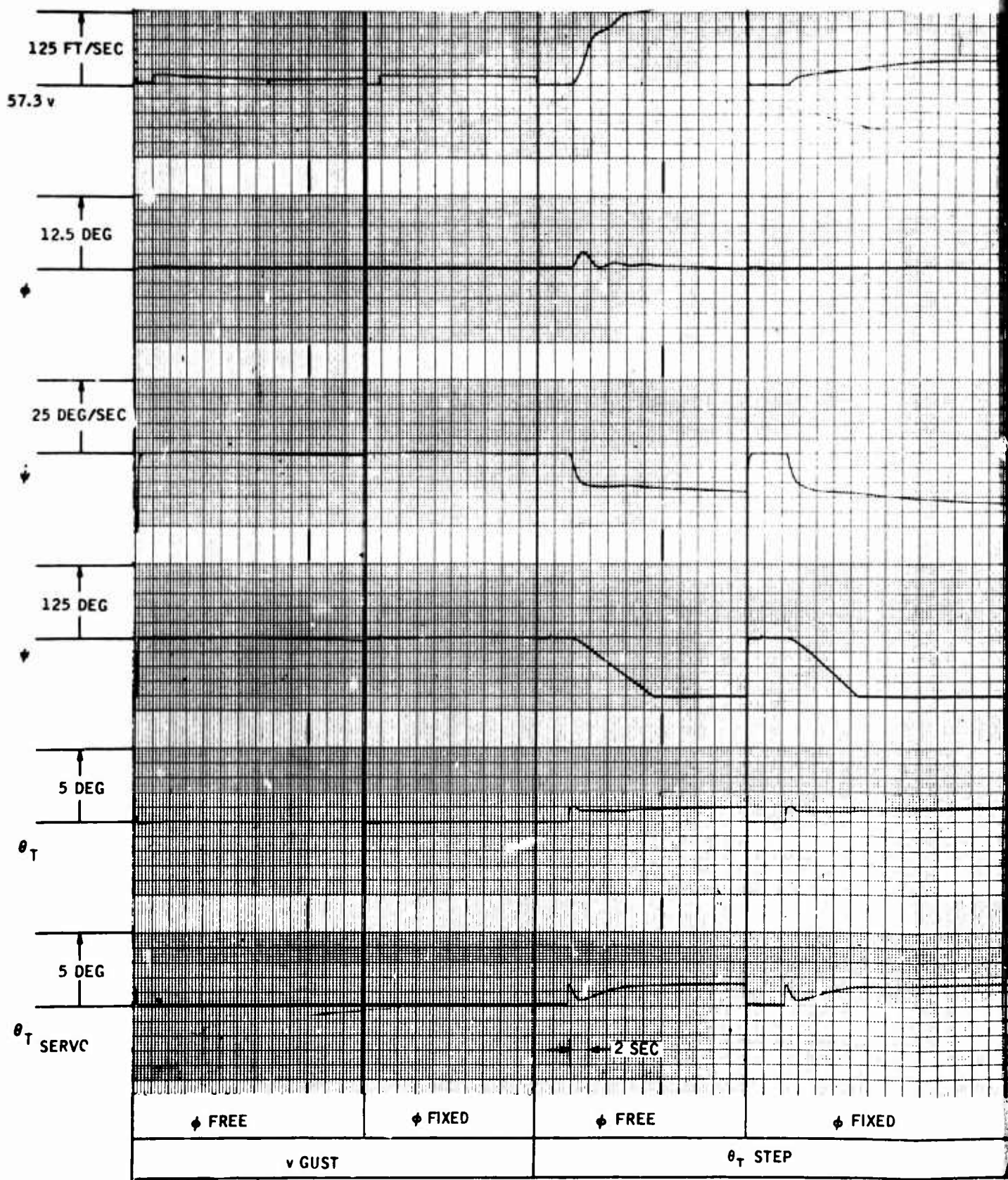
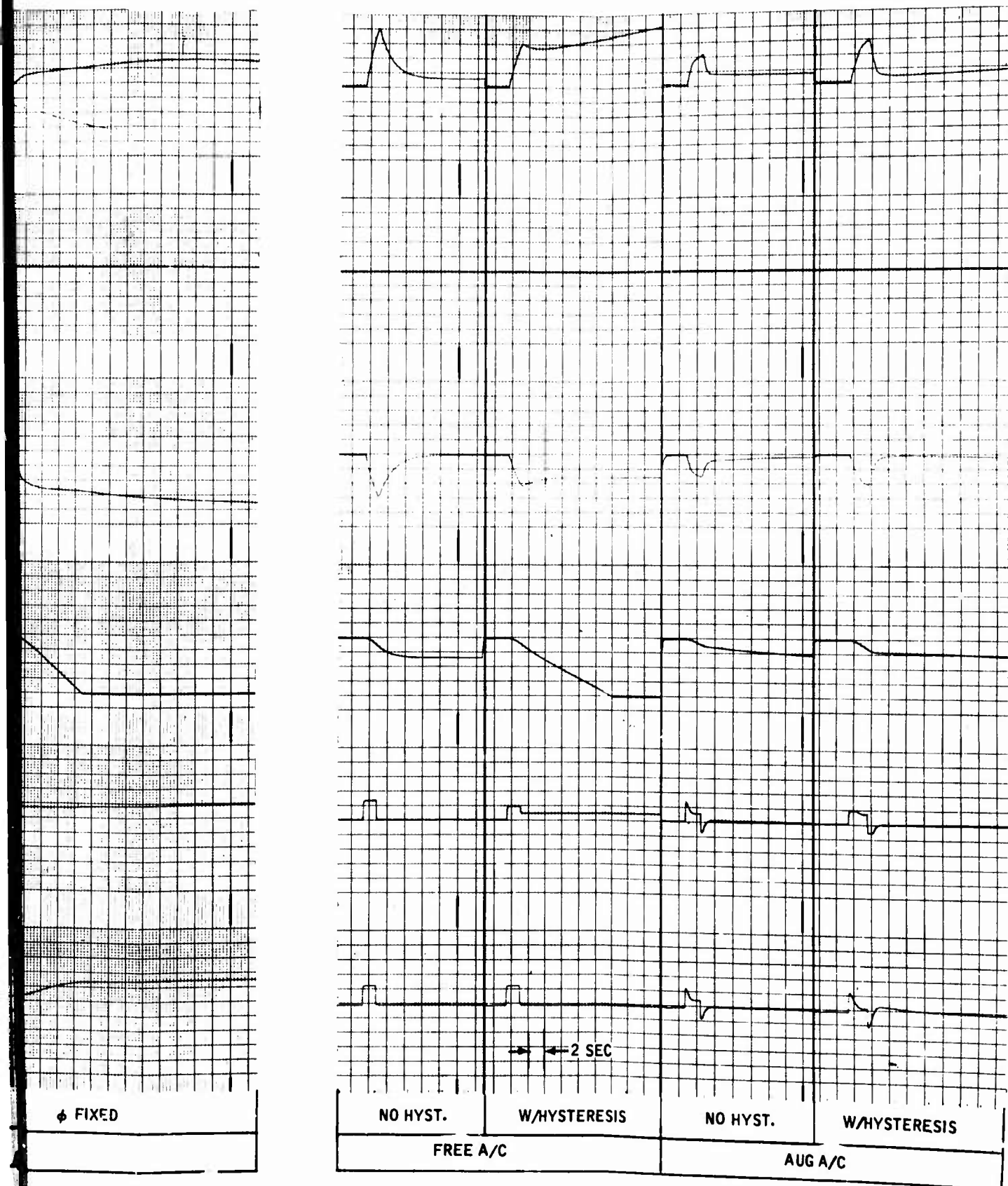


Figure 15. Hover - Nominal Performance, with 0.46-Degree Leakage Hys



TAIL ROTOR PULSE

Minimal Performance, Augmented Aircraft
Degree Leakage Hysteresis

B

The hover condition is treated as a separate case since the above criteria do not apply. The yaw damper tends to make the aircraft less sensitive to pedal inputs, in effect reducing yaw rate control effectiveness by two-thirds in the short period. The steady-state yaw rate attained for a given tail rotor input is the same in both cases. No conclusion can be drawn relative to hover performance with the yaw damper in the absence of some form of outer loop control.

Digital root loci for the four flight conditions are shown in Figures 16 through 19. Only the significant loci, the dominant aircraft and critical gain, are shown in detail, although the complete locus was obtained in the digital program output. In all cases, the hi-pass time constant for the nominal case was one second. The effect of varying the hi-pass time constant is shown in Figure 18 for the 90-knot case.

Of particular significance is the increased damping (the locus is on the negative, real axis) for the higher time constant at the operating gain, and the consistency in critical gain level, independent of the hi-pass time constant.

Further analog-root locus correlation is shown in the analog trace of Figure 20, which shows system responses for various gains and hi-pass time constants for 90 knots. The trend of "frequency" and "damping" of the analog response (β trace) can be seen to follow the prediction of the dominant aircraft locus as shown in the expanded origin portion of Figure 18.

Parametric Studies

A series of parametric studies was made to determine the optimum nominal system configuration and to evaluate the effect of off-design effects on system performance.

Total Loop Gain Variation

The choice of 0.15 deg/deg/sec. as nominal loop gain was determined from the traces of Figures 21, 22, and 23. The criteria applied were minimization of overshoot in gust response, yet maintaining the fast response of the free aircraft. The qualitative trend of these criteria with loop gain is seen to be as shown in Figure 24.

Hi-Pass Time Constant

Figures 21, 22 and 23 also show variations in the hi-pass time constant. With hysteresis in the loop, time constants greater than one second give essentially the same responses. Without hysteresis (see Figures 20 and 22), a time constant of at least 3 seconds is indicated

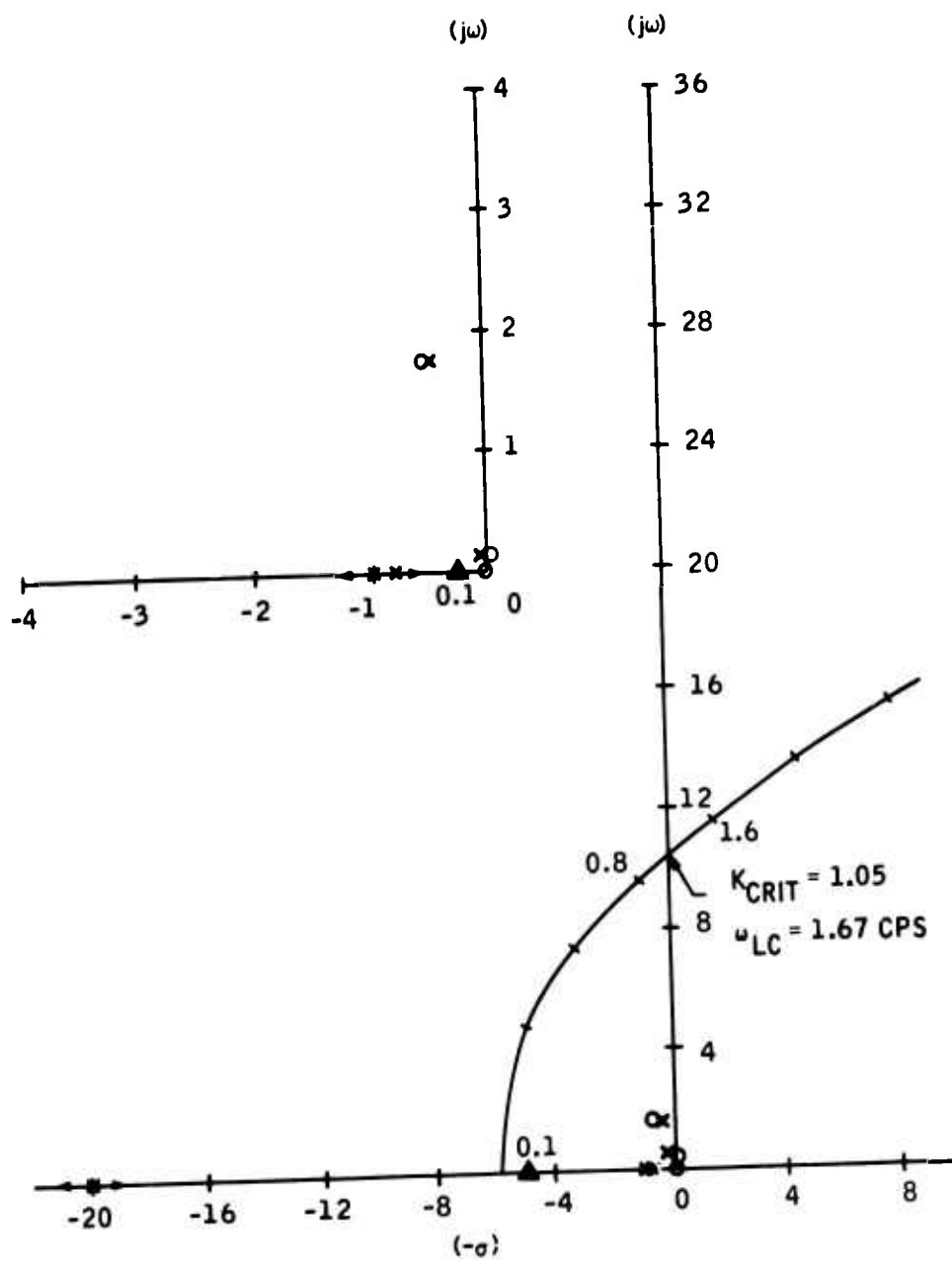


Figure 16. Root Locus Nominal (Hover)

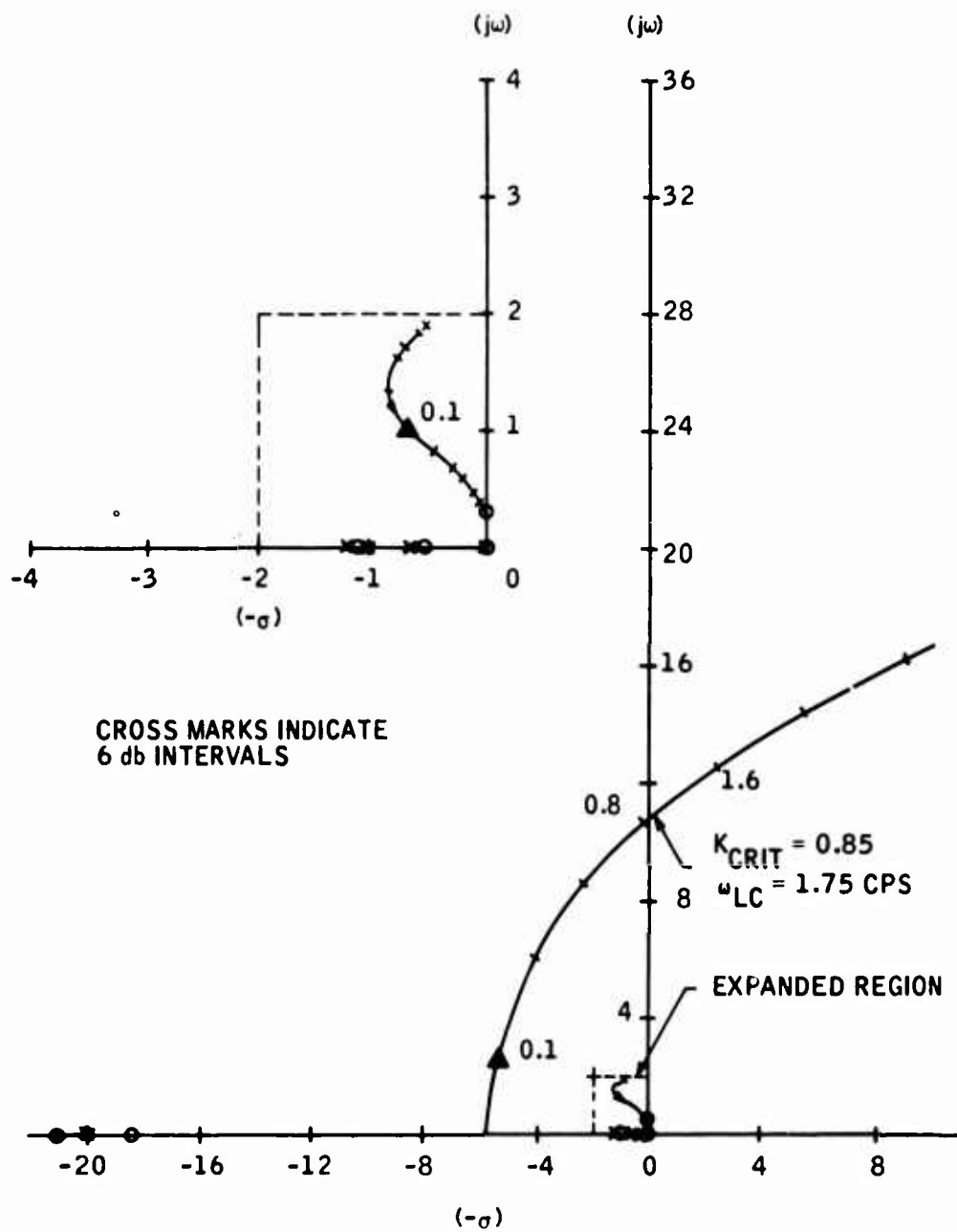


Figure 17. Root Locus Nominal (60 Knots)

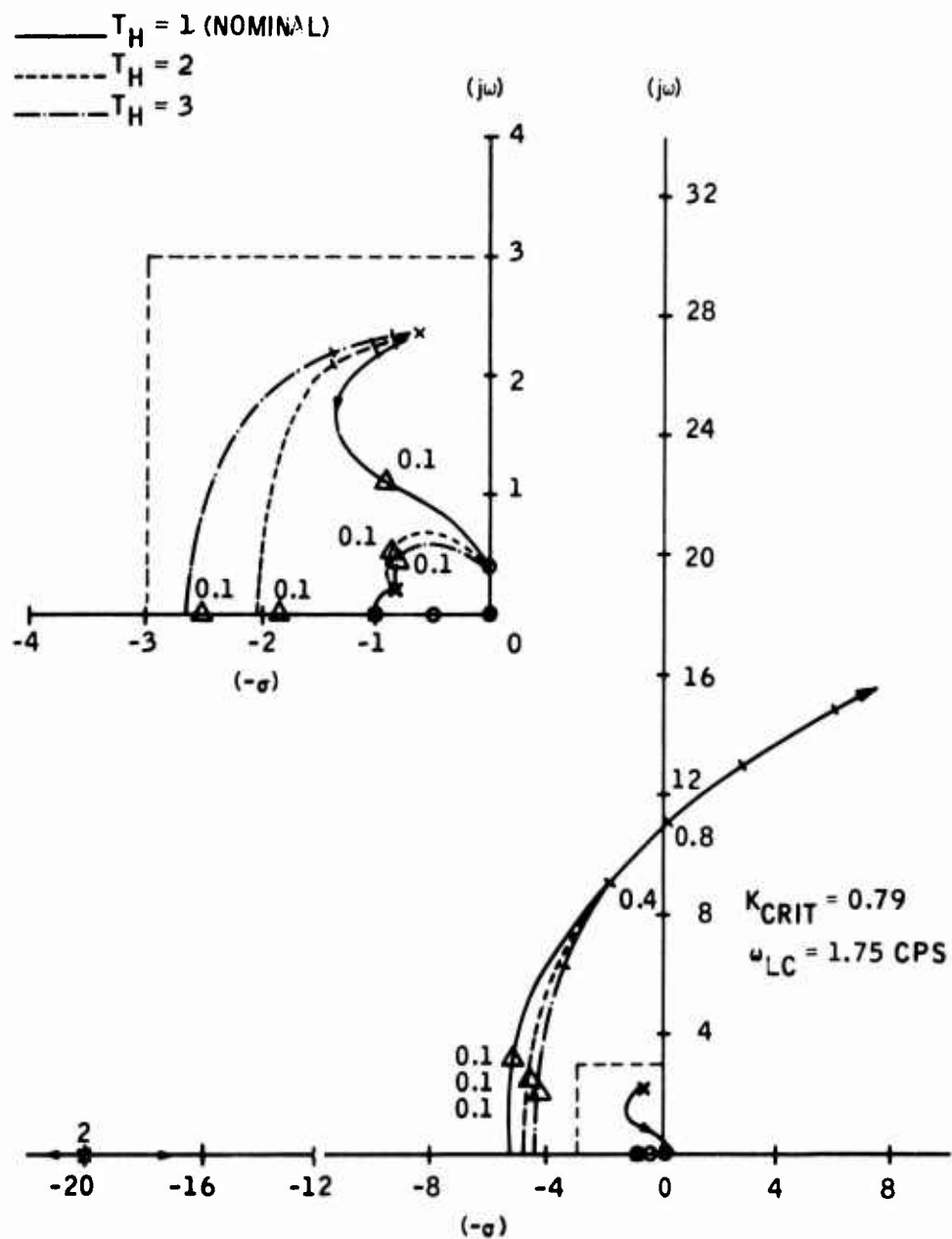


Figure 18. Effect of Hi-Pass Time Constant Variation (90 Knots)

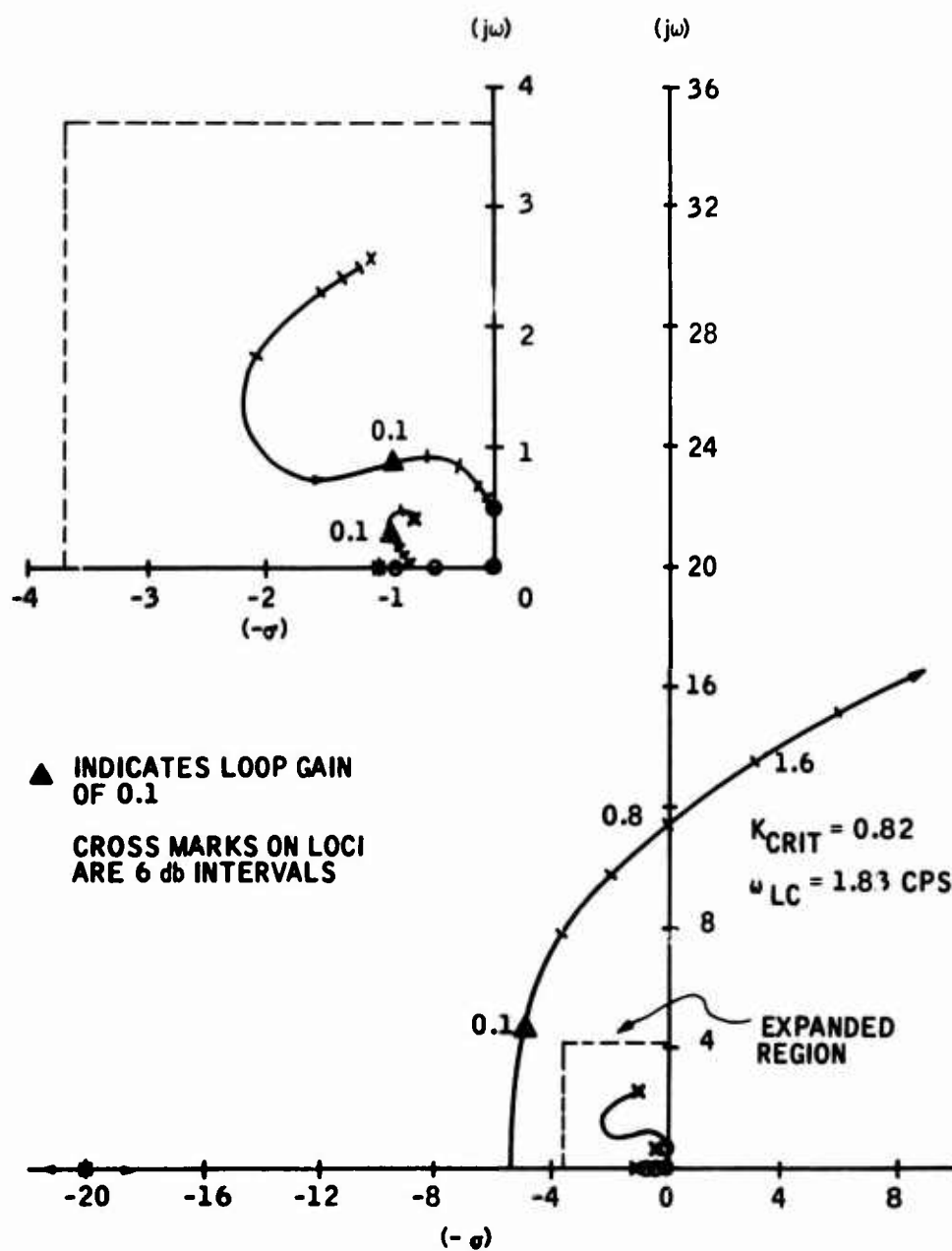


Figure 19. Root Locus Nominal (120 Knots)

BLANK PAGE

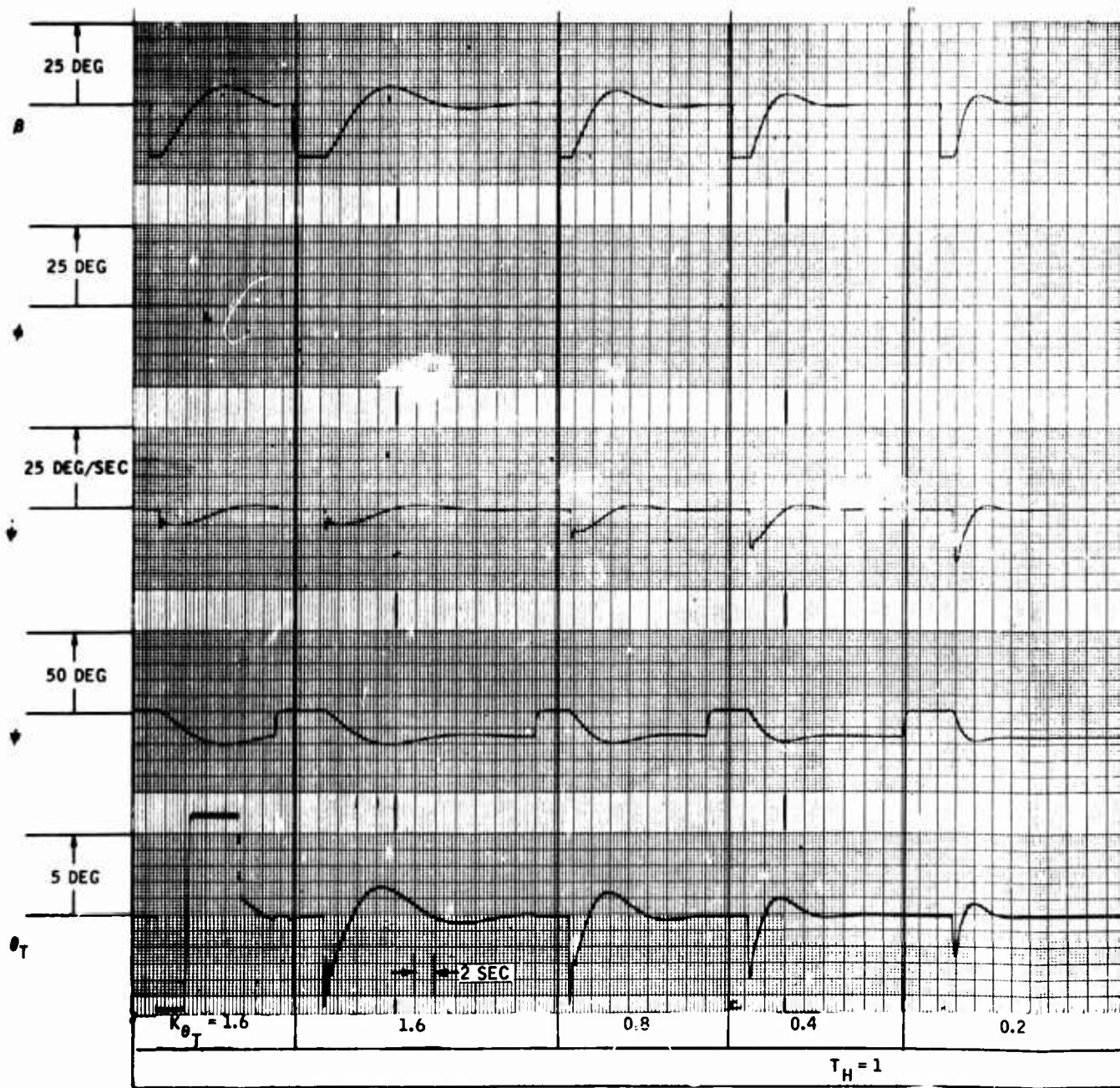
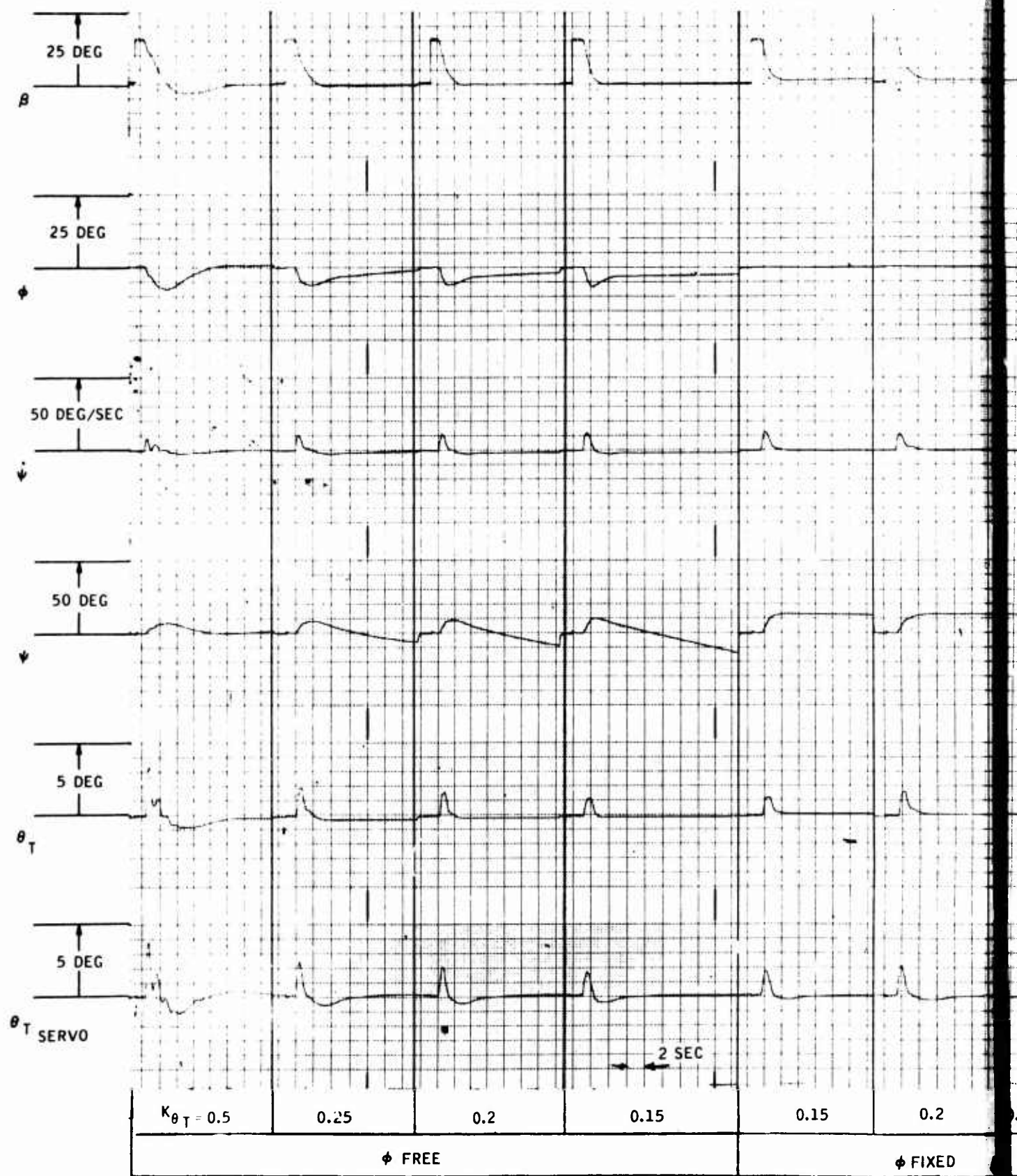


Figure 20. Root Locus Correlatio



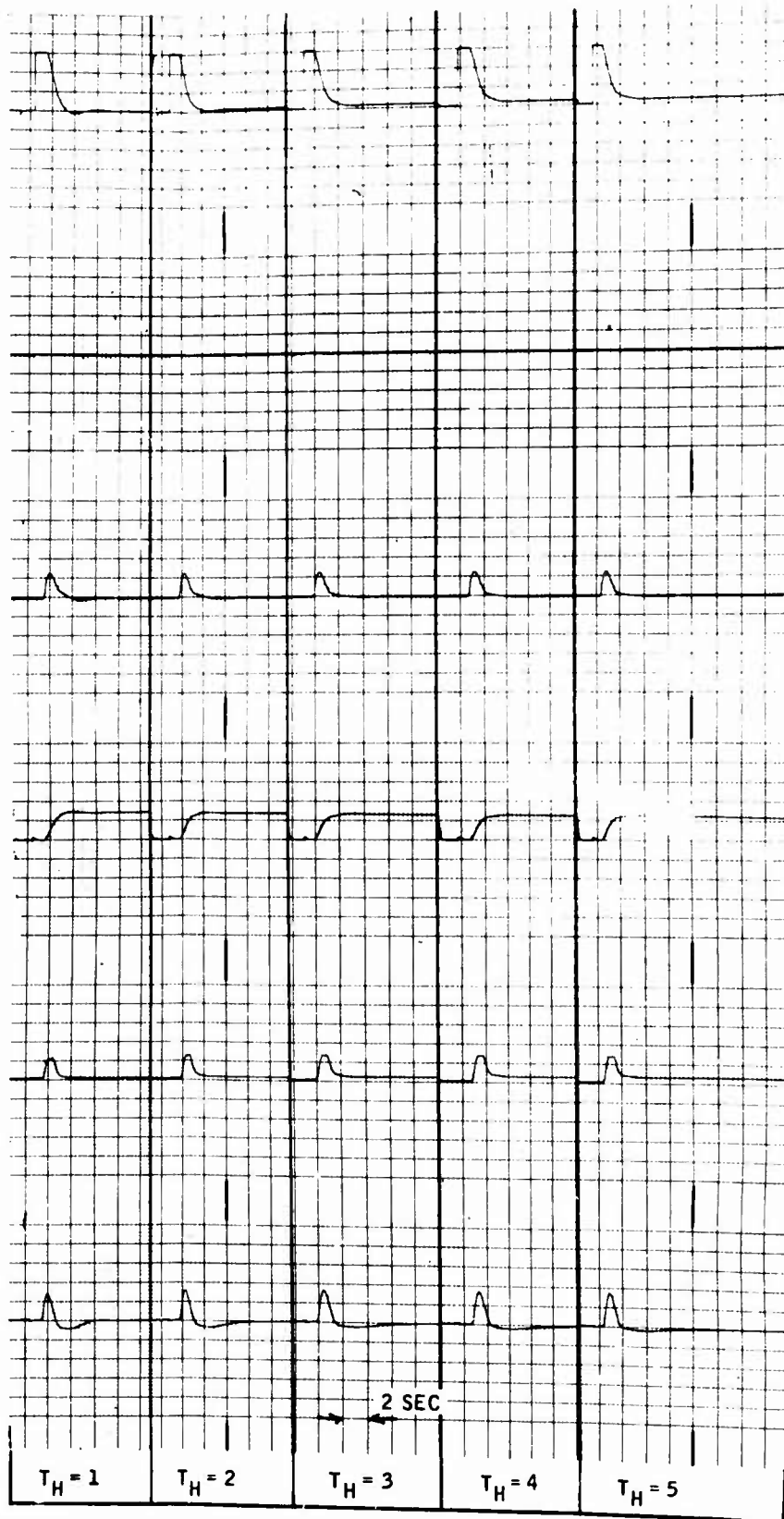
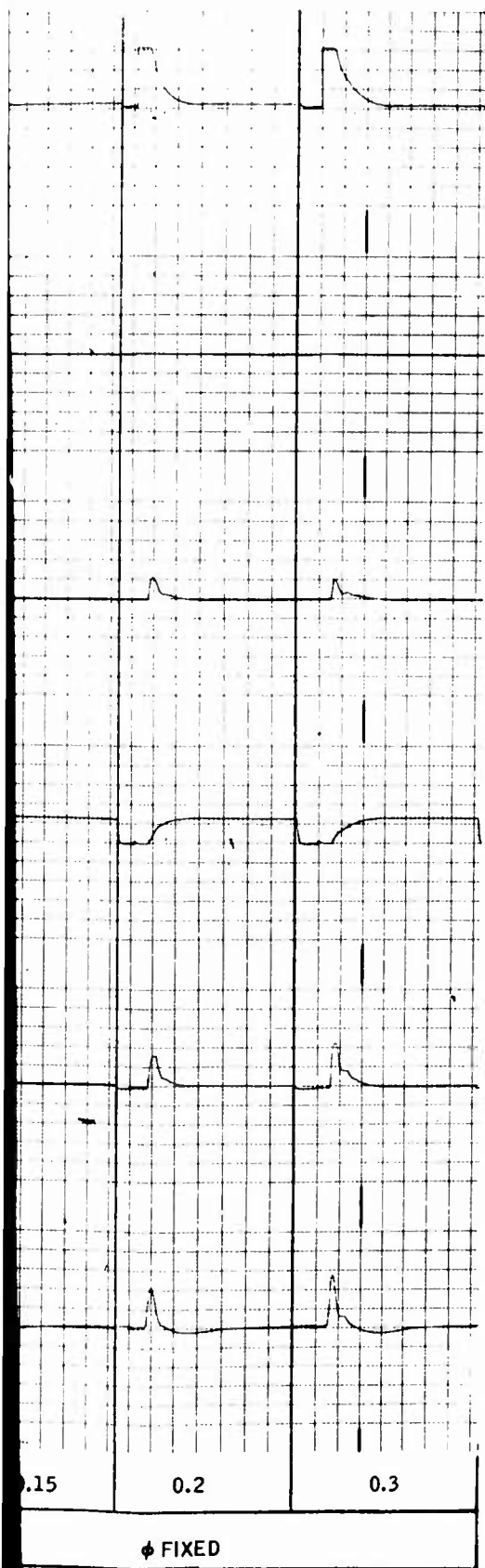
ion Focus Correlation Runs (90 Knots)

B



VARIATION IN TOTAL LOOP GAIN

Figure 21. 60 Knots - P



VARIATION IN HI-PASS TIME CONSTANT

21. 60 Knots - Parametric Study

13

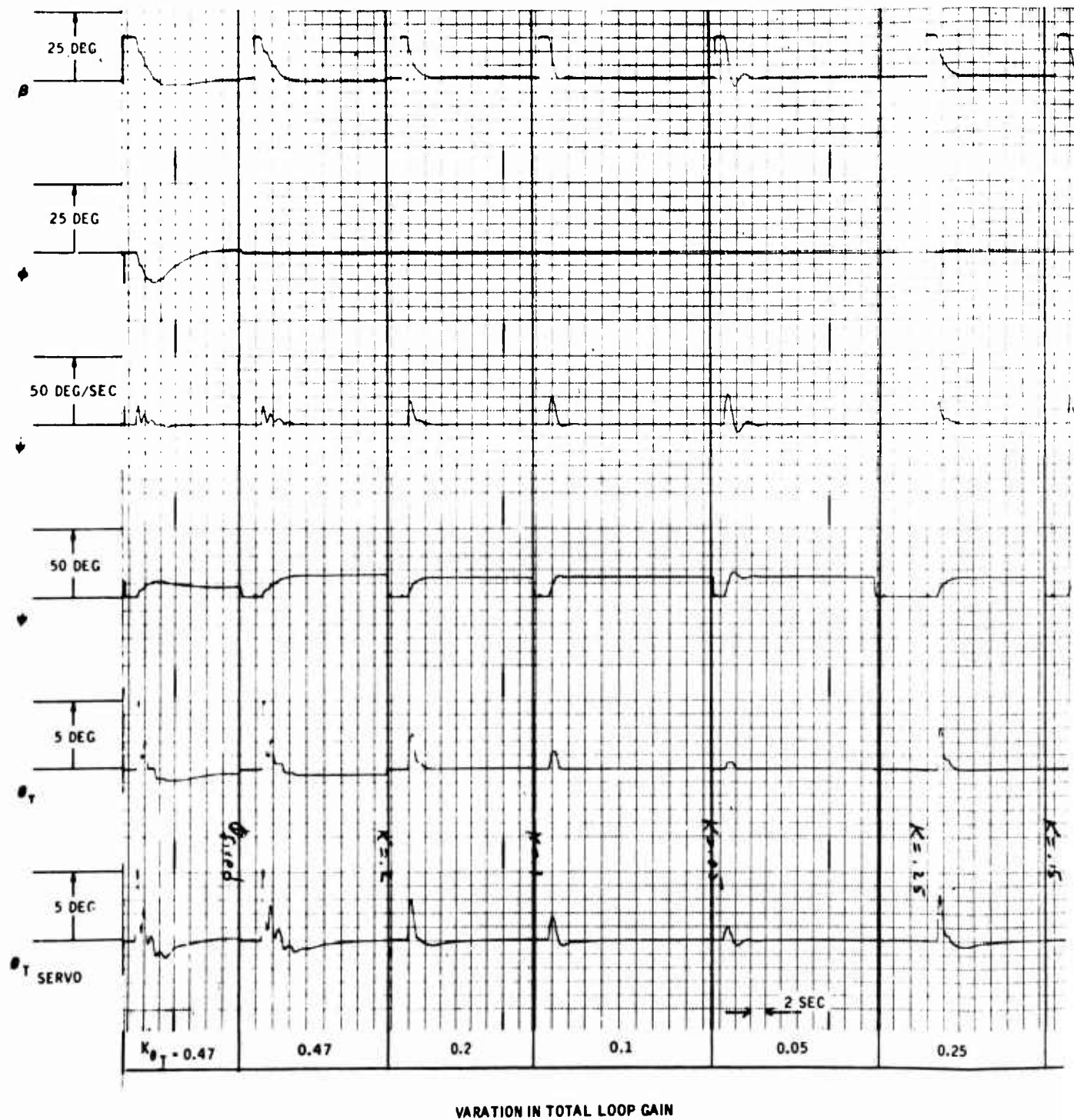
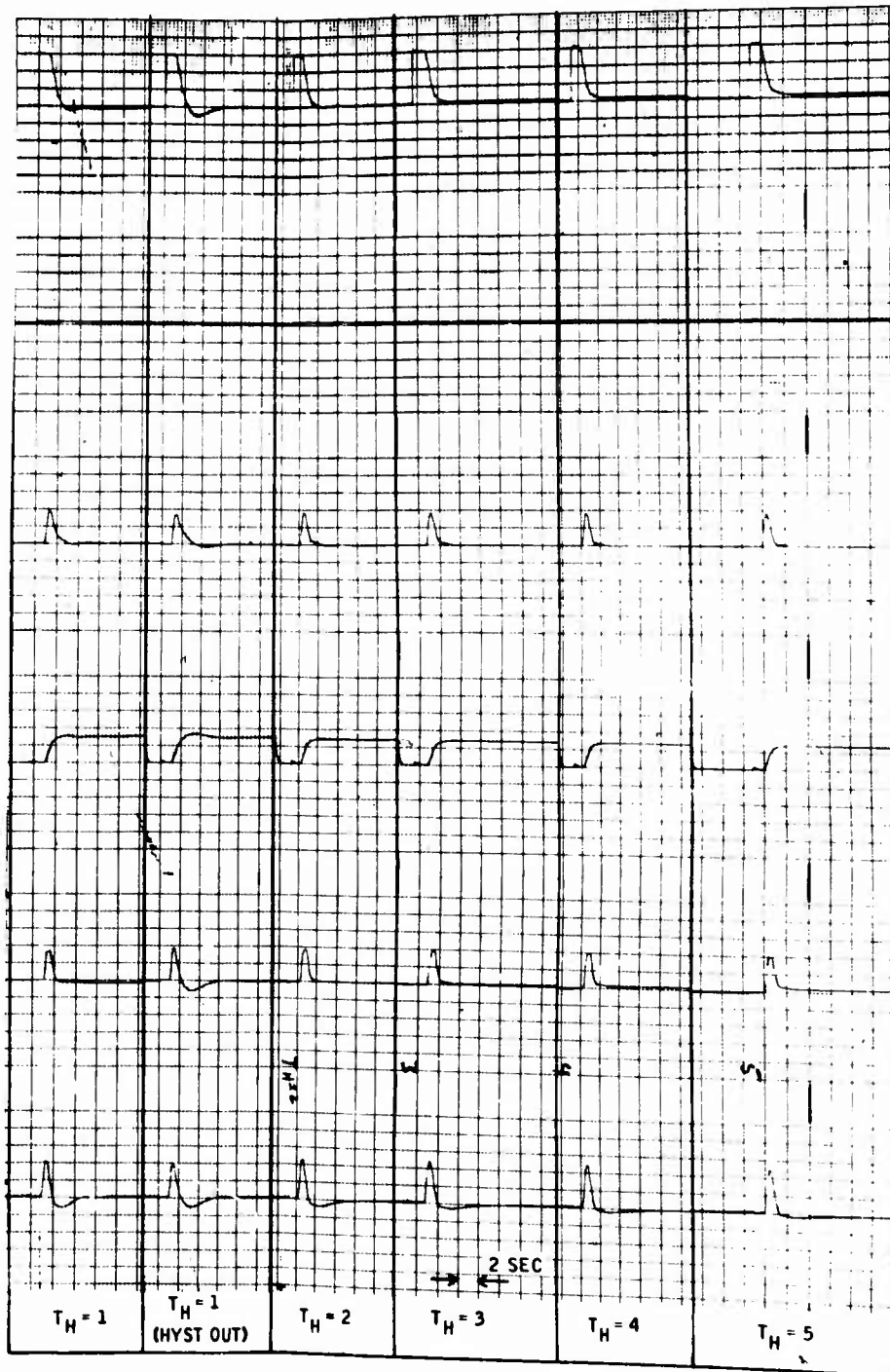
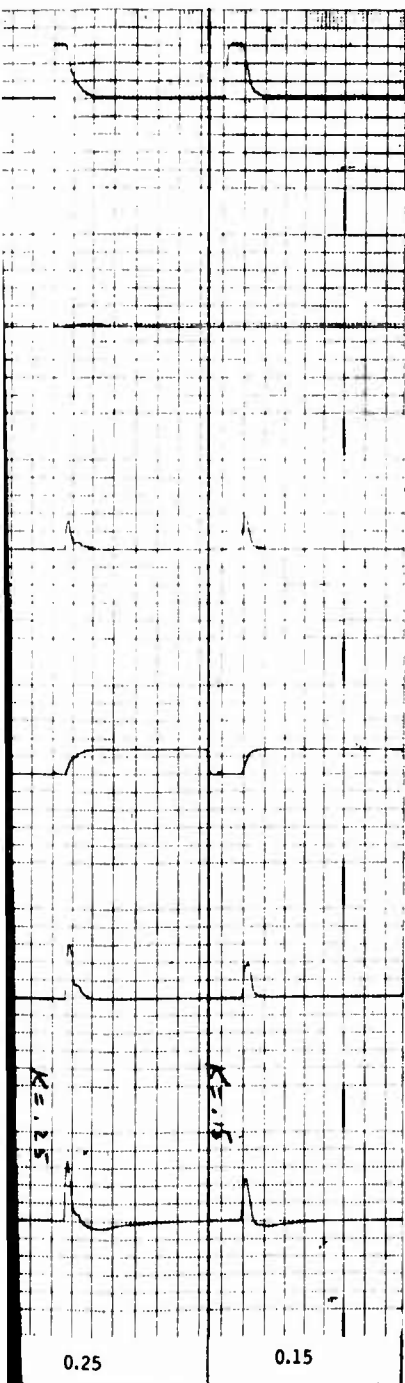
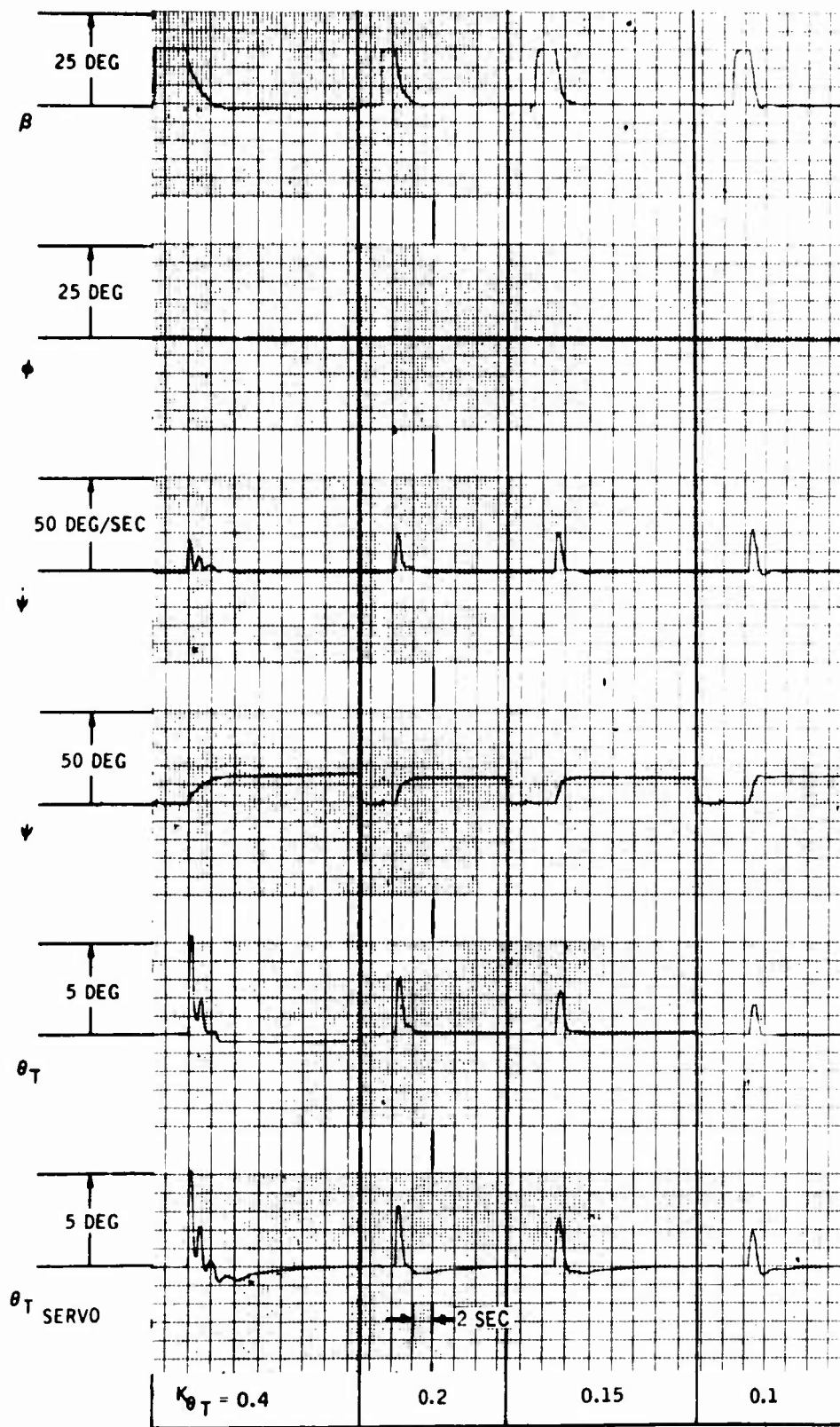


Figure 22. 90 Knots - Par



VARIATION IN HI-PASS TIME CONSTANT

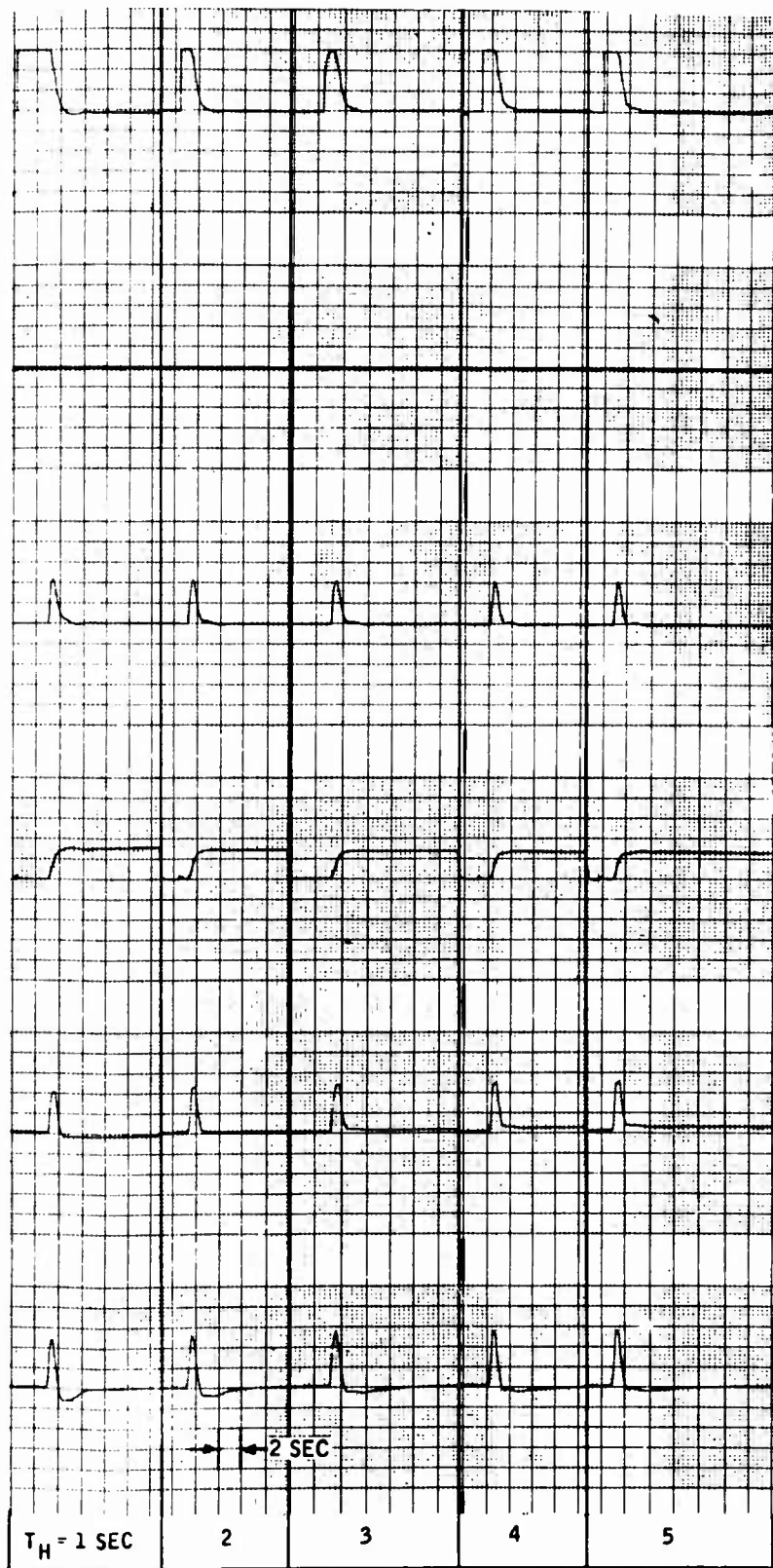
0 Knots - Parametric Study



VARIATION IN TOTAL LOOP GAIN (120 KNOTS)

VA

Figure 23. 120 Knots - Parametric Study



VARIATION IN HI-PASS TIME CONSTANT (120 KNOTS)

Parametric Study

B

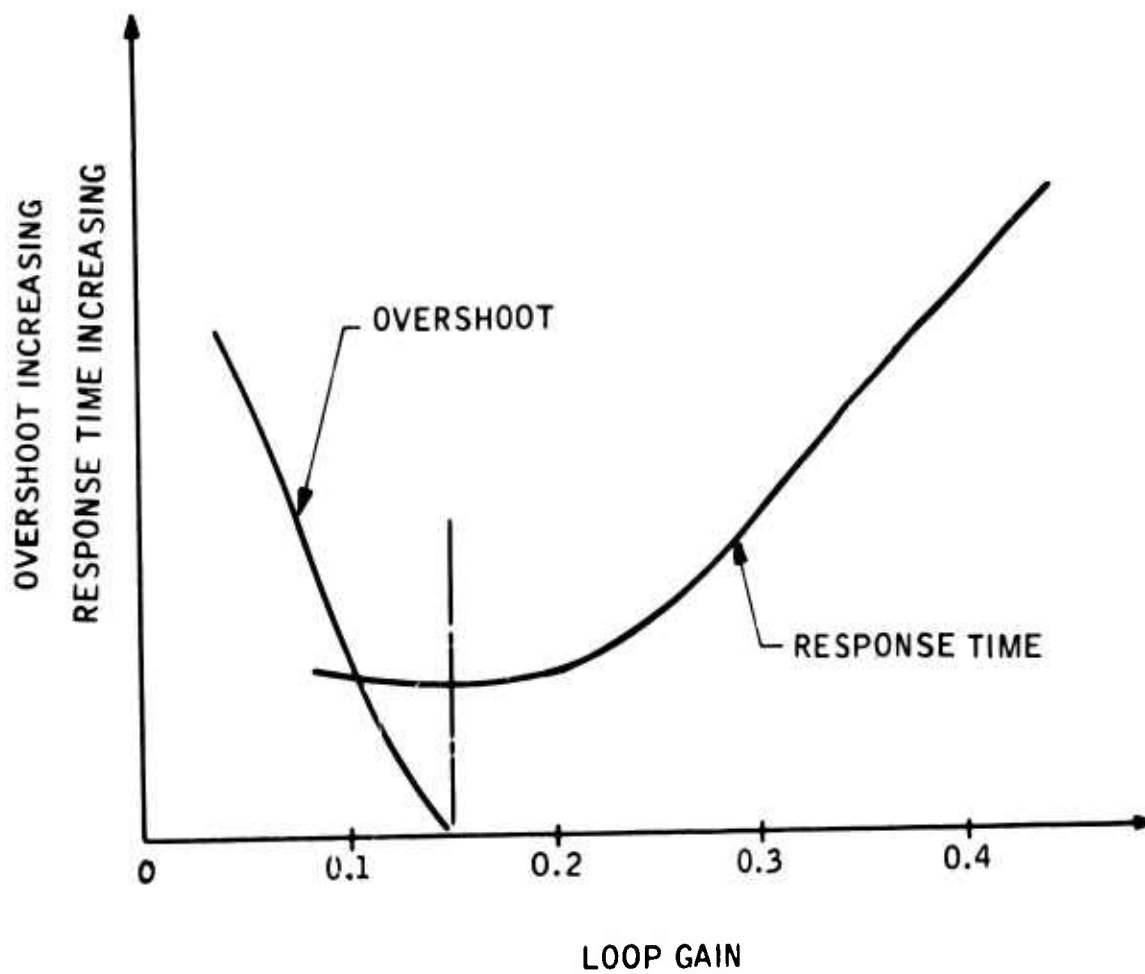


Figure 24. Overshoot and Response Time Qualitative Trend

to give dead-beat response. Because some level of hysteresis will undoubtedly be present, a range of time constant is recommended between 2 and 3.5 seconds, with 3 seconds as nominal. It should be kept in mind that the response of the aircraft to tail rotor inputs in hover is dependent on the hi-pass, with short-period tail rotor effectiveness decreasing with increasing time constant.

Hi-Pass Mechanization

Schematically, the hi-pass is mechanized as shown in Figure 18. With the gains K_{θ_1} and K_{θ_2} both equal to unity, a pure hi-pass results. The general expression for the hi-pass transfer function is:

$$\frac{(K_{\theta_1} - K_{\theta_2}) + K_{\theta_1} T_H S}{1 + T_H S} \quad (1)$$

or

$$K_{\theta_1} \left(\frac{S + \frac{K_{\theta_1} - K_{\theta_2}}{T_H K_{\theta_1}}}{S + \frac{1}{T_H}} \right) \quad (2)$$

Table II shows the variations investigated as being reasonable mechanization deviations.

Note that the positive numerator results when the lagged gain is greater than the straight-through gain. Increasing the hi-pass time constant reduces the magnitude of this right-hand zero.

The analog traces of Figures 25, 26, and 27 show the system response resulting from K_{θ_1} and K_{θ_2} variations, including more extreme deviations than may be expected. Although some difference is noted in response, particularly in response frequency, no deterioration in damping results from variations between K_{θ_1} and K_{θ_2} of up to 20 percent.

Primary Control System Non-Linearities

Except where noted, all the analog traces include a 0.46-degree linkage backlash as shown in Figure 4. The effect of the backlash on tail rotor position can be seen by comparing the servo output ($\theta_{T\text{Servo}}$) with actual rotor position (θ_T).

TABLE II REASONABLE MECHANIZATION DEVIATIONS		
K_{θ_1}	K_{θ_2}	Resultant Transfer Function
1.0	1.1	$0.1 \left(\frac{1 - 30S}{1 + 3S} \right)$ or $1 \left[\frac{(S - 0.033)}{(S + 0.333)} \right]$
1.0	0.9	$0.1 \left(\frac{1 + 30S}{1 + 3S} \right)$ or $1 \left[\frac{(S + 0.333)}{(S + 0.333)} \right]$
1.1	1.0	$0.1 \left(\frac{1 + 33S}{1 + 3S} \right)$ or $1.1 \left[\frac{(S + 0.0303)}{(S + 0.333)} \right]$
0.9	1.0	$0.1 \left(\frac{1 - 27S}{1 + 3S} \right)$ or $0.9 \left[\frac{(S - 0.037)}{(S + 0.333)} \right]$

BLANK PAGE

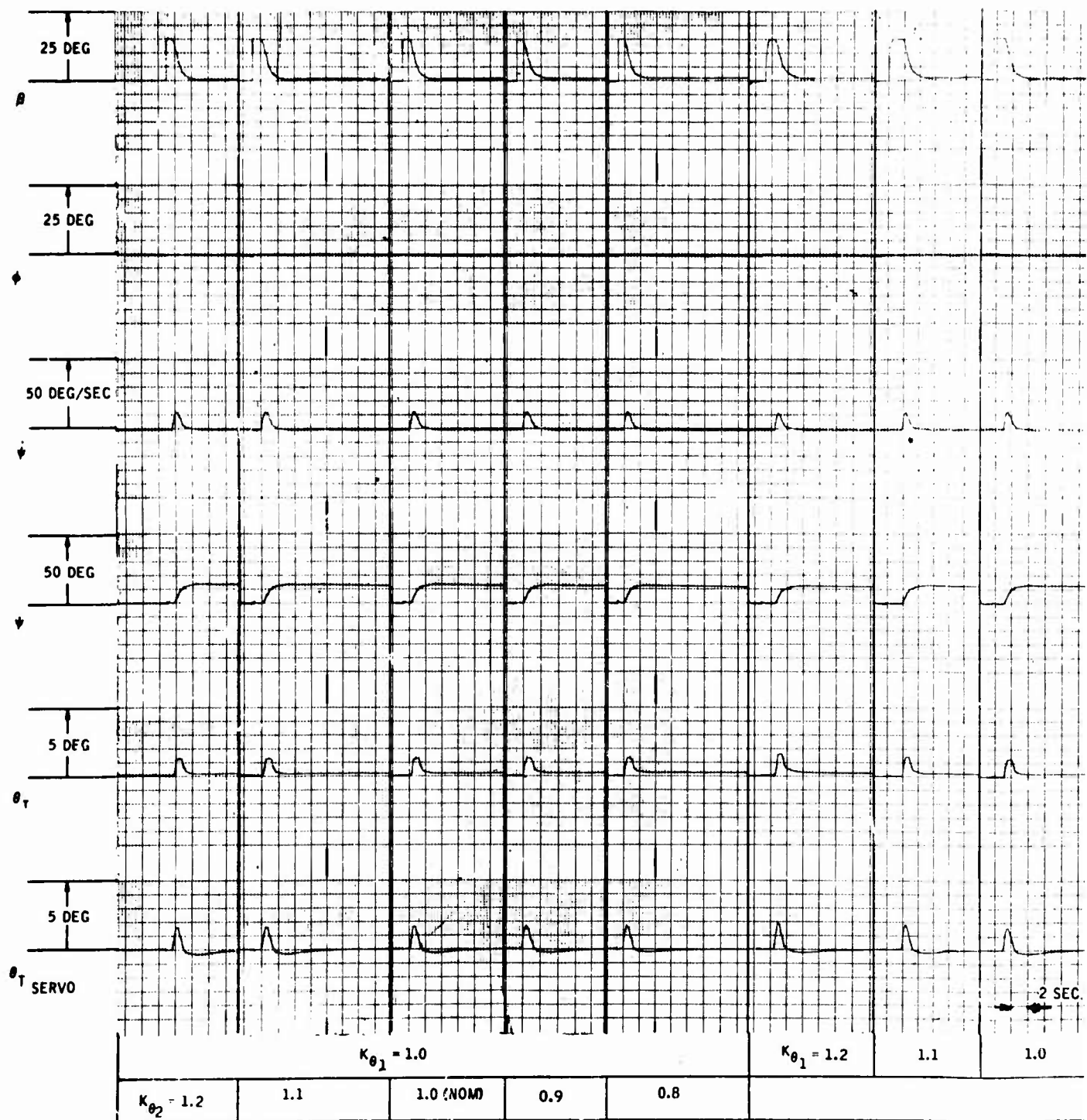
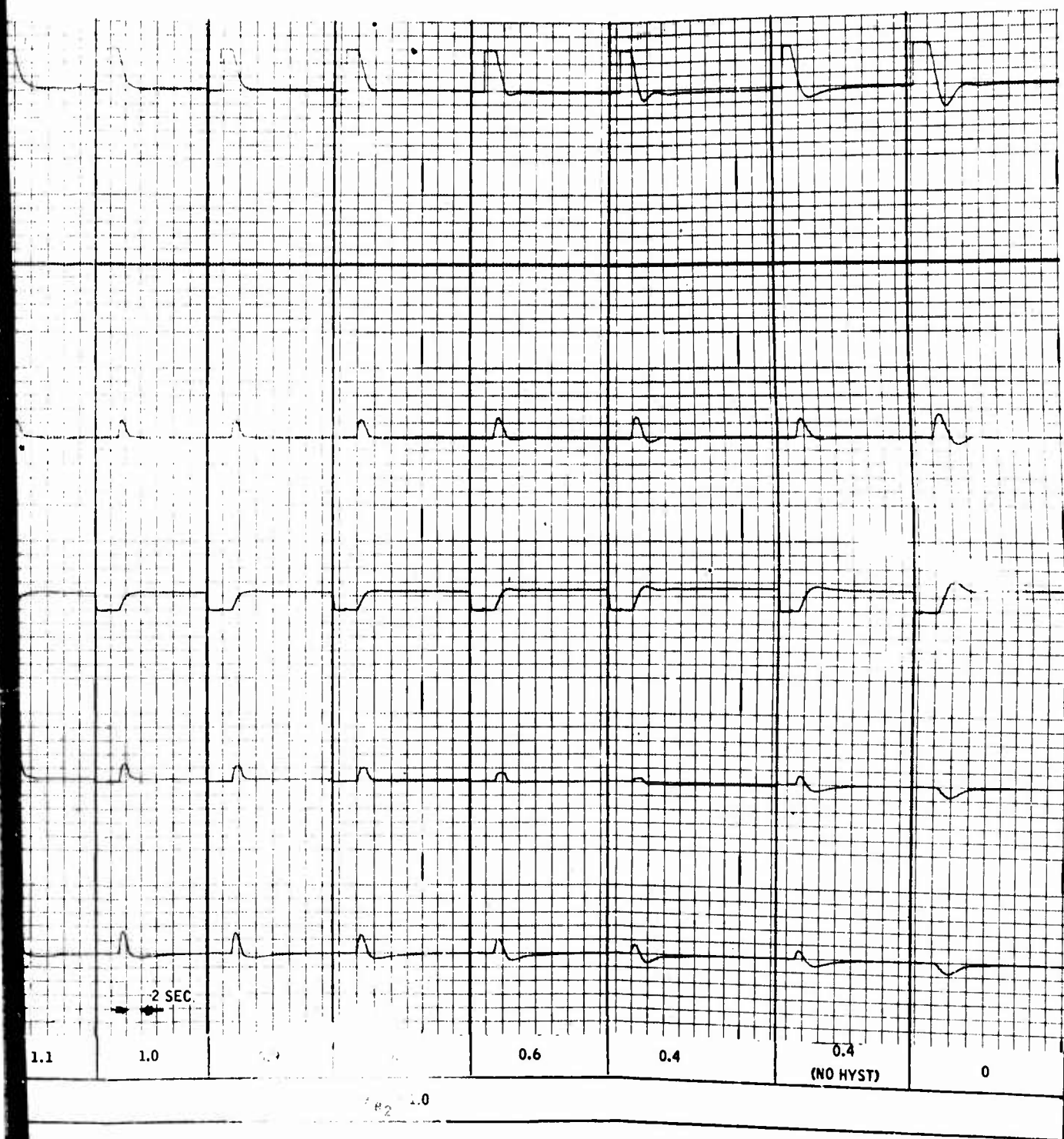


Figure 25. Gain Variation in Hi-Pass

A



tion in Hi-Pass Mechanization (60 Knots)

B

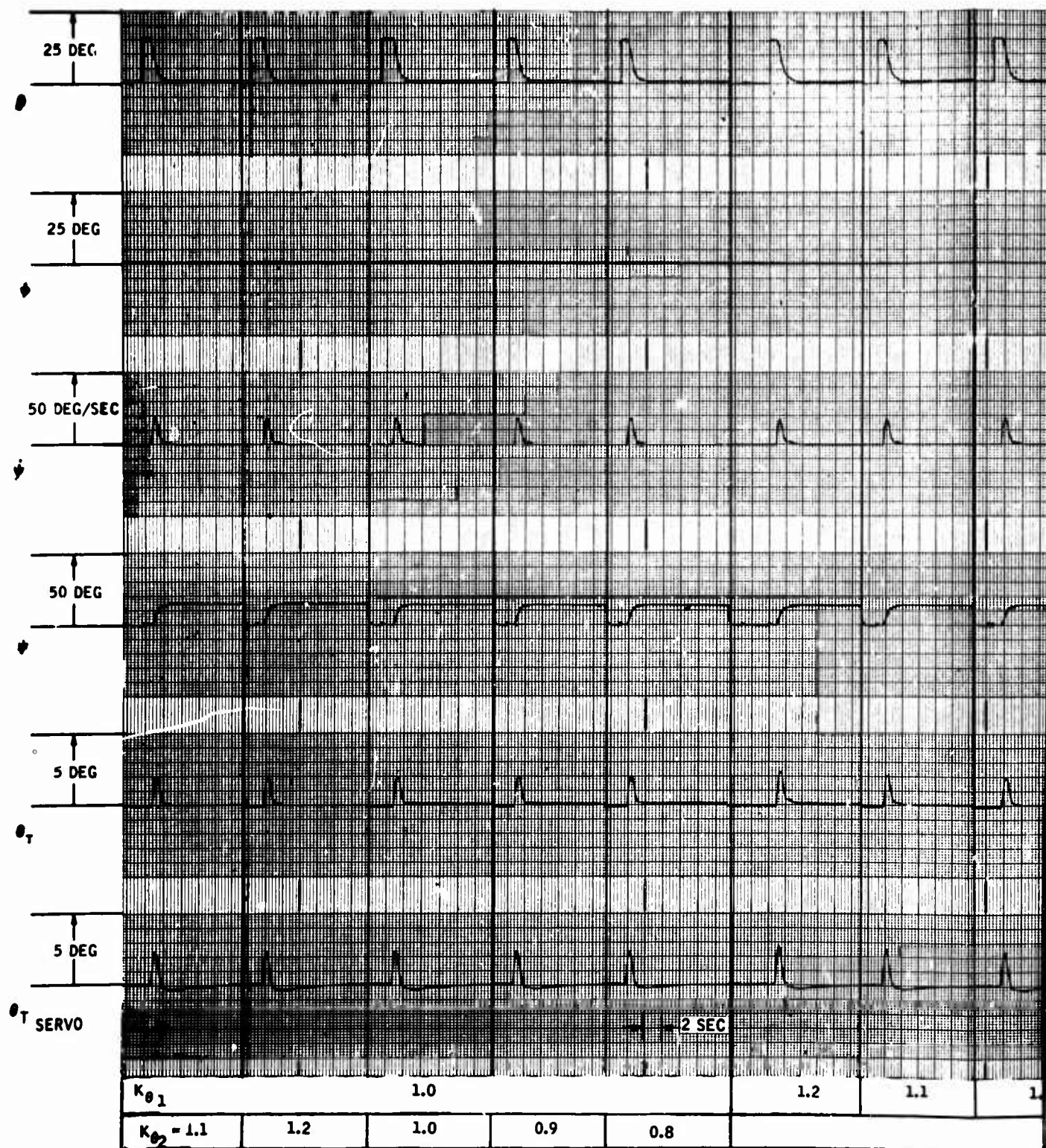
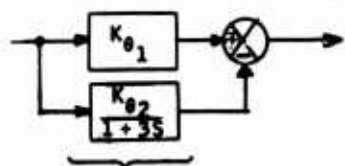


Figure 26. Gain Variation in Hi-Pass Mechaniz



iz ss Mechanization (90 Knots) $\frac{3s}{1+3s}$ (IF $K_{\theta 1} = K_{\theta 2} = 1$)

B

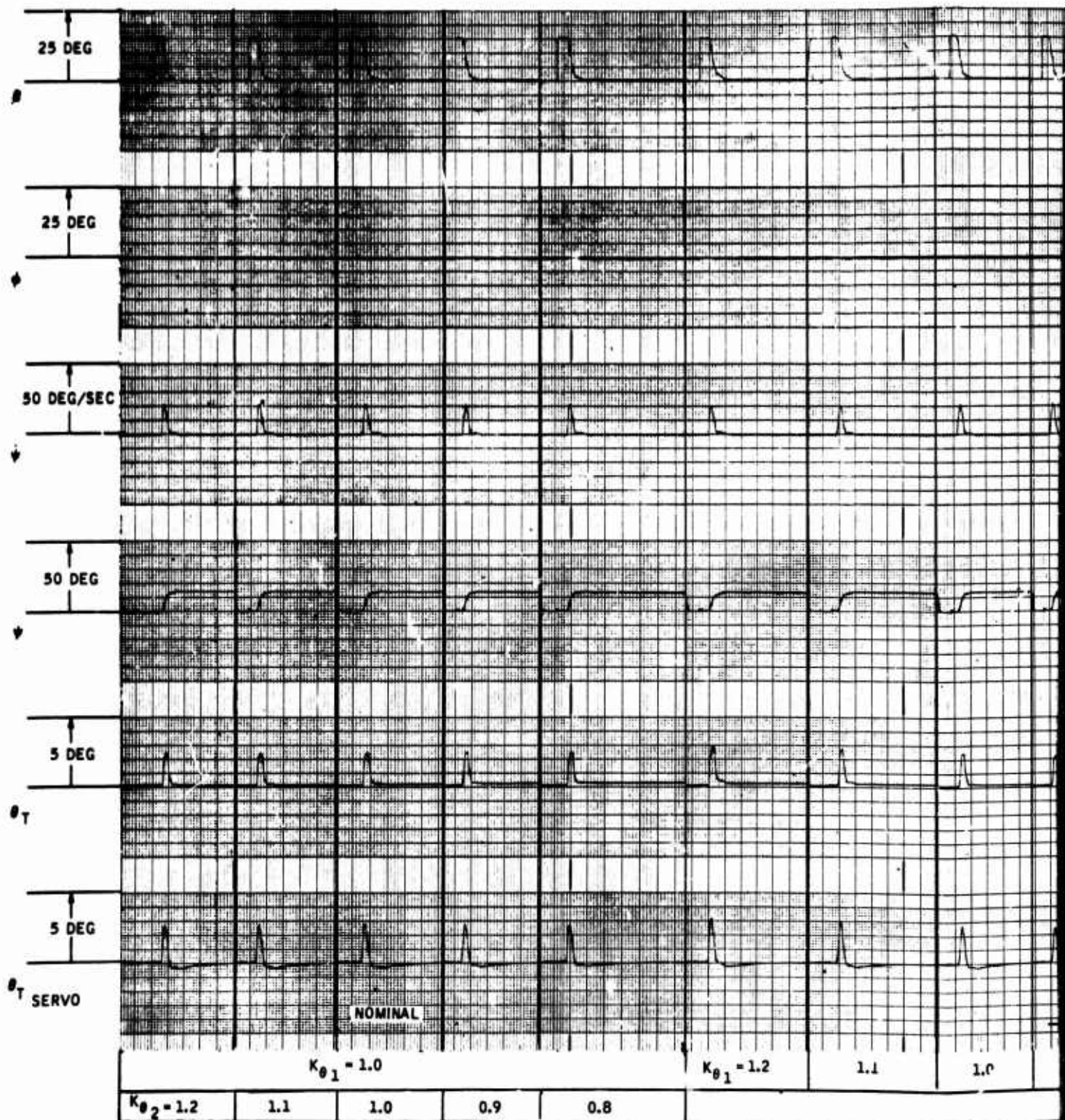
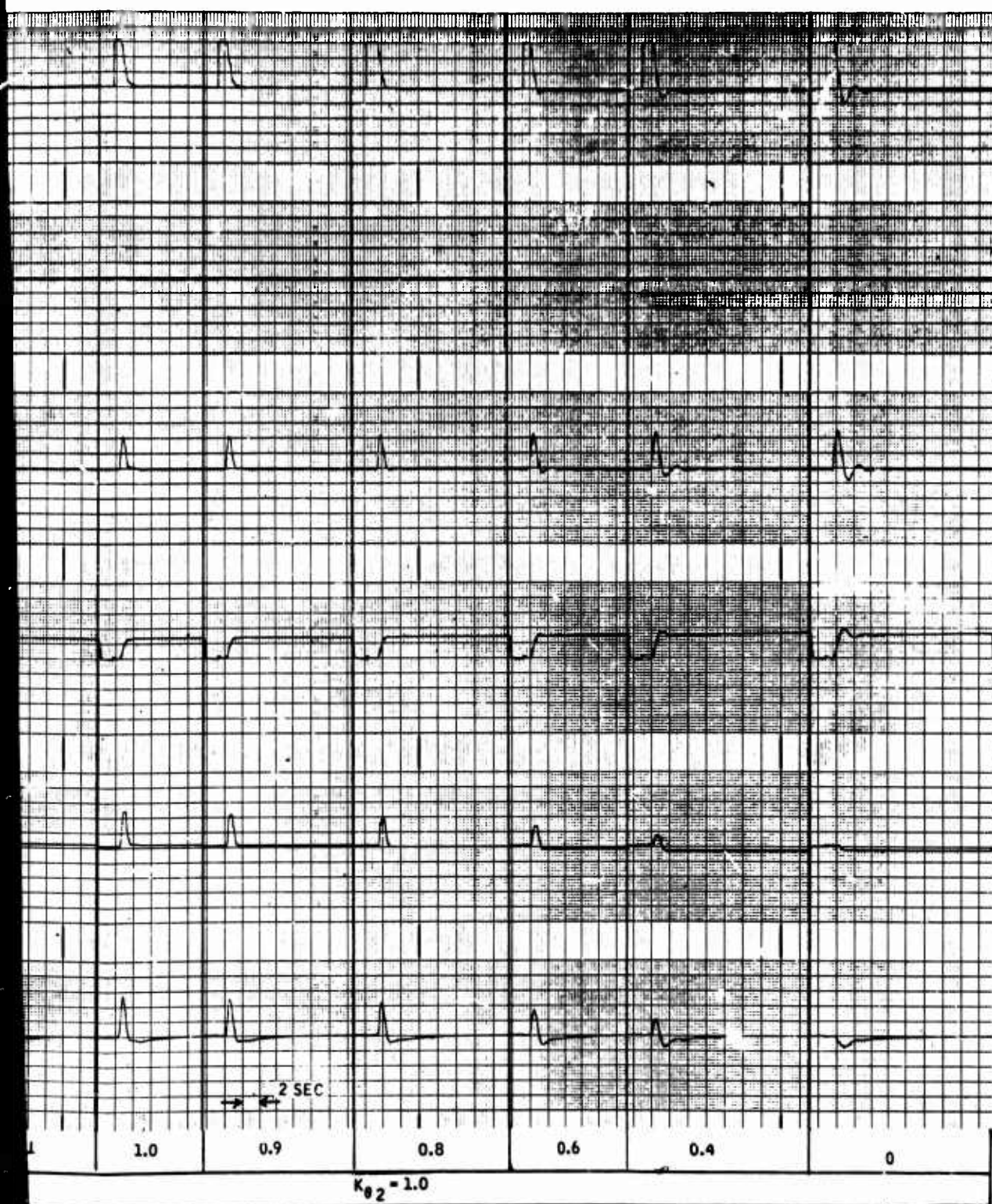


Figure 27. Gain Variation in Hi-Pass Mechanism



Hi-Pass Mechanization (120 Knots)

B

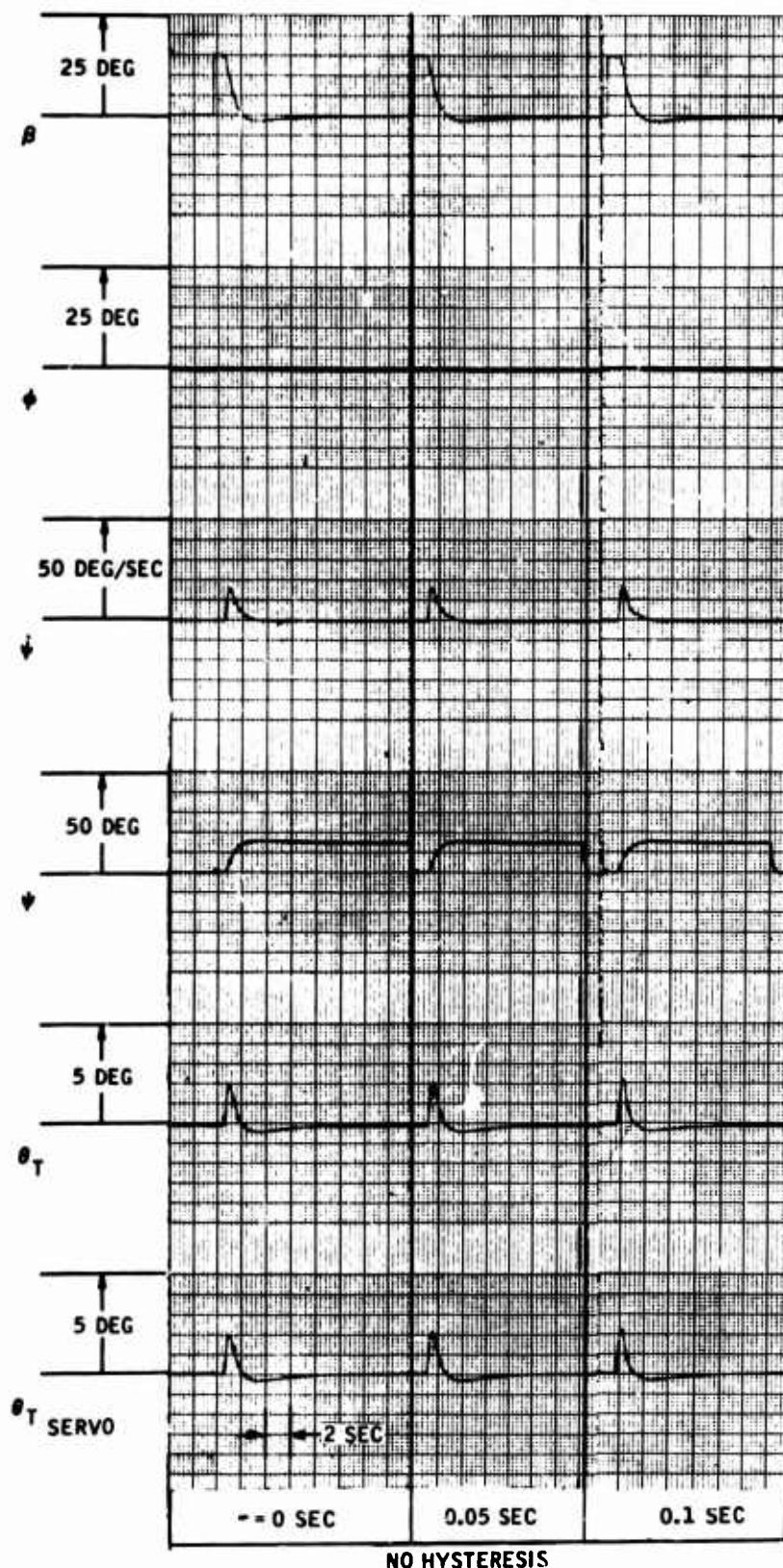
Some difficulties were experienced in simulating the boost element non-linearity as shown in Figure 4. A model of the non-linearity was mechanized on the REAC computer using the analog simulation which successfully duplicated the non-linearity. It was found that for small inputs, on the order of one degree, at a frequency of about one cycle per second, the boost element acts in a manner similar to classical hysteresis. Consequently, the boost element was simulated as a hysteresis, with a magnitude equal to that of the linkage hysteresis. The resulting effect on performance with the two 0.46-degree hysteresis in series is shown in Figure 28.

CONCLUSIONS

The simulated yaw damper configuration has been shown to be strongly tolerant to a wide range of mechanization characteristics and control system non-linearities.

The degree of damping provided by the proposed augmentation is shown to be significant, increasing the free aircraft damping ratio from approximately 0.3 to at least 0.6.

BLANK PAGE



YAW RATE SENSOR TRANSPORT LAG

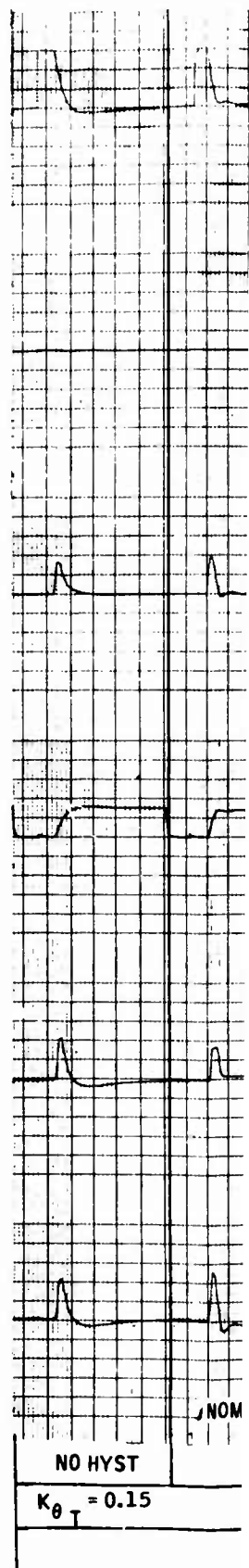
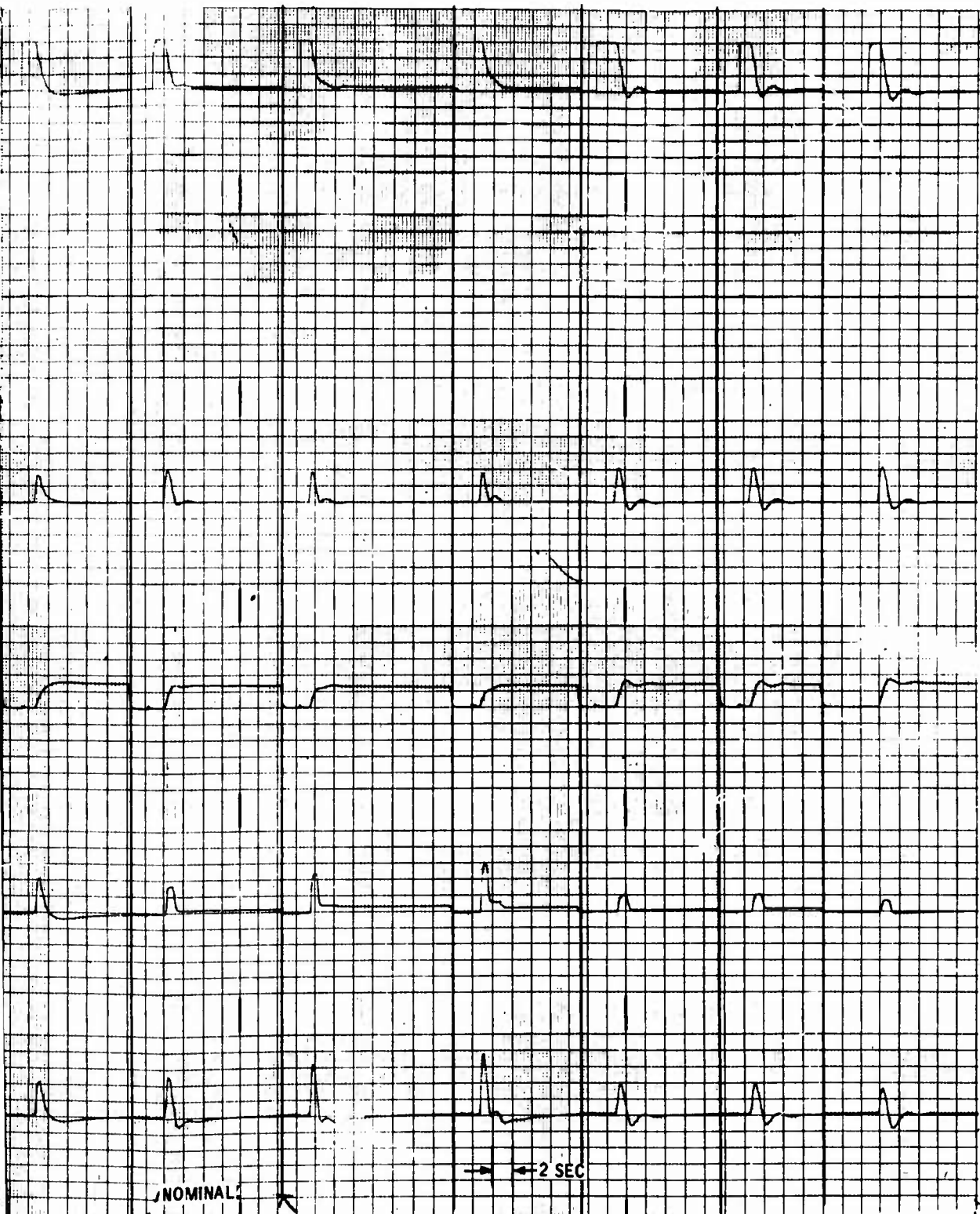


Figure 28. Parametric Variation - Sensor



NO HYST		TWO SERIES 0.46 DEG HYSTERESIS			
$K_{\theta T} = 0.15$		0.2	0.25	0.1	
$T_H = 3$				$T_H = 5$	$T_H = 1$

ation - Sensor Logic, Linkage Hysteresis

B

BLANK PAGE

CHAPTER 3

MECHANIZATION DESIGN

SUMMARY

An all-hydraulic yaw rate damper mechanization was defined based on the results of the system analog simulation, and preliminary component specifications were issued. The rate sensor and fluid amplifier network requirements were reduced to hardware design drawings through use of a mathematical design procedure developed by Honeywell prior to this contract. A servoactuator design was generated by the selected vendor.

DISCUSSION

A system mechanization was selected based on the results of the preliminary system analysis. A schematic of the mechanization is shown in Figure 29. The damper consists of a rate sensor, preamplifier, shaping (hi-pass) network, bias trim control, and servoactuator. The damper is a closed-conduit system in that all fluid amplifier crossover chambers and rate sensor exhaust ports are connected to the return line of the system. This type of system can be operated with the return side of the system supercharged, if desired.

The fluid amplifier (vented, proportional, stream deflection - type 20329) used in the system is a design that was conceived and reduced to practice under a Honeywell independent development program prior to this contract. The salient feature of the amplifier is that the load side (receiver ports) is isolated from the input side (power and control nozzles) such that power can be delivered to the load without affecting the input side operating points. The amplifier performance can be predicted by mathematical means with a reasonable degree of accuracy.

The shaping network consists of a straight-through amplifier cascade with a lagged amplifier cascade parallel in-phase connected at the input and parallel out-of-phase connected at the output. Both cascades have the same gain. The lagged cascade is a low-pass filter with the RC time constant being produced by the hydraulic resistances of the input amplifier receiver ports and the output amplifier control ports in conjunction with parallel connected hydraulic capacitors (metallic bellows).

The shaping network cancels the effect of d-c input signals by subtraction at the output but permits the passage of a-c input signals by attenuating these signals in the low-pass filter section. In this manner,

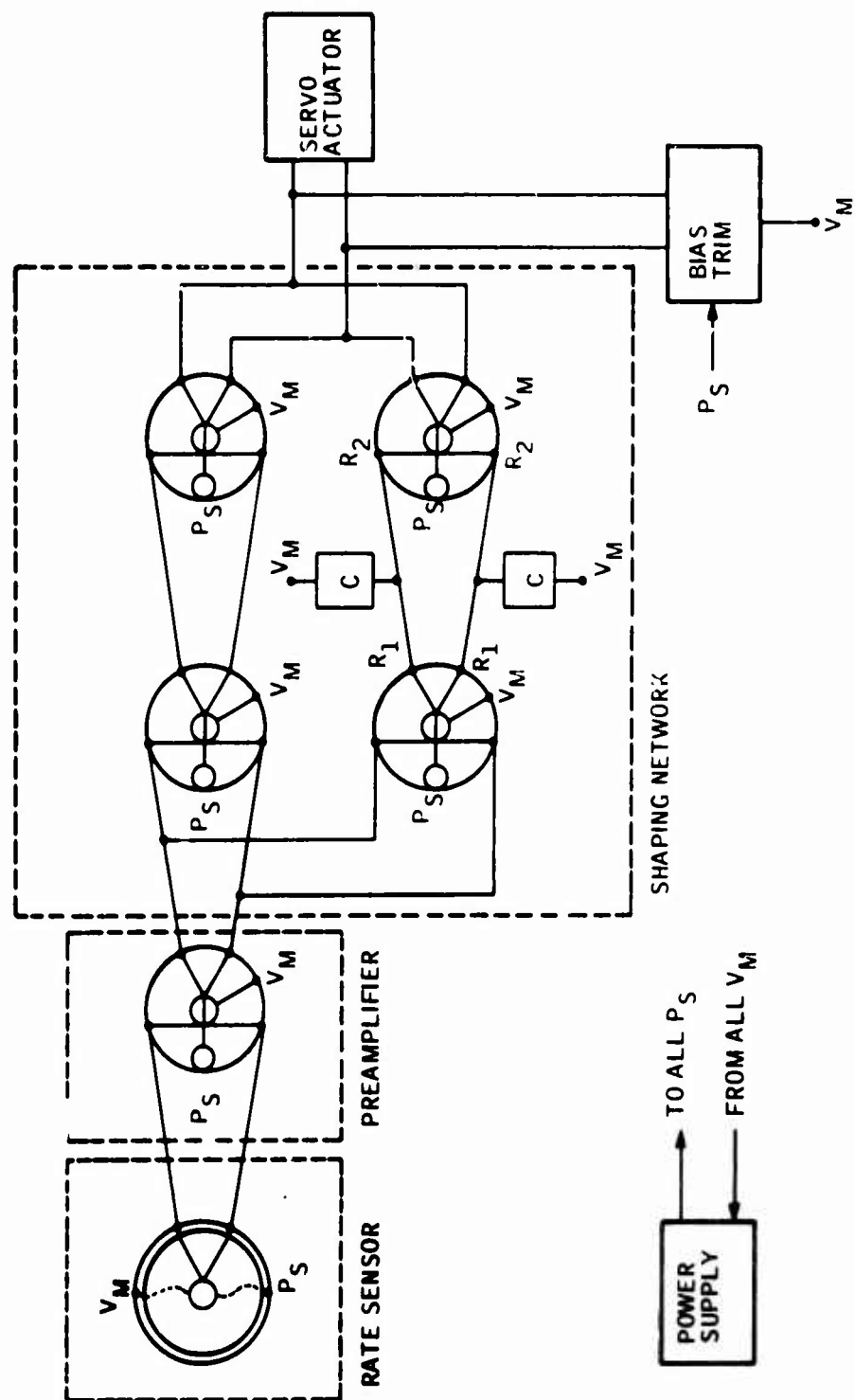


Figure 29. Fluid Schematic - Fluid State Hydraulic Damper

steady-state command signals are washed out and the damper responds to damp out external disturbances.

SYSTEM DESIGN CRITERIA

As a result of the preliminary system analysis, damper system design criteria in the form of a technical development specification were generated. The purpose of this document was to facilitate the design of hardware with the specification serving to set forth developmental design aims. The technical development specification is presented in Appendix I.

RATE SENSOR DESIGN

Starting with the developmental design aims outlined in the technical development specification (Appendix I), an analytical investigation of the important design parameters was made using mathematical models established prior to this contract. This investigation resulted in a preliminary design layout.

Rate Sensor Operation

The vortex rate sensor is a pure fluid device that senses angular velocity about its input axis and provides a fluid signal which is proportional to that velocity. There are no moving parts within the device, and it employs a pattern of fluid flow to sense angular rotation. This pattern of flowing fluid is contained within a cylindrical chamber and is made up of two superimposed flow fields: a "sink" flow field, as shown in Figure 30, where the streamlines are radial and the flow path is straight to the center outlet; superimposed upon that, a rate-imposed tangential flow with a resulting vortex pattern as shown in Figure 30. In the resulting superimposed flow pattern, the streamlines assume a logarithmic spiral as they flow towards the center outlet.

The logarithmic spiral results because of one of the basic principles of motion: the conservation of angular momentum. This principle states that the total angular momentum of a body about an axis remains constant in the absence of restraining forces. As shown in Figure 31, any turning rate about the input axis of the vortex rate sensor imparts a tangential velocity component at the outer ring to the already-present radial component.

The resulting angular momentum is conserved as the fluid is drawn towards the center outlet. Therefore, the component of tangential velocity increases to a maximum at the outlet and is proportional to R_0^2/R_1 , where:

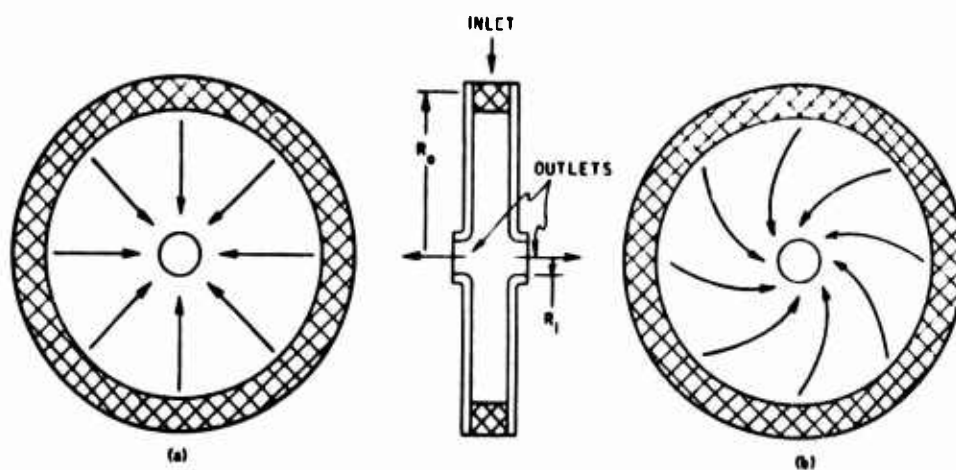


Figure 30. Vortex Rate Sensor Flow Fields

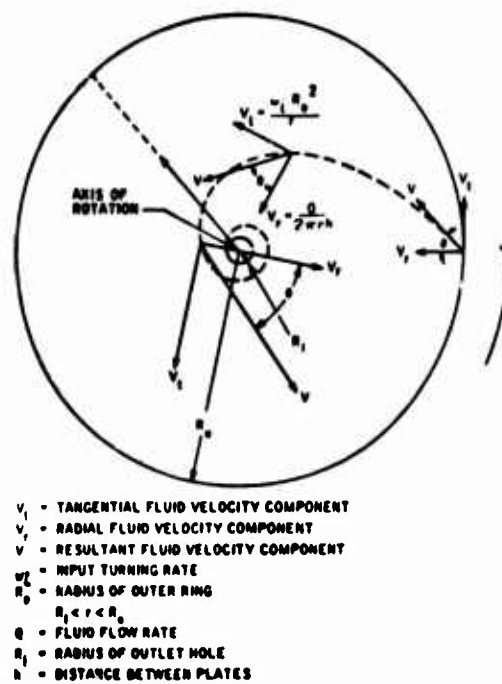


Figure 31. Velocity Components in Vortex Chamber

R_0 = radius of the outer ring

R_1 = radius of the outlet hole

The radial velocity component also increases in proportion to the reciprocal of the radius, resulting in a constant angle (θ) between the final velocity vector and the radial velocity vector. A constant angle is the basis of a logarithmic spiral.

As shown, there is an amplification of the tangential velocity component of the fluid between that imparted at the outer ring and that at the outlet hole. This inherent amplification is utilized by a pickoff which is sensitive only to the tangential velocity component.

The three basic parts of the vortex rate sensor are the coupling element, the vortex chamber, and the signal pickoff. The fluid enters through the inlet, disperses around an annular plenum chamber, and after passing through the coupling element, flows towards and out the center outlets. The coupling element is made of a porous material and imparts any turning motion of the case to the fluid flowing through it. The turning motion imparted to the fluid is amplified as it flows inward towards the outlet, by "free-vortex" action.

The major breakthrough in the development of the vortex rate sensor was the development of a low noise pickoff. The pickoff consists of a thin blade extending across the outlet hole with pressure taps located near its leading edge. The pressure taps sense pressure changes as the fluid flow changes angle of attack with input turning rates. In the absence of case rotation, the fluid flow over the pickoff is at zero angle of attack. However, with input turning rates applied to the case, the stream flows over the pickoff at some angle of attack proportional to the helix angle, the flow angle in the vortex chamber, and the case turning rate.

Initial Design Tradeoffs

In most rate sensor applications, the important performance characteristics are sensitivity, accuracy, and response time. Performance with respect to these characteristics depends upon several parameters, the most important being the dimensions of the vortex chamber and the flow rate through it. A large vortex chamber, a small outlet, and a low flow rate generally result in a larger and more stable vortex motion. This is conducive to a more sensitive and accurate output signal. However, this also results in a slow response, for the response time of the vortex rate sensor is dependent upon the chamber volume and flow rate through it. A sensor with a fast response requires a small chamber volume and a fast flow rate; sensitivity is sacrificed. Because of these two conflicting requirements, a tradeoff is generally necessary between size and power (flow rate) to obtain the best compromise between accuracy and response.

The major criteria for the initial design tradeoffs for the helicopter rate sensor were the following:

- Maximum flow rate of 2.5 GPM of MIL-H-5606
- Phase lag of 90° at 5 cps (corresponds to a 0.050-second response time in the sensor)
- Impedance match sensor output with a 0.025 x 0.025 amplifier orifice
- Maximize scale factor and minimize threshold

Based on these guidelines, the initial design was generated from previously developed mathematical models.

The resulting vortex rate sensor is contained within a 2.875-inch-diameter by a 2.0-inch-long cylinder and weighs about 0.75 pound. The vortex chamber is a 2.0-inch-diameter cylinder 0.08 inch in length. The primary outlet is 0.100 inch in diameter and the pickoff consists of a 0.002-inch-thick blade with two 0.020 x 0.040 pressure taps. The secondary outlet is 0.125 inch in diameter. The sensor was designed to operate on 2.5 gallons per minute of MIL-H-5606 hydraulic oil at a differential pressure of 20 pounds per square inch at nominal conditions. The scale factor when driving the pre-amplifier was predicted to be approximately 0.003 psid/deg/sec.

SERVOACTUATOR DESIGN

The servoactuator design requirements as outlined in the technical development specification (Appendix I) were forwarded to the selected vendor (Hydraulic Research and Manufacturing Company). The servoactuator supplied is a modification of a unit employed for an earlier directional augmentation system for the UH-1B helicopter. The modification included the conversion of the electrically-operated torque motor to a fluid-operated force motor, and the lockout spring centering feature of the actuator main piston was replaced with a positive pressure-operated mechanical-locking device.

FLUID AMPLIFIER NETWORK DESIGN

The fluid amplifier network design was accomplished using a mathematical design procedure established prior to this contract. Past experience has shown reasonable agreement between predicted results

and actual results for nominal operating conditions. The mathematical design procedure has not been refined to a sufficient degree to predict performance accurately during environmental conditions such as substantial fluid temperature variation. This is mainly due to the absence of sufficient experimental data to include these effects.

The design of the fluid amplifier network was undertaken with the following criteria established by the preliminary system analysis and the technical development specification (Appendix I):

- Based on the nominal loop gain requirement of 0.10 deg/deg/sec from the preliminary analog simulation and the anticipated rate sensor and servoactuator gains, the fluid amplifier cascade d-c gain (shorted hi-pass) should be 25 psi/psi or greater.
- The hi-pass network time constant should be in the range of 2 to 3 seconds.
- Null static pressure at the servoactuator force capsules should be 4 psig above return pressure to provide a linear output range of at least double that required at the servoactuator input.
- Based on previous experience, the amplifier power nozzle supply differential pressure should be 10 psid or greater to minimize gain variations with supply pressure change.
- Past experience indicates that fluid amplifier power or control nozzle areas should not be less than 6.25×10^{-4} square inches from a reliability standpoint.
- Total network power flow rate held to a minimum consistent with reliable amplifier performance.

From a configuration standpoint, a modular type fluid amplifier construction was selected to facilitate individual component changes, if the need arose. The rate sensor was also to be manifolded to the fluid amplifier network. The bellows-type fluid capacitors were to be external to the fluid amplifier network.

The fluid amplifier functional dimensions governing gain, range, static output pressures, and power flow rates were calculated. The hi-pass network fluidic resistance and capacitance values to provide the proper shaping were calculated. Fluid amplifier transport lags, as well as the additional system lag due to dynamic operation of the servoactuator force capsules from a fluid amplifier, were also computed.

TRIM CONTROL

The bias trim control is basically a hydraulic bridge circuit which provides a differential output pressure in proportion to the displacement of the input member.

Since the fluidic system is a low-impedance type of circuit, the design of the trim control must be carefully considered so that its insertion into the control system will not result in unwanted dynamic effects. The actual location of the device in the aircraft with the associated line lengths can have a significant effect on response rates and determination of the required hydraulic resistance values. For these basic reasons, trim control will be simulated by a hydraulic valve bridge circuit, where necessary. The procurement of a special trim control will be deferred until the system development reaches flight test status.

CONCLUSIONS

The system components, as defined from the Honeywell fluidic system mathematical design procedure, should meet the system performance as outlined in the technical development specification (Appendix I). It is further concluded that the major divergence between actual performance and predicted performance may occur at environmental condition extremes since the precise effects of these conditions are, at present, not included in the mathematical design procedure.

CHAPTER 4

COMPONENT TEST RESULTS

This section contains all results from component testing conducted during the program. The components are the rate sensor, fluid amplifiers shaping network, and servoactuator. Each area of work is discussed separately.

RATE SENSOR

SUMMARY

The rate sensor was tested in its original configuration (not manifolded to preamplifier) and in the manifolded to the preamplifier configuration. Test results were in close agreement with design goals. The transport time measurement indicates that the sensor dynamic response will be satisfactory for system use.

DISCUSSION

Configuration

A photograph of the rate sensor is shown in Figure 32.

Test Results

The initial testing was done on a rate table setup using orifices to simulate the anticipated preamplifier load. A block diagram of the setup is shown in Figure 33. Due to the rotating joint and plumbing arrangement, the rate sensor ambient pressures were significantly in excess of those to be encountered in the aircraft. Since this was the case, the sensor was retested using a tilt table which permitted a plumbing arrangement more nearly like that to be encountered in the aircraft.

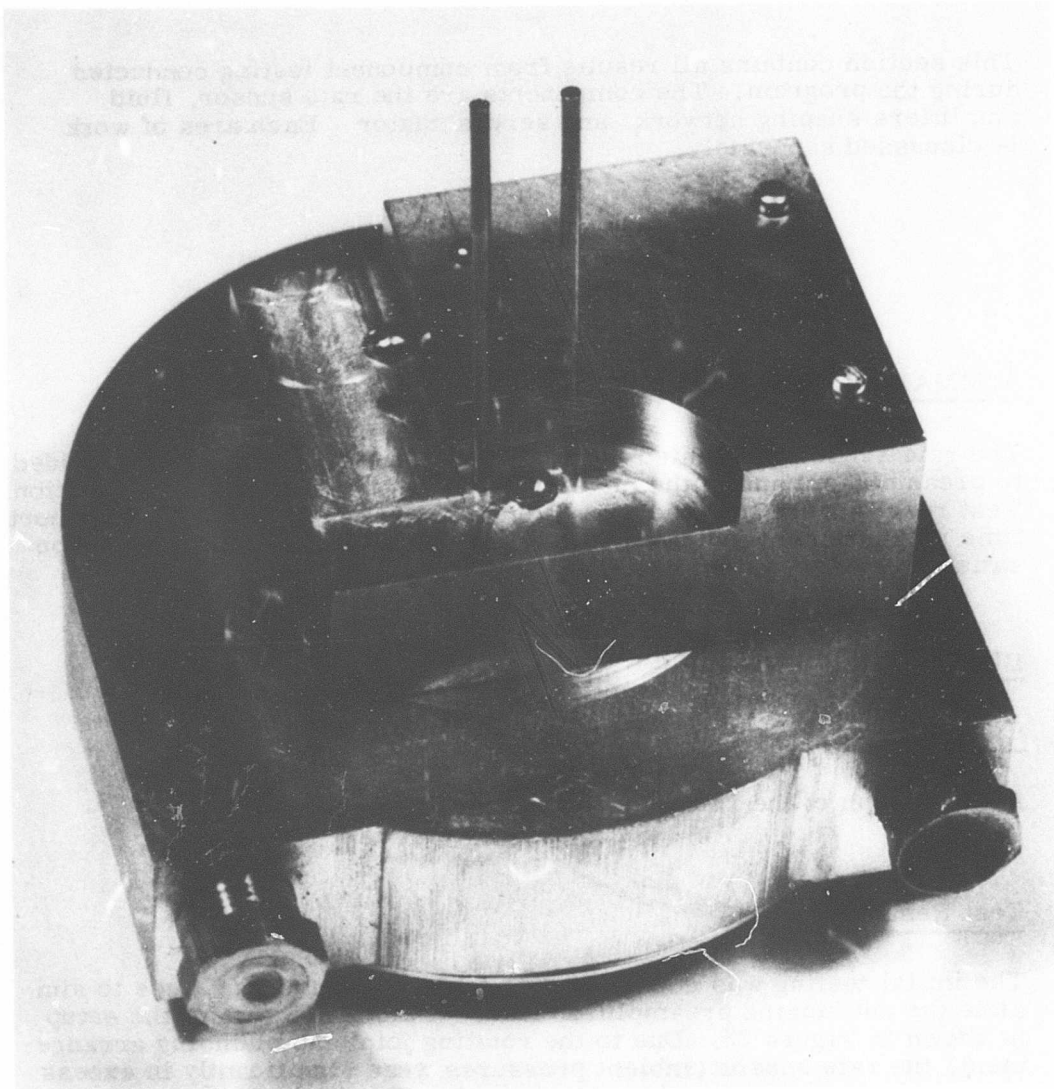


Figure 32. Vortex Rate Sensor

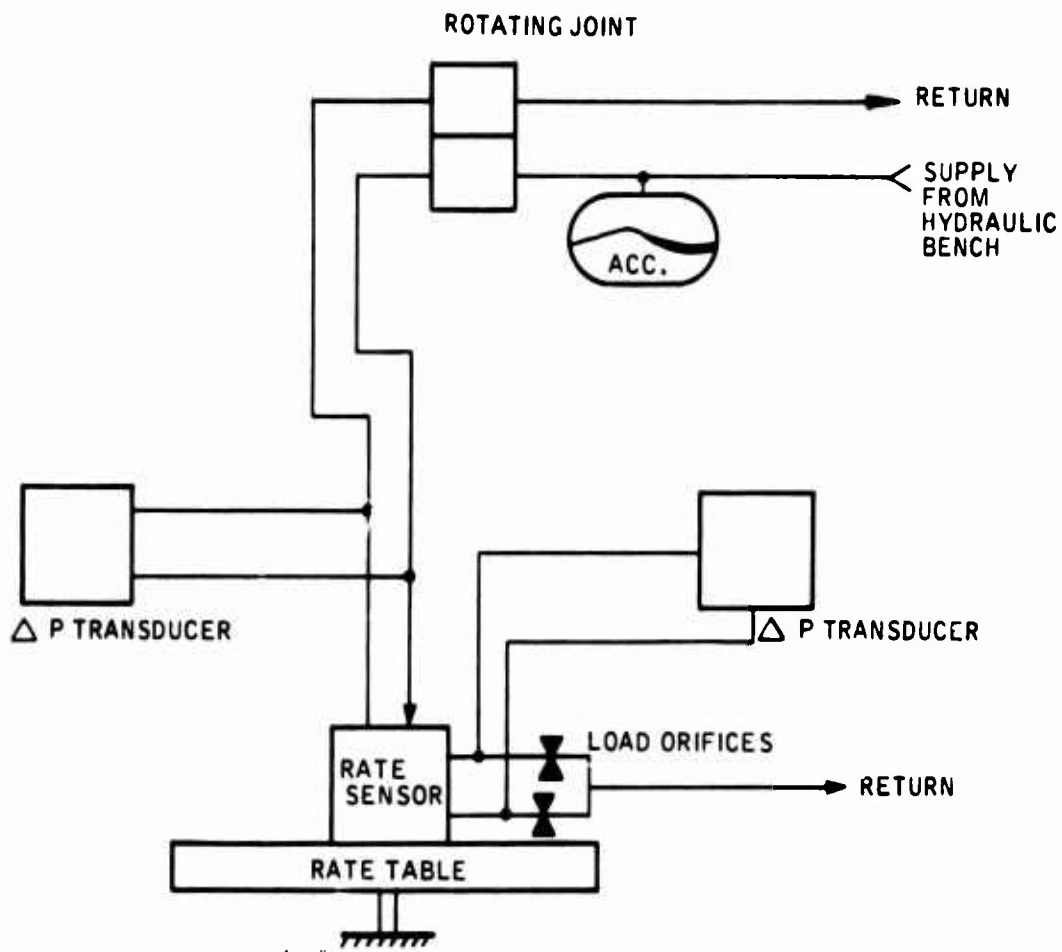


Figure 33. Rate Table Test Setup

The tilt table setup block diagram is shown in Figure 34. Since the rate sensor was manifolded directly to the preamplifier, no connection was available to obtain sensor pickoff output directly. The preamplifier was tested with a deadhead load (ΔP transducer) and the pressure gain was measured. During this test the sensor output was amplified by the preamplifier and readout on the differential pressure transducer. This output was divided by the known preamplifier gain to obtain the output at the sensor pickoff ports. A comparison of the test results obtained from the two test methods and the pertinent design goals is shown in Table III. It is seen that in most cases the measured performance was in close agreement with the design goals.

A plot of the rate sensor scale factor is shown in Figure 35.

CONCLUSIONS

The rate sensor measured performance was in close agreement with the design goals. The transport time measurement indicates that the sensor dynamic response is satisfactory for system use.

FLUID AMPLIFIERS

SUMMARY

The fluid amplifiers fabricated in accordance with the design criteria generated during the preliminary design phase were tested as individual devices and as cascades. Test results were in close agreement with design goals. Test results also verified that the mathematical design procedure was valid for preliminary design purposes. "Built-in" null bias was found to be a problem area which was considered to be a function of the manufacturing process.

The fluid amplifiers were considered satisfactory for use in the system.

DISCUSSION

Design and Fabrication

Fluid amplifier cascades were fabricated from aluminum alloy blocks with power nozzle, control nozzle and receiver port configuration being cut with an engraving machine. 10x size metal templates of the required detail configurations were used. This method permitted fabrication of

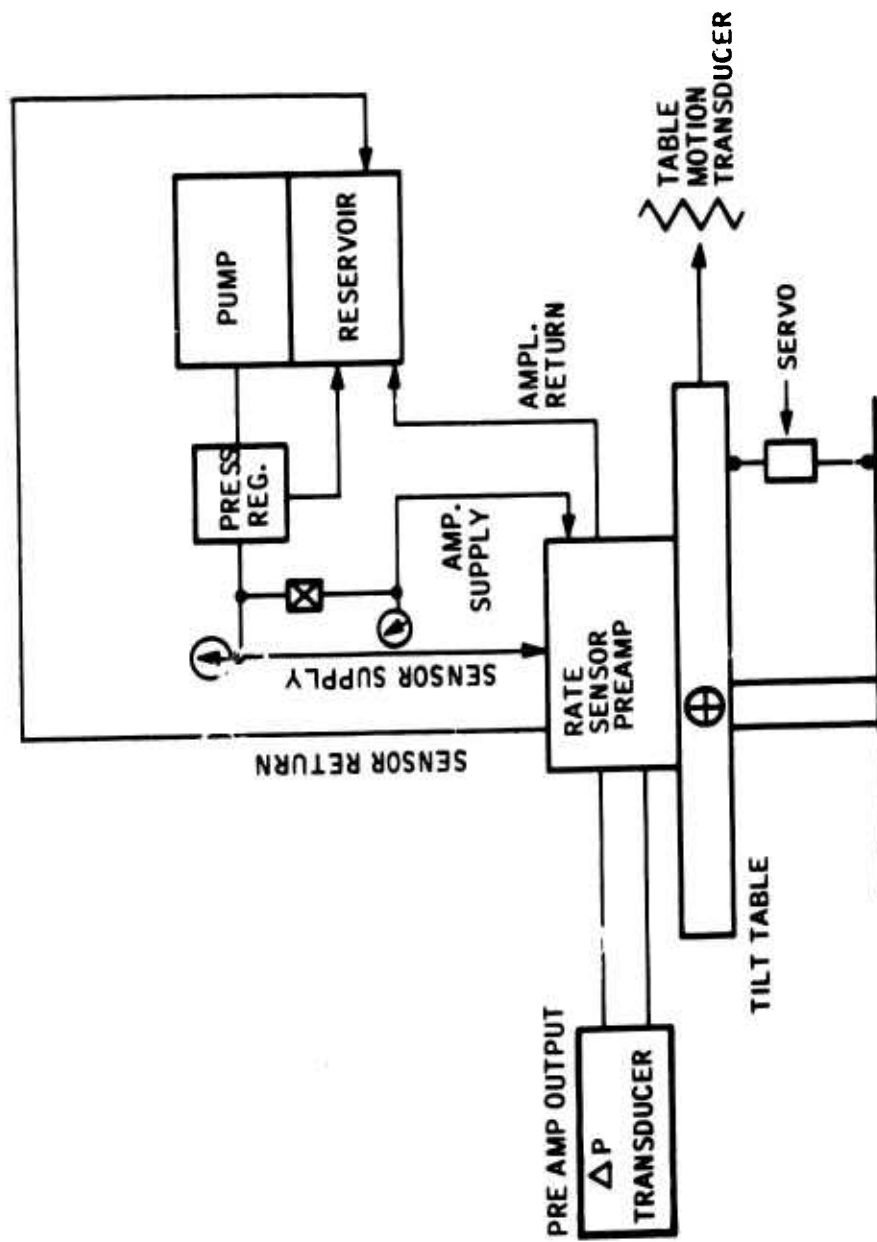


Figure 34. Tilt Table Test Setup

TABLE III RATE SENSOR TEST RESULTS TABULATION			
Parameter	Design Goal	Rate Table Test - Simulated Load	Tilt Table Test - Preamp. Load
Scale factor at 2 gpm pick- off sink flow rate	≥ 0.003 psi/°/sec	0.0053 psi/°/sec with 0.0225 dia orifices	0.00318 psi/°/sec with 0.0250 square nozzles 0.0375 long
Linearity	5 % of full scale	4.7% of full scale	6.1% of full scale (includes preamp.)
Range	$\pm 60^\circ/\text{sec}$	$\pm 60^\circ/\text{sec}$	$\pm 42.5^\circ/\text{sec}$ (maximum rate of tilt table)
Transport time at 2 gpm pickoff sink flow rate	50 milliseconds	Not measured	37.5 - 50 milliseconds
Noise	Not specified - design aim was 0.10°/sec	~ 0.5 to $0.8^\circ/\text{sec}$	$\sim 0.9^\circ/\text{sec}$ (includes preamp)
Supply pressure differential for 2 gpm flow	20 psi	35 psi	29 psi
Null shift with supply pressure differential	0.6°/sec/psi	$\sim 0.50^\circ/\text{sec/psi}$	$\sim 0.40^\circ/\text{sec/psi}$
*Difficult to measure precisely due to non-linearities in tilt table linkage and differential pressure transducer dynamics.			

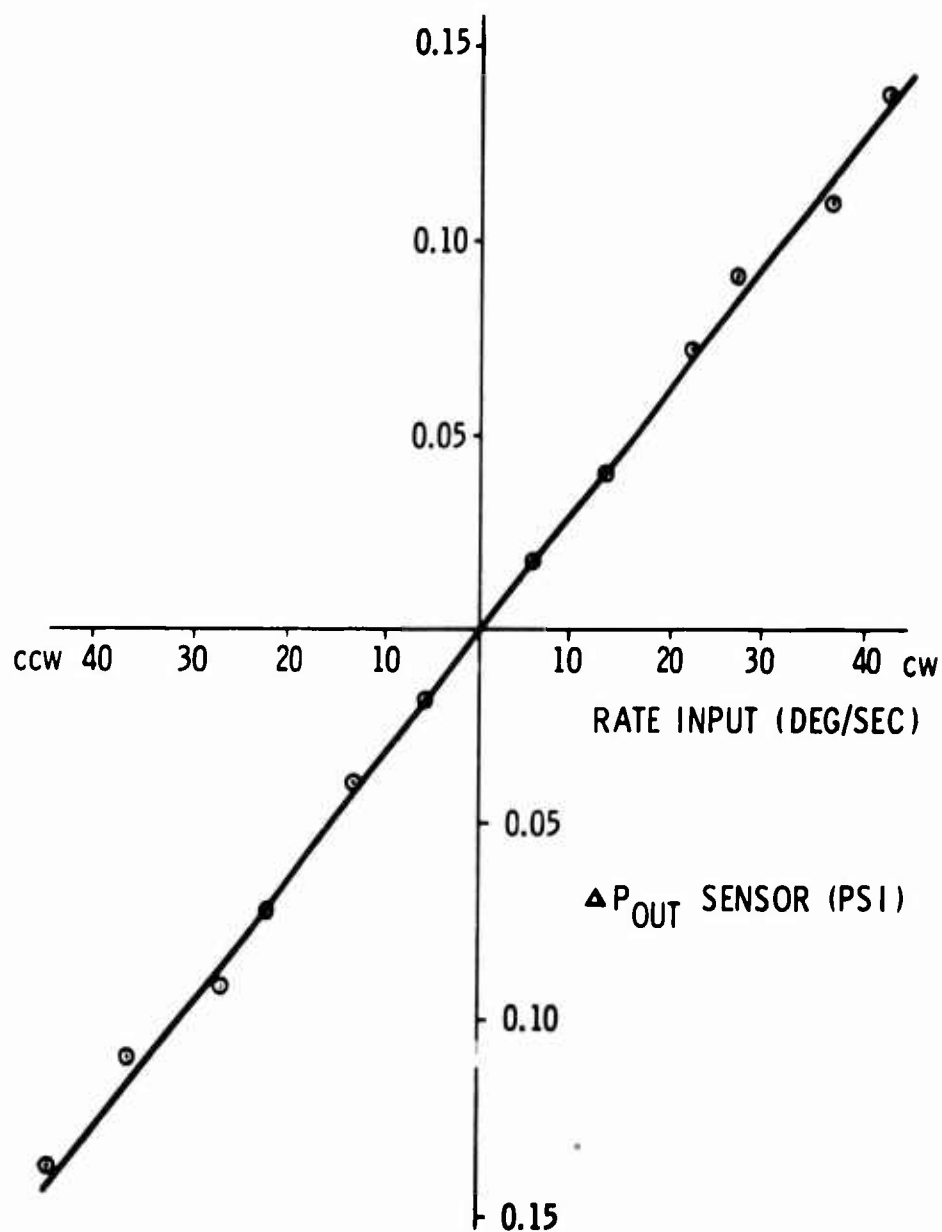


Figure 35. Rate Sensor Scale Factor

developmental amplifier pairs identical in detail except for machine variables and cutting tool flexure variations. Based on an evaluation of test results on the amplifiers made to date, the only significant variable has been "null bias" as a percent of full signal. This variation was attributed to cutting tool flexure when the initial cut was made to form the splitter and receiver detail. Since the probability of cutting tool flexure is related to the tool size, the excessive "built-in" null bias has been encountered primarily in the smallest size amplifiers (preamplifier and shaping input amplifier). Although excessive "built-in" null bias can be taken out by injecting bias adjust signals, it is felt that bias adjust signal should be held to one signal injection point for a three-stage cascade. In general, the amplifier fabrication technique has been quite successful, insofar as development hardware is concerned. Manufacturability studies could result in techniques to minimize "built-in" null bias.

Test Results

The fluid amplifier steady-state gain tests were conducted on the fluid amplifiers connected in cascade in order to have each component loaded properly. The differential pressure input to the cascade was varied and the differential pressure output was measured at the various stages. Figure 36 shows a schematic of the test setup.

All fluid amplifiers were operated with 11.4 psig supply pressure, with all crossover chamber return lines tied together and exhausting to atmosphere. The fluid temperature was $100^{\circ}\text{F} \pm 10^{\circ}\text{F}$.

Table IV shows a tabulation of amplifier measured performance as compared to the design goals. It is seen that the measured results generally met or exceeded the design goals. Figures 37, 38, 39, 40, and 41 are point-to-point plots showing amplifier performance.

A second set of shaping input amplifier blocks was fabricated to see if the difference in null bias could be eliminated. These amplifiers were tested in a cascade, and it was concluded that their gain was the same as the other shaping input amplifiers. It was also concluded from the cascade gain plots that both amplifiers had their "built-in" null bias in the same direction and that they were approximately 5 percent to 7 percent of full signal. This larger than expected null bias was attributed to the tool flexure situation previously discussed.

Figures 42 and 43 show point-to-point plots of the cascade performance. The difference in null bias of the cascades may have to be adjusted out with an external signal when used in the damper system.


$$ALL P_S = 11.4 \text{ psig}$$

**ALL V_M 'S TIED TOGETHER EXHAUSTING
TO ATMOSPHERE**

Figure 36. Fluid Amplifier Test Setup

**TABLE IV
AMPLIFIER TEST RESULTS TABULATION**

Amplifier Stage	Parameter	Design Goal	Measured Result
Preamplifier ($P_s = 11.4$ psig)	Gain	≥ 2.18 psi/psi	2.35 psi/psi
	Linear Range	± 0.030 psid	+ 2.0 - 2.5 psid
	Saturation	≥ 2.50 psid	+ 2.2 - 2.7 psid
	Null Bias	$\leq 5\%$ of full output	2% of full output
Shaping Input Amplifier No. 1 ($P_s = 11.4$ psig)	Gain	≥ 2.00 psi/psi	2.35 psi/psi
	Linear Range	± 0.50 psid	± 2.0 psid
	Saturation	≥ 2.50 psid	+ 3.0 - 2.8 psid
	Null Bias	$\leq 5\%$ of full output	10% of full output
Shaping Input Amplifier No. 2 ($P_s = 11.4$ psig)	Gain	≥ 2.00 psi/psi	2.35 psi/psi
	Linear Range	± 0.50 psid	+ 2.0 - 1.5 psid
	Saturation	≥ 2.50 psid	+ 2.7 - 3.0 psid
	Null Bias	$\leq 5\%$ of full output	2% of full output
Shaping Output Amplifier No. 1 ($P_s = 11.4$ psig)	Gain	≥ 8.25 psi/psi	8.2 psi/psi
	Linear Range	± 2.0 psid	+ 6 - 5 psid
	Saturation	± 7 psid	+ 8.1 - 7.2 psid
	Null Bias	$\leq 5\%$ of full output	0% of full output
Shaping Output Amplifier No. 2 ($P_s = 11.4$ psig)	Gain	≥ 8.25 psi/psi	8.2 psi/psi
	Linear Range	± 2.0 psid	+ 6 - 8 psid
	Saturation	± 7 psid	+ 7.8 - 8.8 psid
	Null Bias	$\leq 5\%$ of full output	1.5% of full output

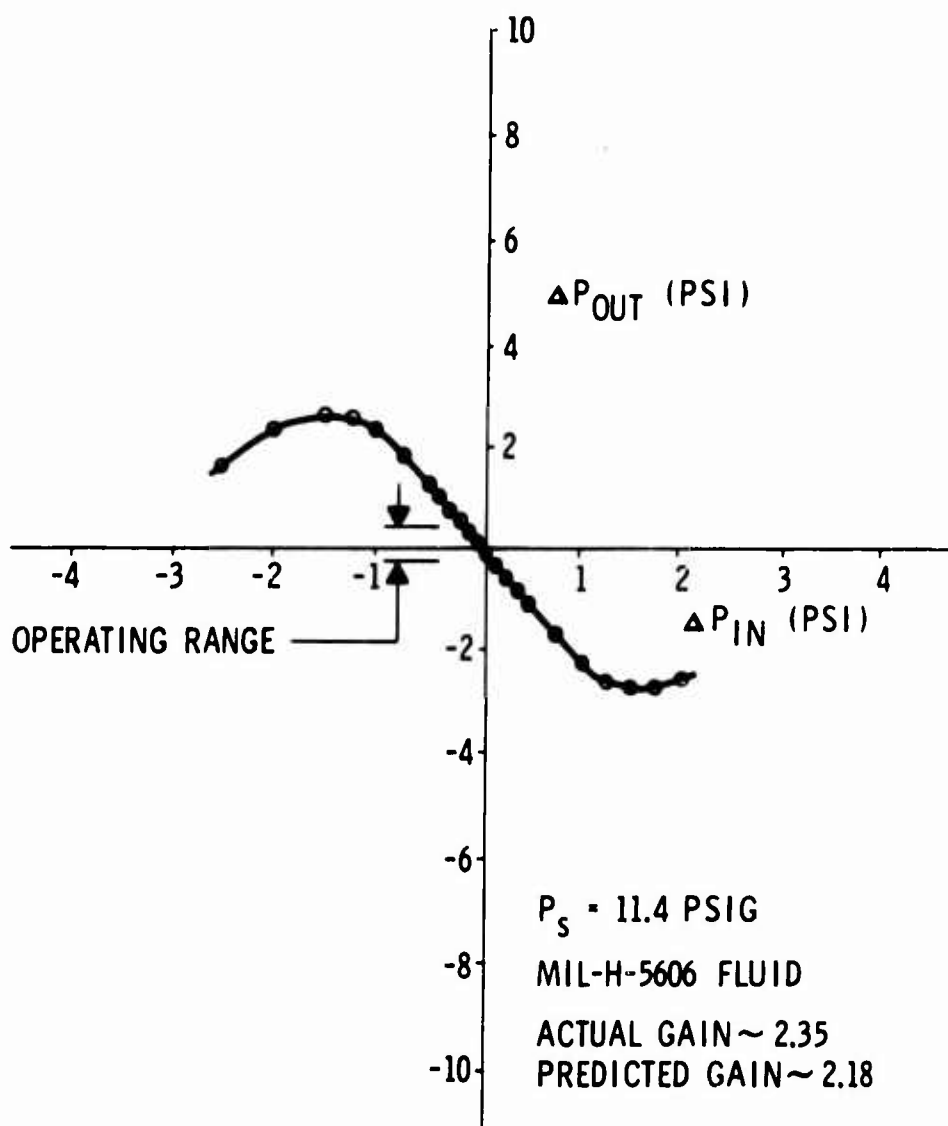


Figure 37. Preamplifier Driving Shaping Input Amplifiers

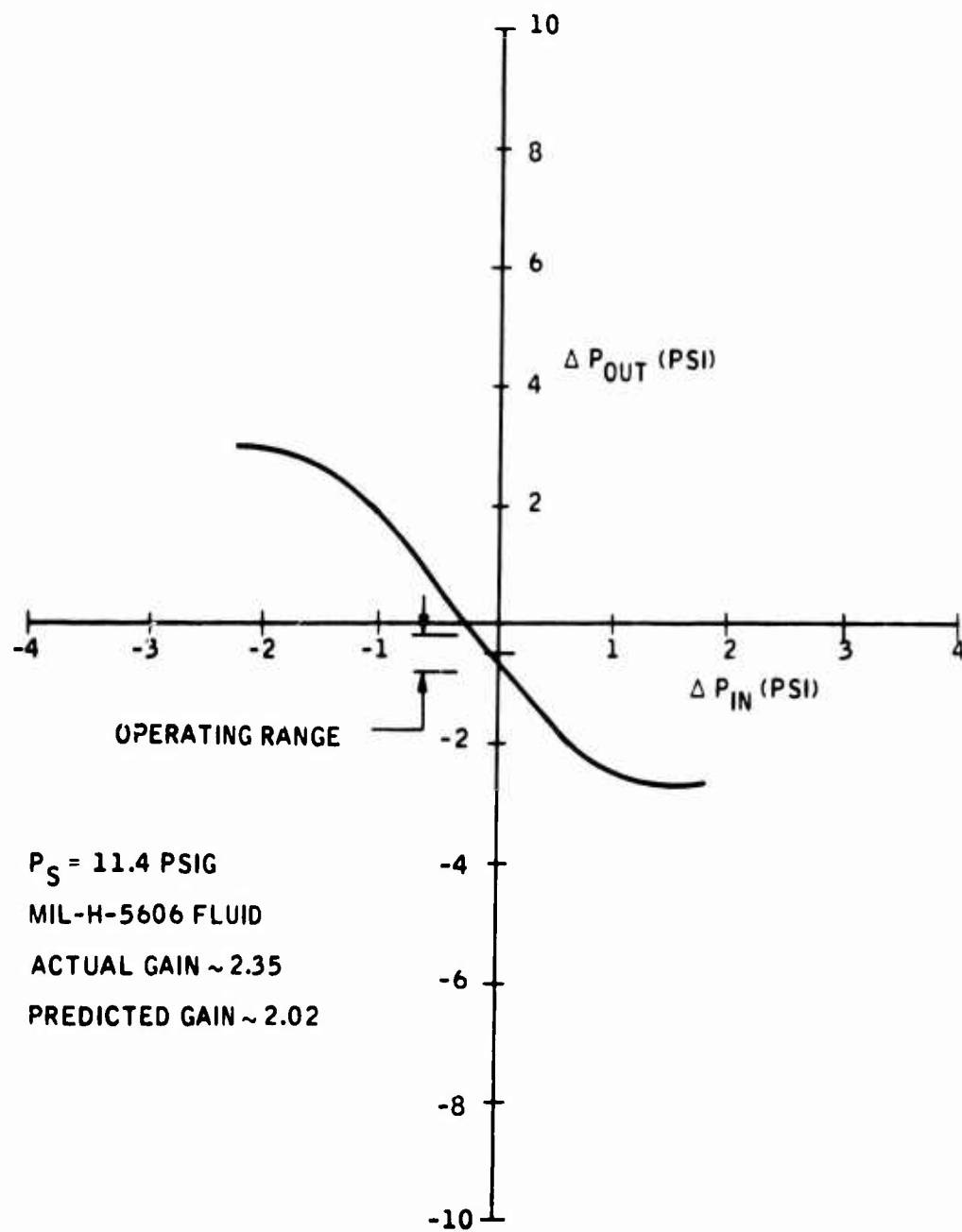


Figure 38. Shaping Input Amplifier No. 1 Driving Shaping Output Amplifier No. 1

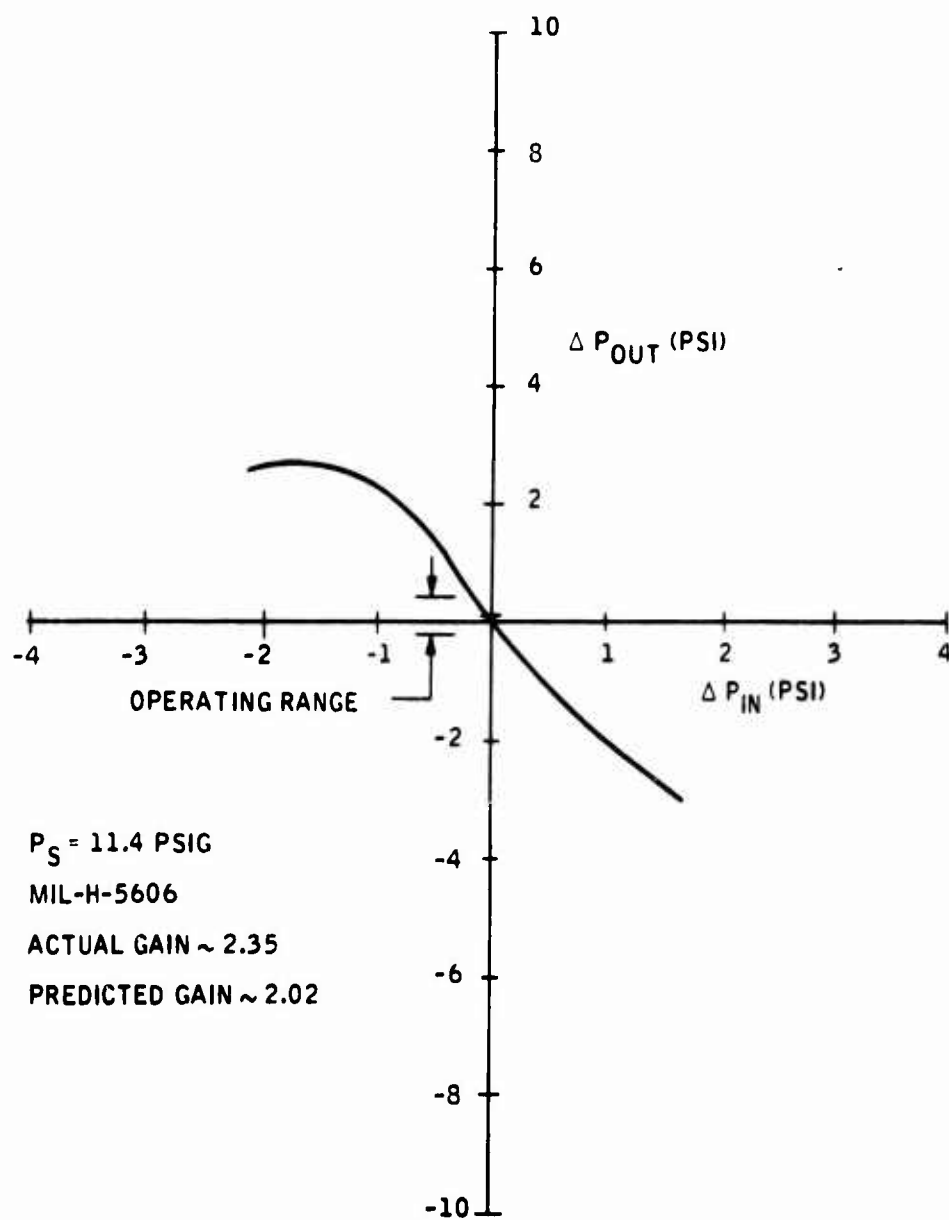


Figure 39. Shaping Input Amplifier No. 2 Driving Shaping Output Amplifier No. 2

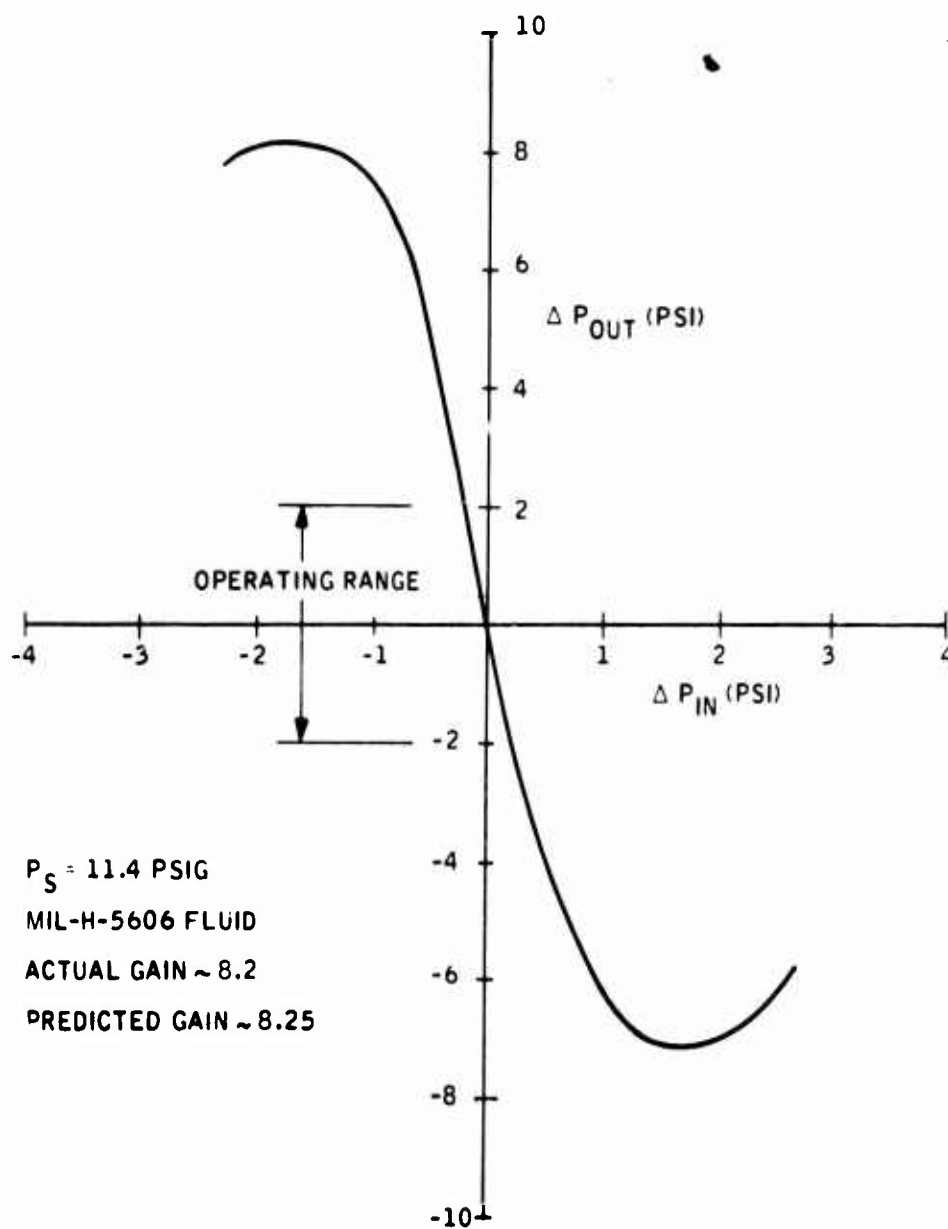


Figure 40. Shaping Output Amplifier No. 1 (Deadhead Load)

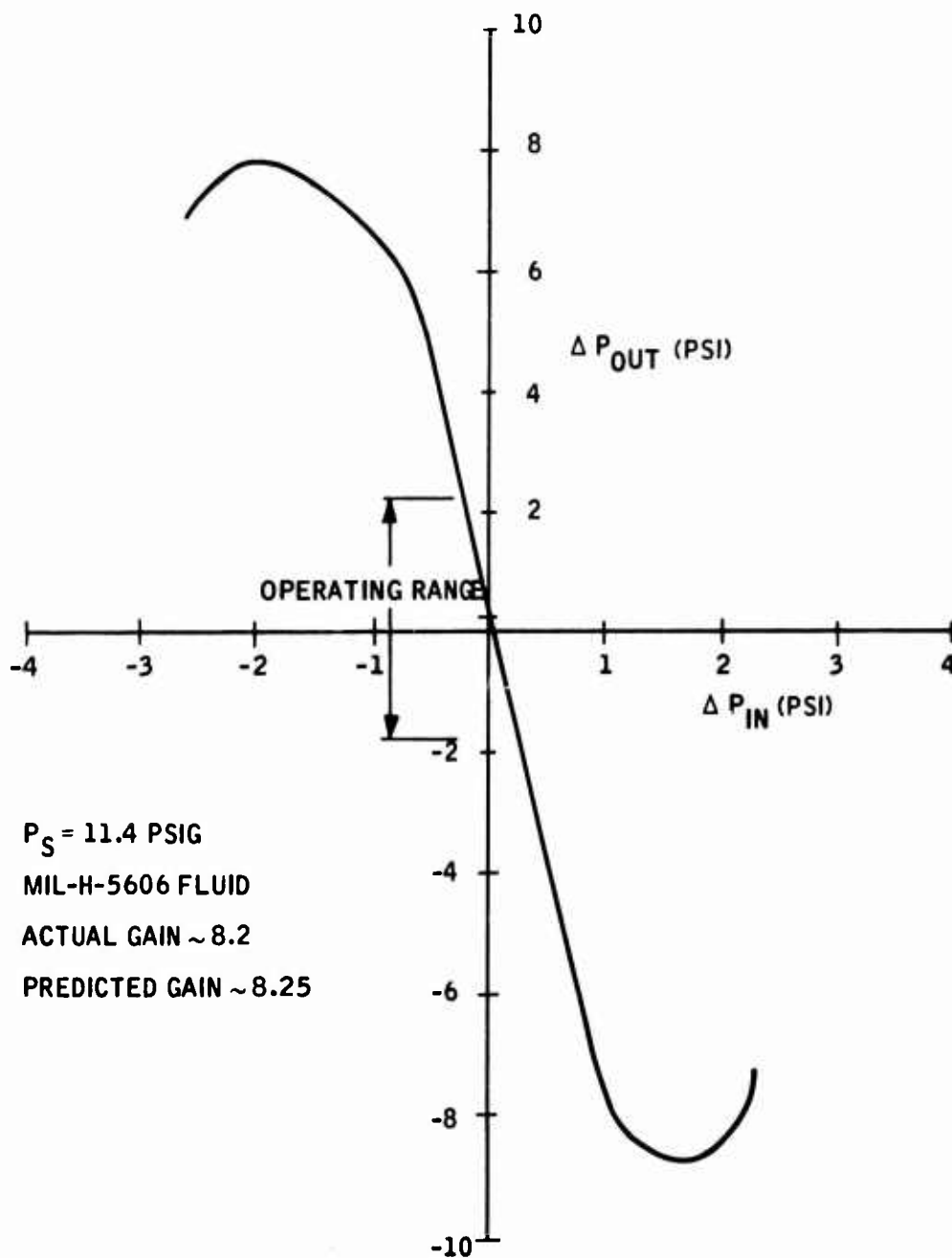


Figure 41. Shaping Output Amplifier No. 2 (Deadhead Load)

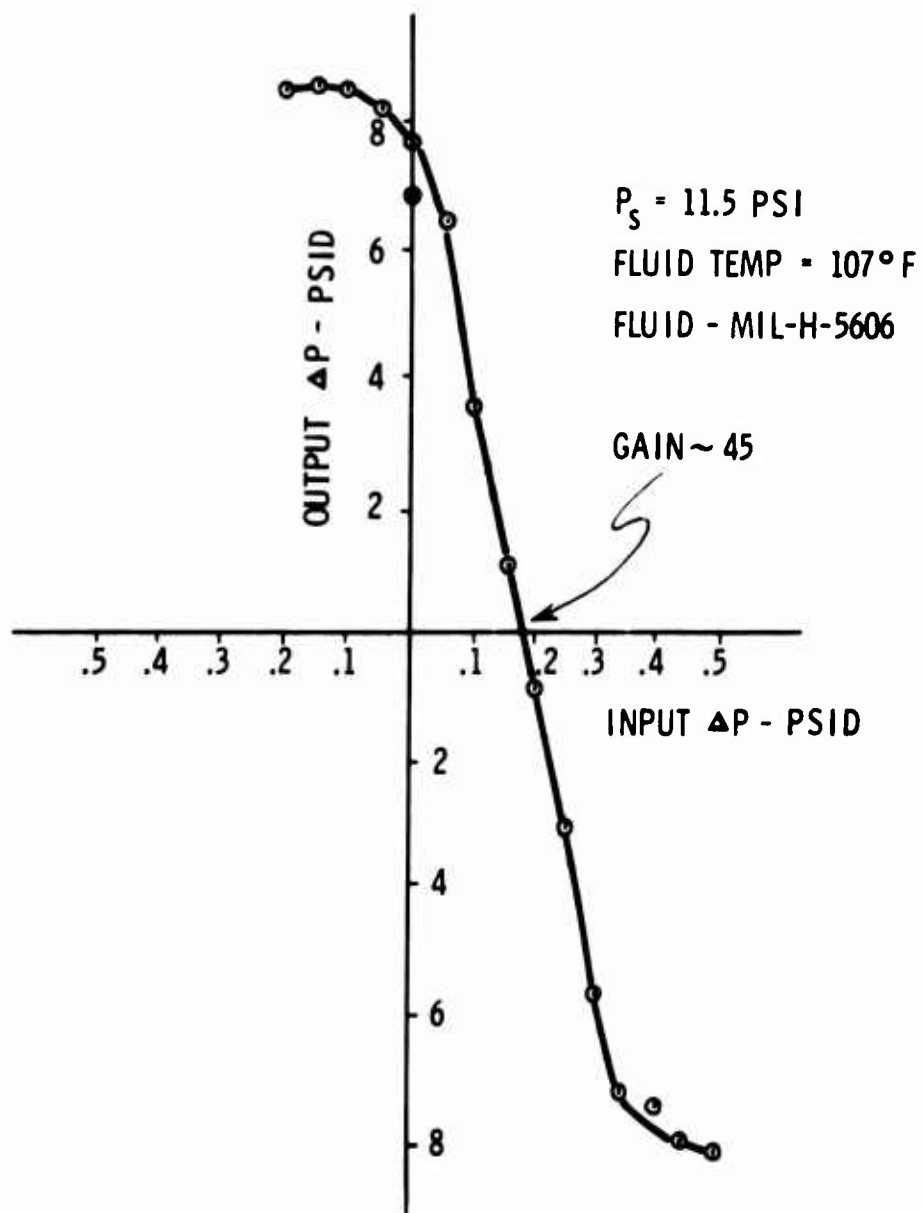


Figure 42. Straight Cascade (Includes Preamp)

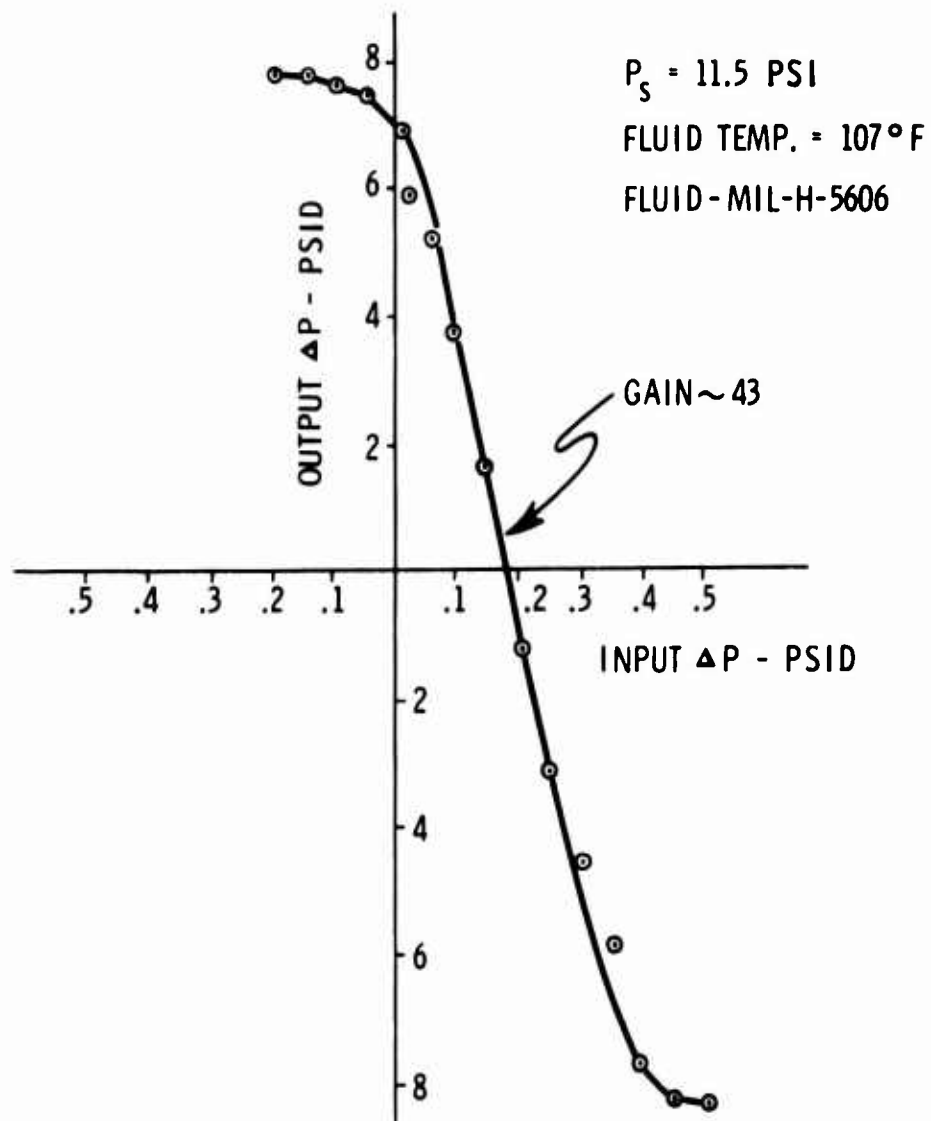


Figure 43. Lag Cascade Gain (Includes Preamplifier)

CONCLUSIONS

The amplifier steady-state performance when compared to the design goals shows that the amplifiers are satisfactory to be used as components in the damper system for purposes of system feasibility demonstration.

SHAPING NETWORK

SUMMARY

The test results on the shaping network show that its performance is in reasonable agreement with the design goals as defined by the analog simulation.

Although some difficulty with instrumentation was encountered in obtaining sinusoidal response results, the data obtained was considered valid.

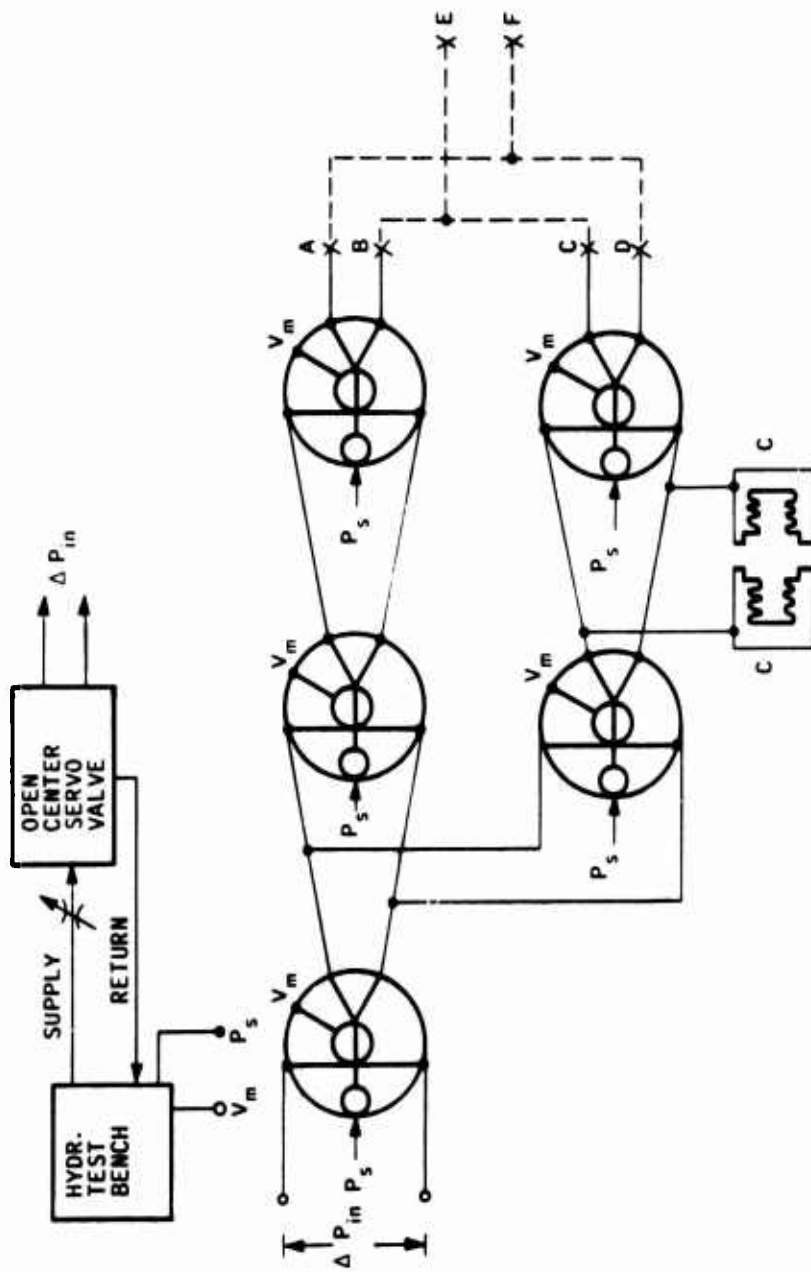
There is a gain reduction between the d-c gain (shorted hi-pass, dead-head load) and the dynamic gain (hi-pass system) due to output amplifiers loading themselves during hi-pass network dynamic operation. This effect was not predicted in the hardware design method.

The shaping network is considered satisfactory for use in the system. The dynamic gain of the shaping network is adequate for system proof of feasibility purposes.

DISCUSSION

Shaping Network Test Setup

Figure 44 shows the schematic of the shaping network test setup. An open-center electrohydraulic servovalve was used to vary the input control pressure sinusoidally or as step inputs. Both ΔP_{in} and ΔP_{out} were measured with differential pressure transducers. For this testing, the ground side of the bellows capacitors was open to atmosphere since the network return pressure (V_m) was low enough so as to not impair the bellows operation. The preamplifier was connected to the shaping network for all tests, since it was convenient to do so. All input signals were supplied to the preamplifier. For the purposes of the following discussions, the term "shaping network" is taken to include the preamplifier.



3. FOR SHAPING NETWORK TEST, B & C CONNECTED TOGETHER, A & D CONNECTED TOGETHER, OUTPUT AT E & F
2. FOR LOW-PASS FILTER SECTION TEST, ΔP_{out} MEASURED AT C & D, NO CROSS CONNECTION TO STRAIGHT-THRU CASCADE.
1. ALL $P_s = 11.4$ PSIG & ALL V_m CONNECTED TOGETHER.

Figure 44. Schematic - Shaping Network Test Setup

Dynamic Performance Test Results

Sinusoidal and transient response to step input tests were conducted on the shaping network to verify that the network had the general functional characteristics essential for application to the control system. The sinusoidal frequency response tests were rather difficult to conduct and the results were difficult to interpret, particularly at conditions of attenuated output amplitude. The major difficulties were in programming pure sine wave inputs, noise pickup due to vibration of the signal transducers, low level pressure signals required, and the effects of air trapped in the pressure transducers.

The presence of trapped air in the output transducer is particularly important since the presence of the transducer presents an RC circuit load to the output fluid amplifier during dynamic operation. The measured frequency response of the system or device will be modified by this circuit time constant unless it is sufficiently small to be ignored over the frequency spectrum of interest. However, in most cases the data up through 5 cps (which exceeds the frequency spectrum of the UH-1B yaw damper) is within the reading capability of our present instrumentation.

Transient responses to step inputs are generally easier to program and may not be as adversely affected by the previously described testing limitations. Transient response tests were made to verify function and to cross check sinusoidal response results, insofar as possible.

Since the shaping network time constant is determined by the low-pass filter section of the network, a sinusoidal response test was made on this section. Figure 45 shows the results of this test. It is seen that the break frequency is about 0.068 cps, indicating a time constant of about 2.4 seconds. The amplitude fall-off is about -20 db per decade indicating that the filter is a reasonable approximation of the desired first order lag. Since the analog simulation indicated that a time constant ranging from 2.0 seconds to 3.5 seconds would be satisfactory, the 2.4-second time constant of the low-pass filter is considered to be in compliance with the design goal.

A sinusoidal response test was conducted on the complete shaping network (connected per note 3, Figure 44). The resulting amplitude response compared to the design goal is shown on Figure 46. Difficulty was encountered in programming input sine waves with minimal distortion. Also, due to the attenuation characteristic of the shaping network, it was difficult to read precisely peak amplitudes. The phase could not be determined precisely due to small amplitude outputs at the low frequencies and, therefore, was not shown on Figure 46.

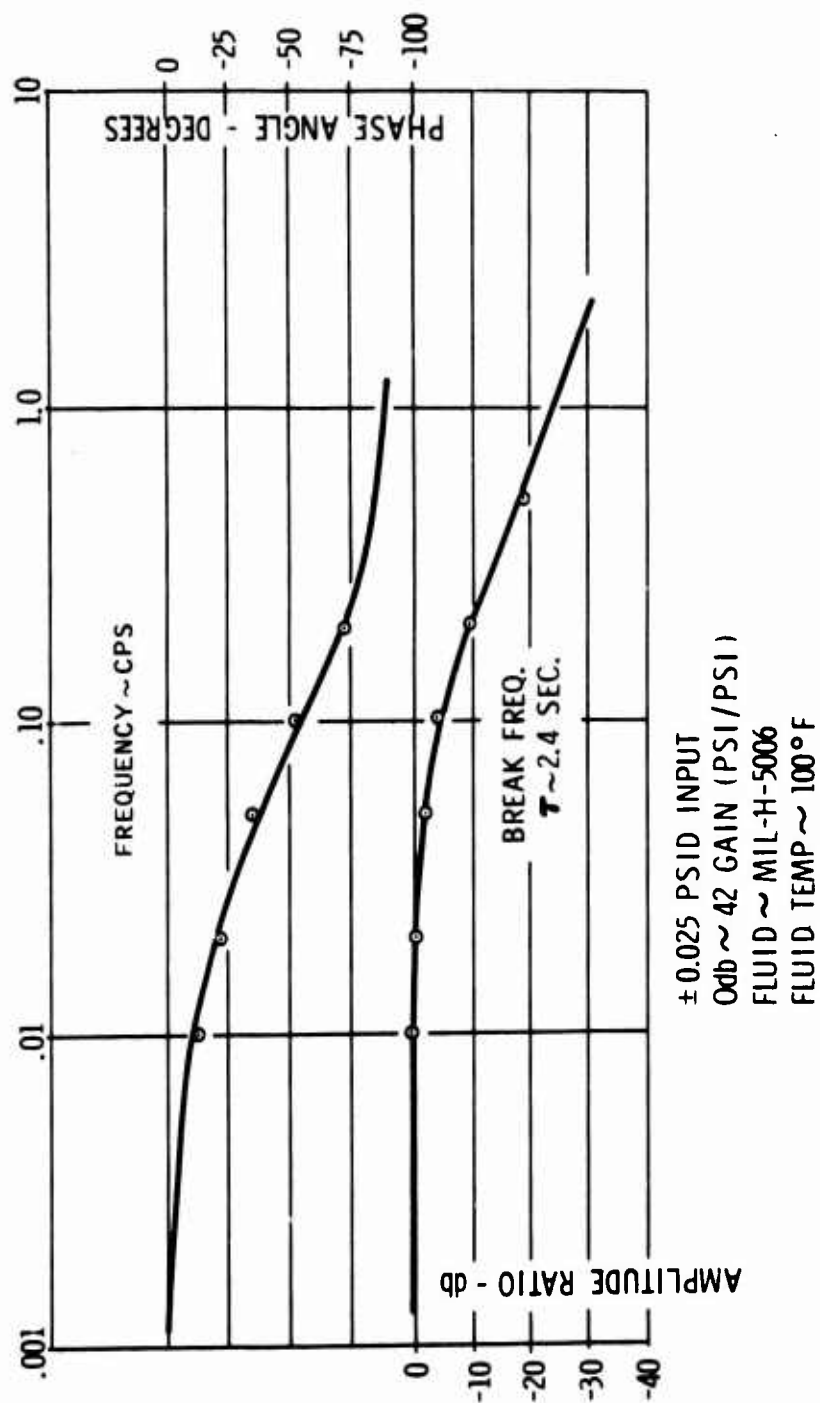


Figure 45. Dynamic Response - Low-Pass Filter Section of Shaping Network

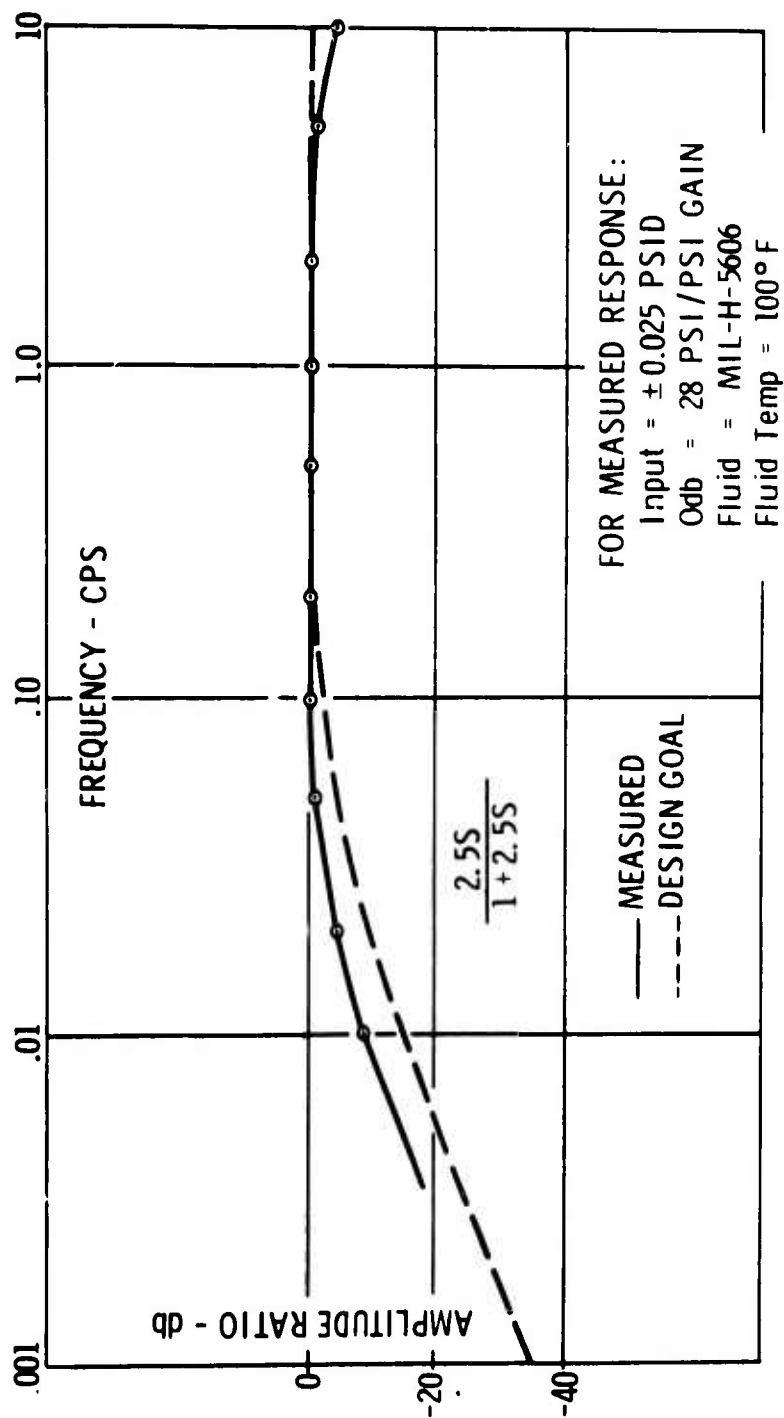


Figure 46. Dynamic Response - Shaping Network (Includes Preamp)

It could be seen, however, that substantial phase advance was occurring at the low frequencies. The measured amplitude response curve would indicate that the time constant was somewhat greater than 2.4 seconds. There may have been some trapped air in the bellows capacitors during the test which could result in a lengthened time constant.

The small attenuation of the measured response in the 5 cps to 10 cps region is believed to be due to the dynamic RC circuit load on the output amplifiers produced by the presence of the pressure transducer, as was discussed previously. It is also noted that the dynamic gain was 28 psi/psi, while the static gain of the cascades was about 43. The gain difference is due to the output amplifiers loading each other during dynamic operation. This situation is not readily calculable and, therefore, was not included in the amplifier design process.

Figure 47 shows a transient response to a step input. It can be seen that the time constant is about 2.5 seconds, which confirms the low-pass filter response results.

Transfer Function

The shaping network transfer function considered as the design goal from the analog simulation is expressed as follows:

$$\frac{\left(1 - \frac{K_{\theta_2}}{K_{\theta_1}}\right) + T_H S}{1 + T_H S}$$

where

$$0.9 < \frac{K_{\theta_2}}{K_{\theta_1}} < 1.1$$

$$2 < T_H < 3.5$$

Considering the fluid shaping network as an equivalent electrical circuit, the open circuit gains of the two cascades are

$$K_{\theta_1} = 45 \text{ (straight-thru cascade)}$$

$$K_{\theta_2} = 43 \text{ (lag cascade);}$$

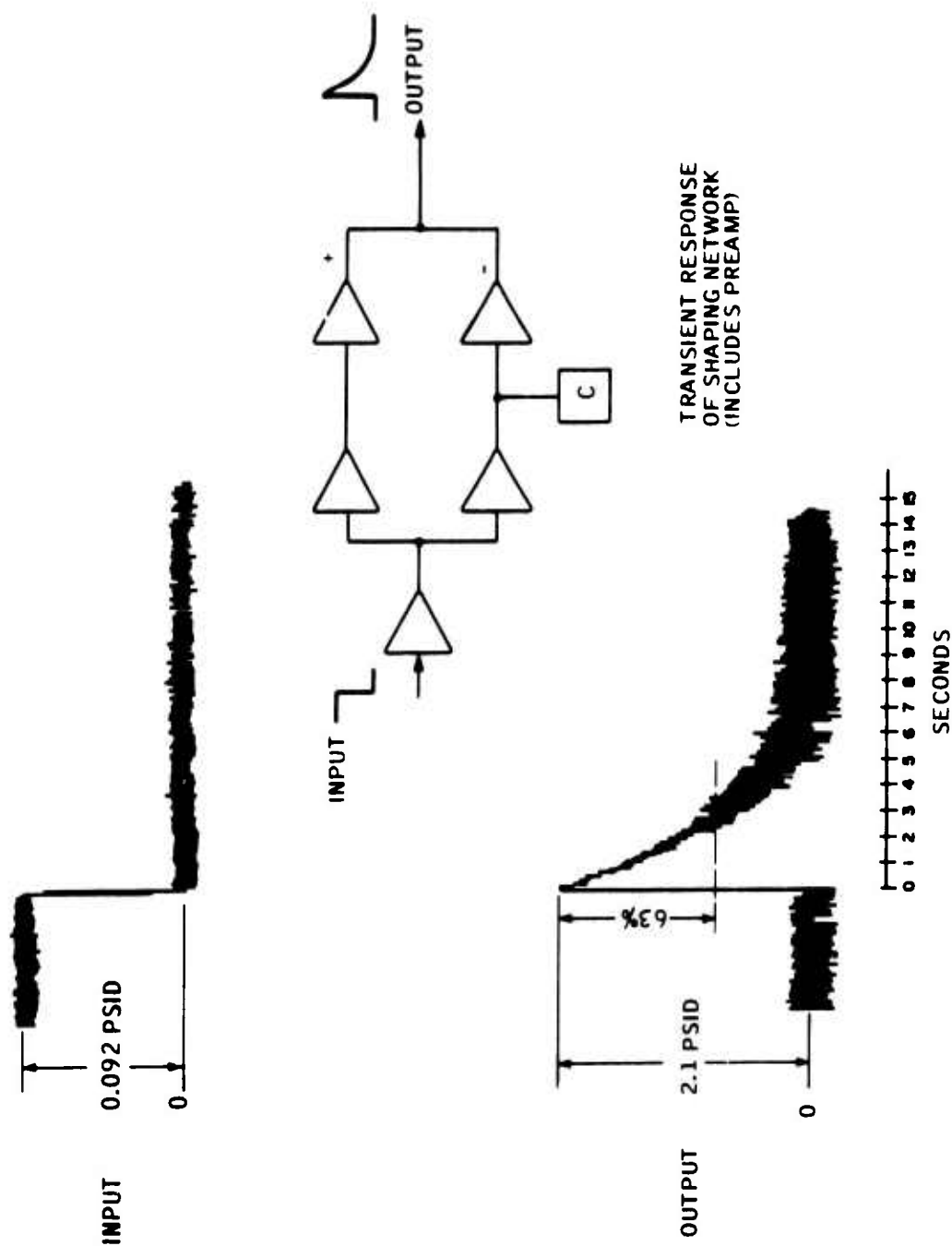


Figure 47. Transient Response - Shaping Network (Includes Preamp)

therefore,

$$\frac{K_{\theta_2}}{K_{\theta_1}} = \frac{43}{45} = \underline{0.955}$$

From the low-pass filter dynamic response (Figure 45)

$$T_H \sim 2.4 \text{ seconds}$$

Since the ratio of K_{θ_1} to K_{θ_2} and T_H is within the limits of the design goal, as prescribed by the analog simulation, the shaping network is considered to have met the design goal objective.

CONCLUSIONS

The sinusoidal and transient response results show that the shaping network has the hi-pass network characteristics necessary for use in the control system. The network output attenuation at the low frequencies should effectively wash out the effects of pilot-commanded yaw ratio on the damper during steady-state maneuvers.

SERVOACTUATOR

SUMMARY

The servoactuator (HRM Part No. 85111200) met the design objectives of the technical development specification (Appendix I) and is considered satisfactory for use in the damper system.

DISCUSSION

The servoactuator was tested by the vendor at the vendor's facility. These test results are listed below and are shown in Figures 48 and 49. The servoactuator dynamic response characteristics are shown in Figures 50 and 51. It should be noted that the input referred to as "pneumatic" was actually hydraulic. To facilitate testing, the force capsules and connecting tubing were filled with hydraulic fluid and then air pressure was applied to the hydraulic fill in order to produce the input differential pressure.

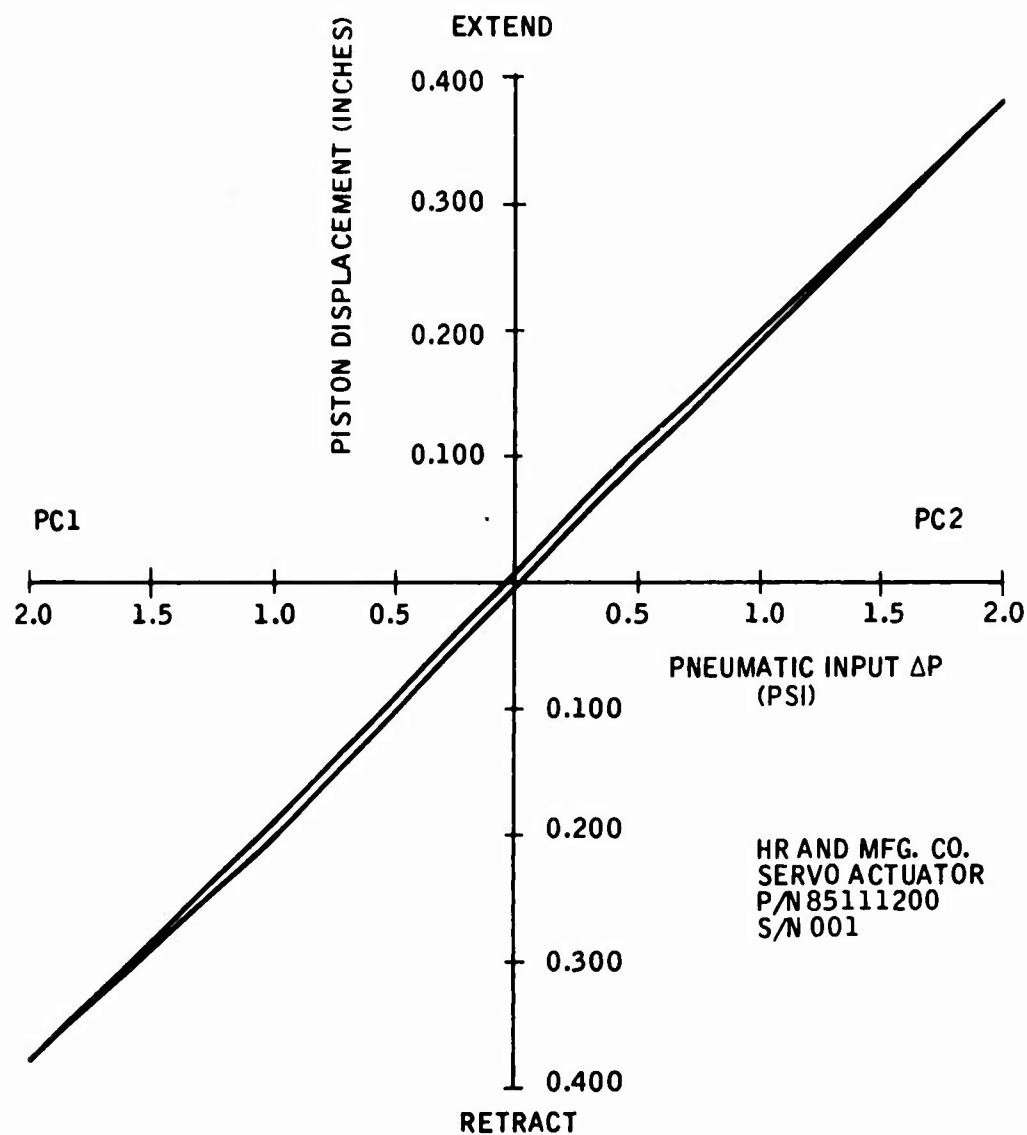


Figure 48. Actuator Displacement Versus Pneumatic Input (S/N 0.001)

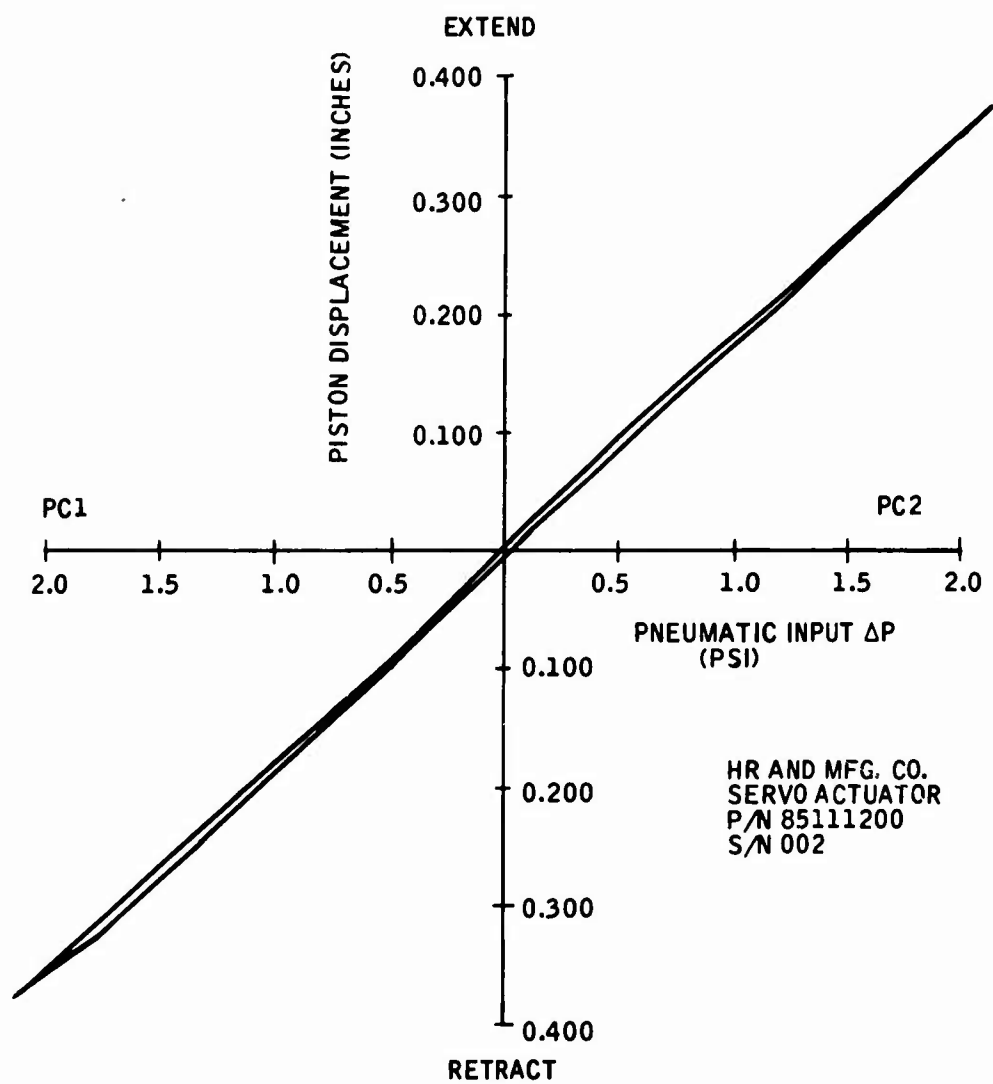


Figure 49. Actuator Displacement Versus Pneumatic Input (S/N 0.002)

HYDRAULIC RESEARCH MFG. CO.
P/N 8511200 SERVO ACTUATOR
S/N 002 3 - 21 - 66

FREQUENCY RESPONSE

AMPLITUDE RATIO AND PHASE LAG OF CLOSED LOOP
POSITION WITH RESPECT TO INPUT SIGNAL

RESPONSE DATA BASED ON 0.075 P TO P ($\pm 10\%$) PISTON
TRAVEL

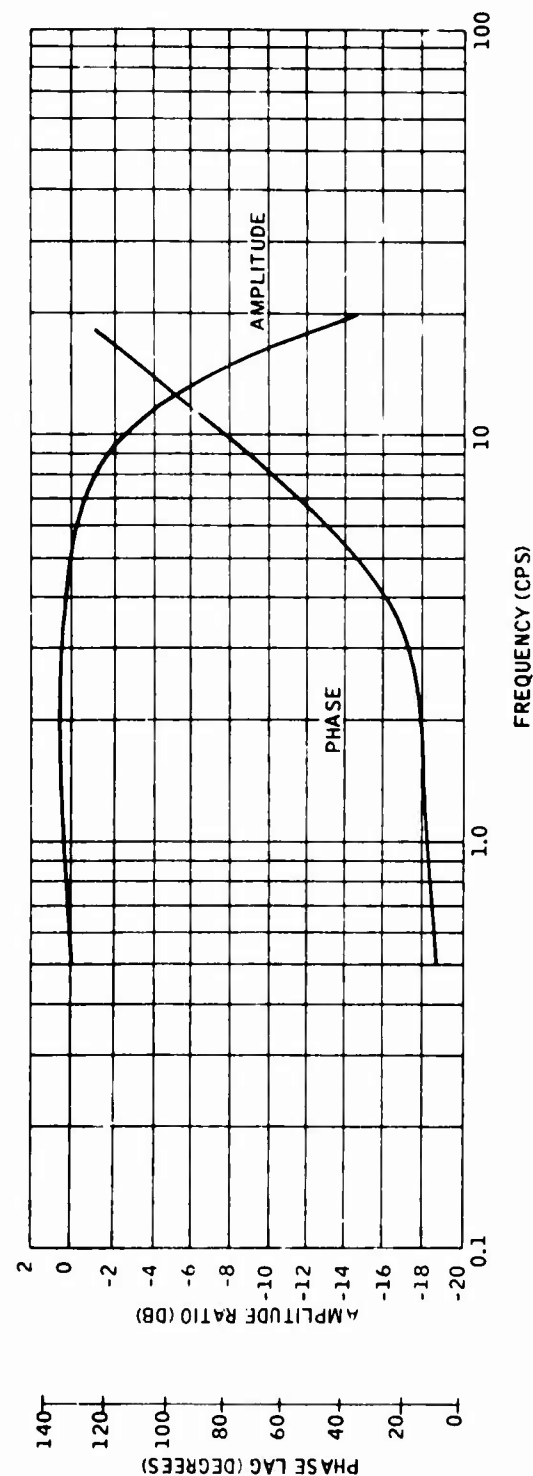


Figure 50. Amplitude Ratio and Phase Lag of Closed Loop Position with Respect to Input Signal

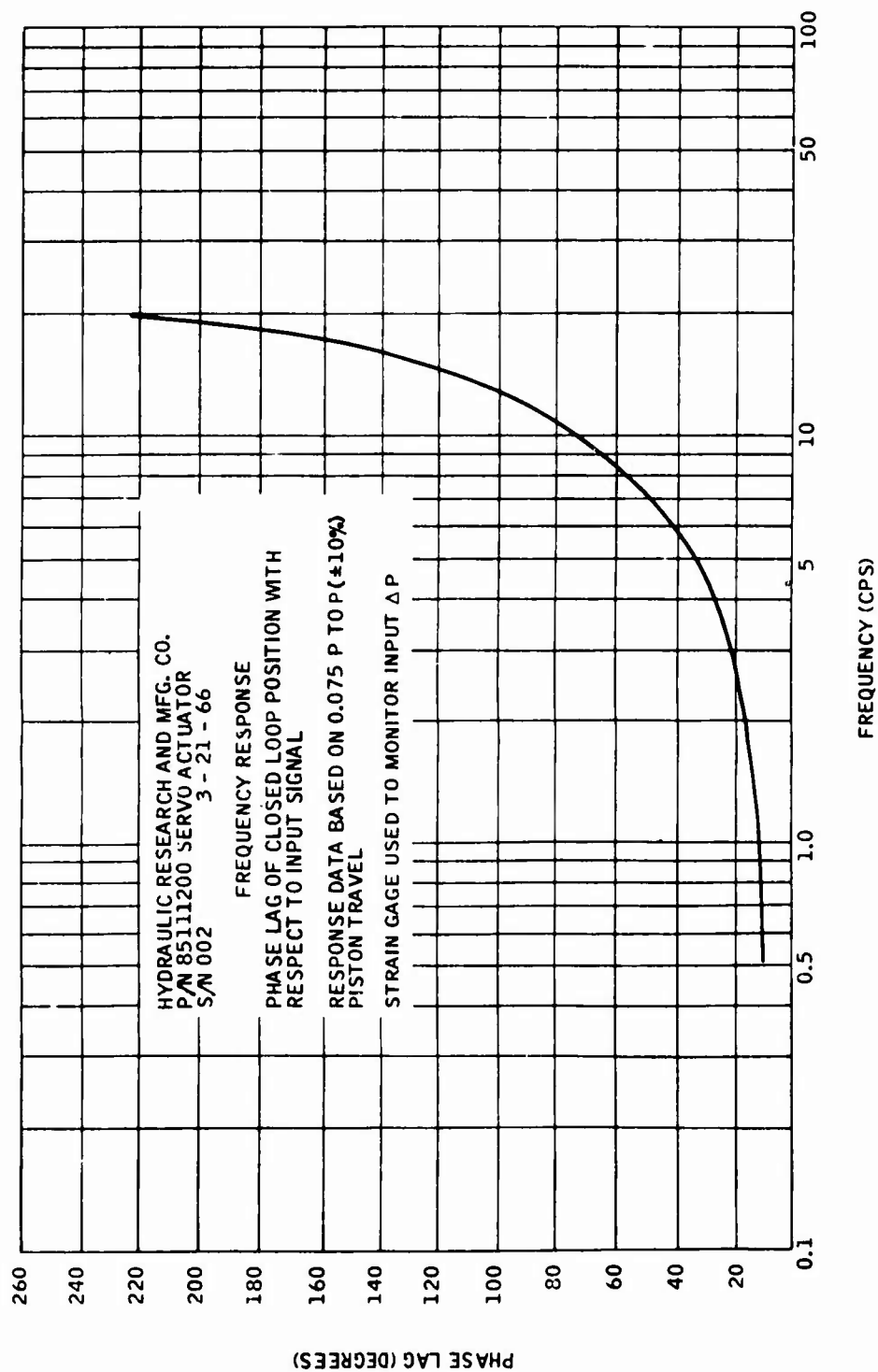


Figure 51. Phase Lag of Closed Loop Position with Respect to Input Signal

TEST DATA FOR 85111200 SERVOACTUATOR

Ser. No. 001

Null reference position of the servoactuator is the center-locked position with pressure off.

	Results
Proof Pressure: 4500 psi supply, return 1000 psi	OK
Gain: See Figure 48	0.190 in/psi
Threshold:	0.3%
Positional deadband following small input signals of opposite polarity.	000
Hysteresis: Position loop width based on full signal swing	0.012 in.
Centering: With 4-psi balanced input pressures actuator position with respect to center-locked position	0.003 in.
Null shift with change in supply pressure	
- from 1000 to 1500 psi	0.003 in.
- from 1000 to 500 psi	0.007 in.
Unlock pressure with rising supply pressure:	660 psi
Locking pressure with decreasing supply pressure:	
Lock piston starting to engage	480 psi
Completion of locking	150 psi

TEST DATA FOR 85111200 SERVOACTUATOR

Ser. No. 002

Null reference position of the servoactuator is the center-locked position with pressure off.

	Results
Proof Pressure: 4500 psi supply, return 1000 psi	OK
Gain: See Figure 49	0.185 in. /psi
Threshold:	0.3%
Positional deadband following small input signals of opposite polarity	000
Hysteresis: Position loop width based on full signal swing	0.008 in.
Centering: With 4-psi balanced input pressures actuator position with respect to center-locked position	0.003 in.
Null shift with change in supply pressure	
- from 1000 to 1500 psi	+ 0.002 in.
- from 1000 to 500 psi	- 0.005 in.
Unlock pressure with rising supply pressure:	575 psi
Locking pressure with decreasing supply pressure:	
Lock piston starting to engage	325 psi
Completion of locking	250 psi
Dynamic Response: See Figure 50	

Figure 52 shows an x-y plot of the servoactuator gain with a steady-state commanded input differential pressure. This test was conducted at Honeywell to cross check HRM's test results.

CONCLUSION

The servoactuator performance is in compliance with the design goals.

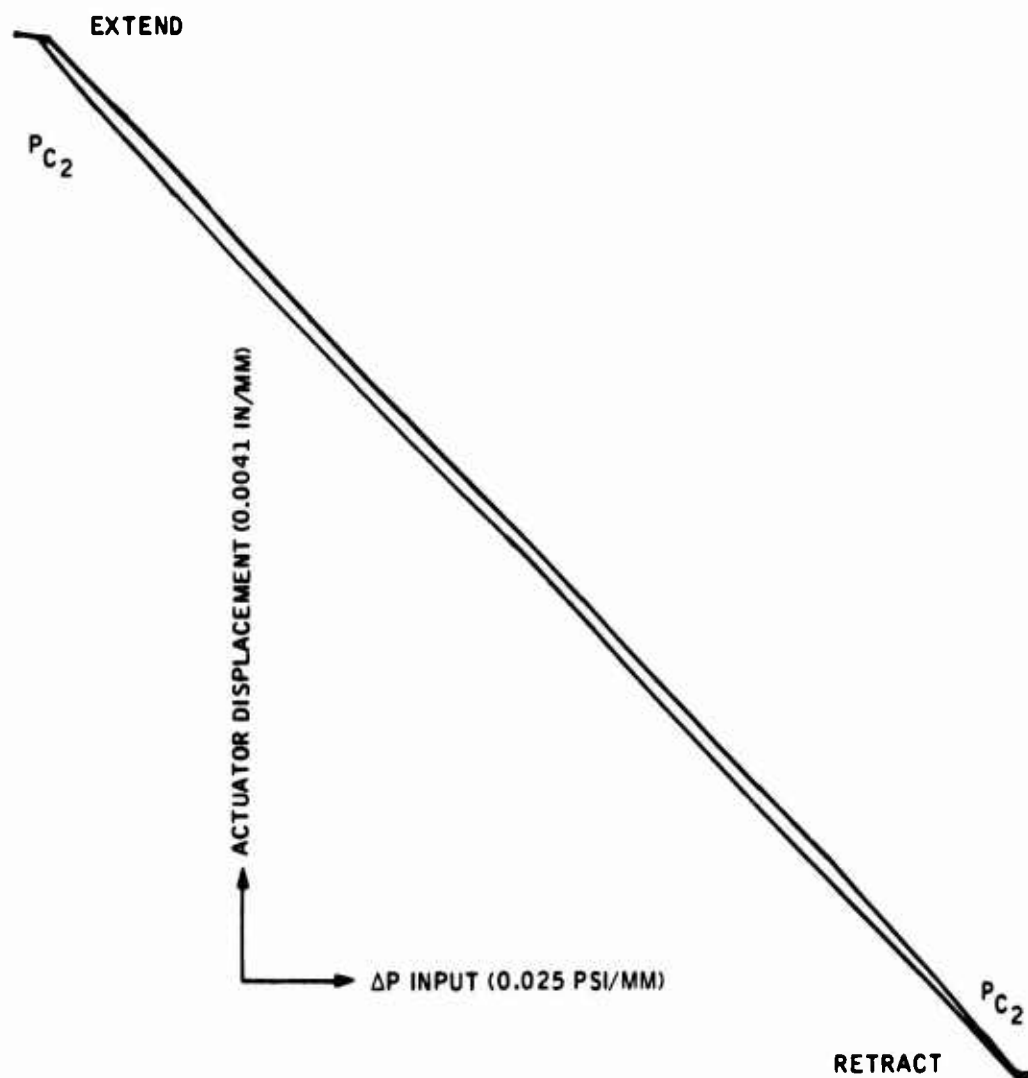


Figure 52. Actuator Displacement versus ΔP Input

CHAPTER 5

SYSTEM TEST RESULTS

This section contains the results of all yaw damper system testing conducted during the program. This work is divided into three major areas: open-loop testing, closed-loop testing, and environmental testing. All test work was conducted in accordance with the procedures outlined in the document "System Test Requirements" shown in Appendix II insofar as possible. Each area of work is presented and discussed separately.

OPEN-LOOP TESTING

SUMMARY

A rate sensor and system operating point different from that used during component testing was selected on the basis of reduced system noise in the form of actuator jitter. Reduction in system loop gain was the tradeoff for reduced system noise. Dynamic response tests show that the system using hi-pass yaw rate is feasible and should provide a significant increase in aircraft damping. Fluid temperature effects are limiting the present system operating range, but this can be improved by shifting the location of the hi-pass network to hi-pass directly out of the rate sensor. Additional experimental work on the rate sensor and fluid amplifiers is recommended in order to include fluid temperature effects in the mechanization design procedure, as well as to reduce sensor null shifts due to fluid temperature changes.

DISCUSSION

The open-loop testing was conducted using a tilt table to apply angular rates to the system. Sinusoidal varying angular rates and step input angular rate signals were applied to the tilt table servo by a function generator. Table angular rates were sensed and read out from a rate gyro mounted on the table. System performance in the form of servo-actuator motion was read out from a potentiometer actuated by movement of the servoactuator piston rod. Figure 53 shows a schematic of the setup. Figures 54, 55, and 56 are photographs showing the yaw damper system and tilt table apparatus.

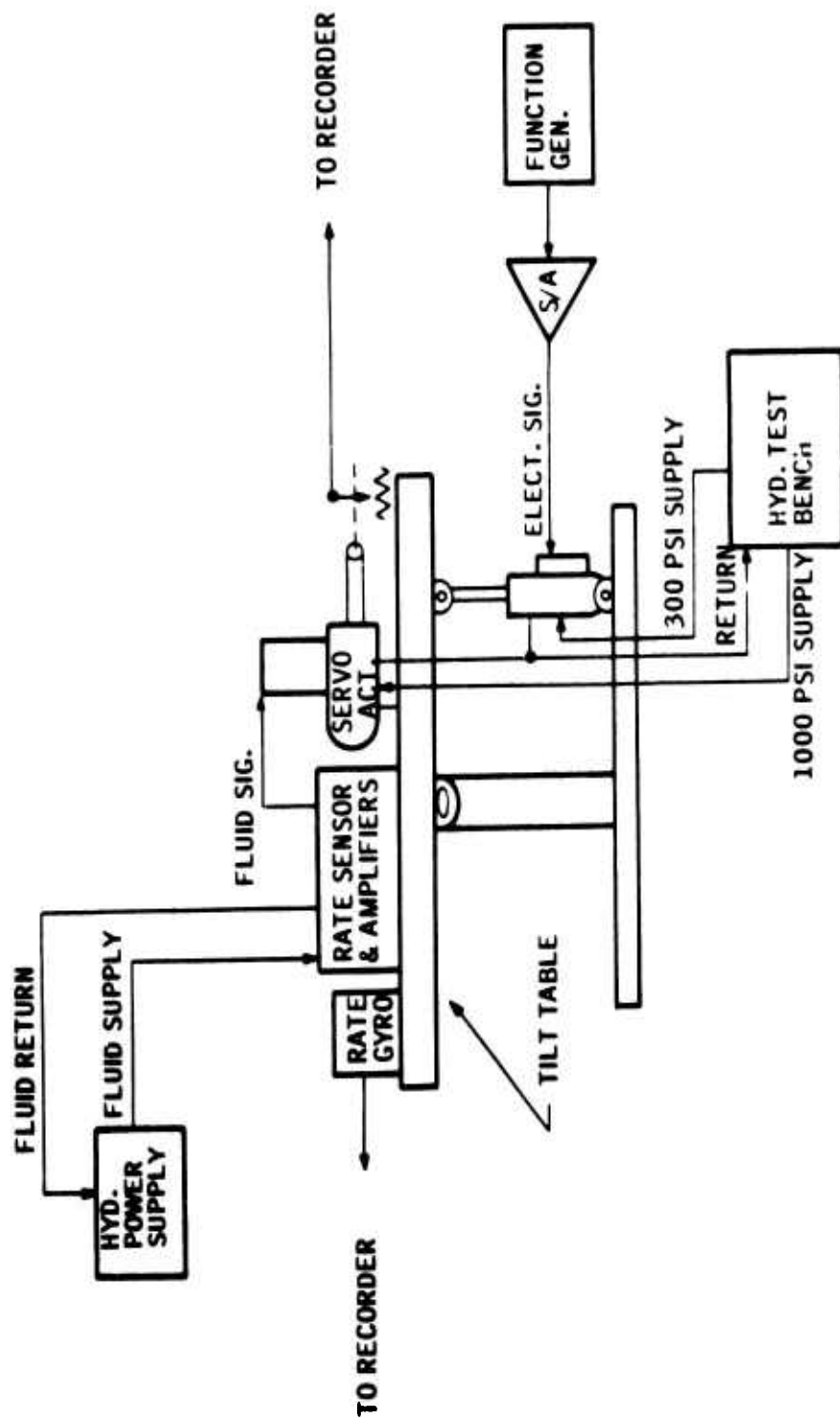


Figure 53. Open Loop Test Setup

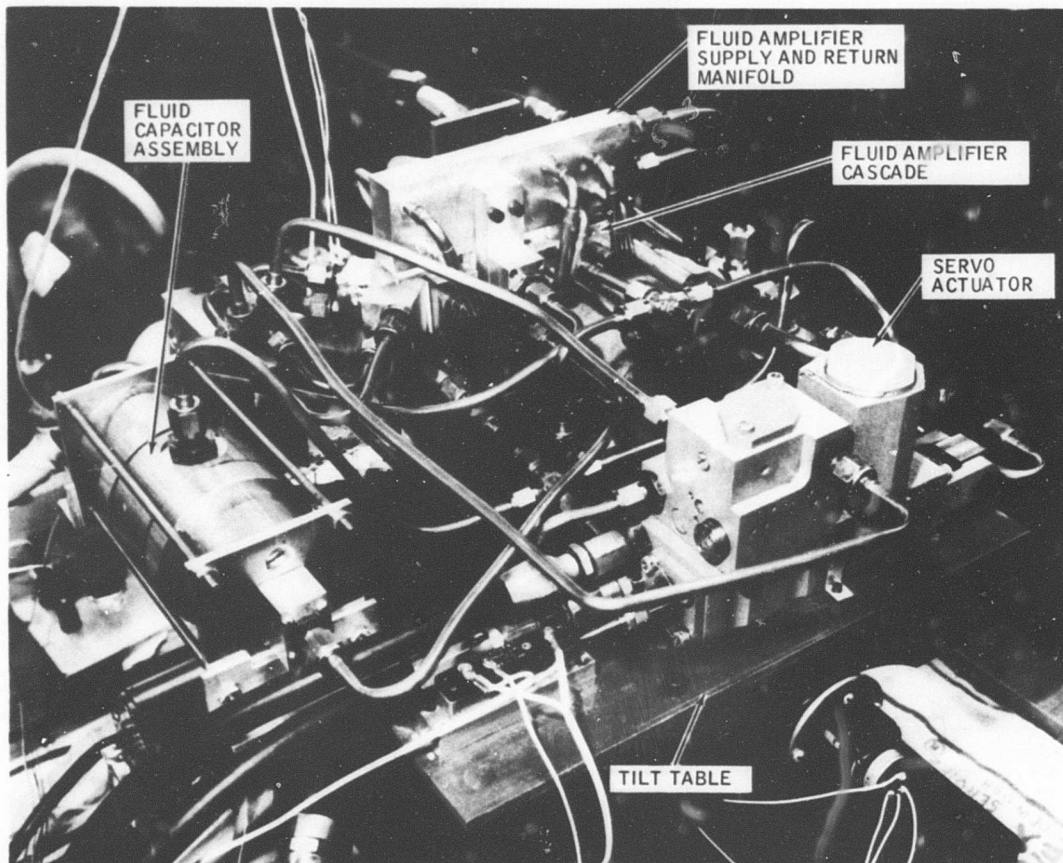


Figure 54. Damper on Tilt Table

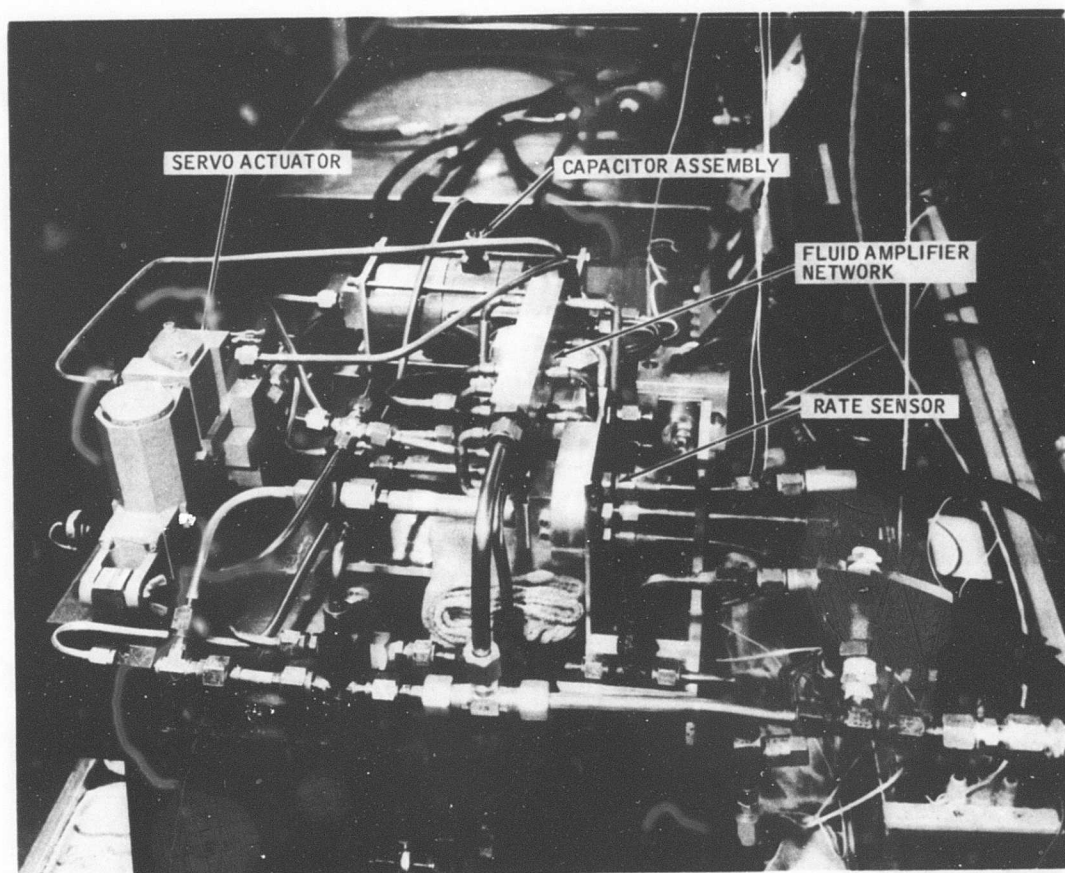


Figure 55. System on Tilt Table

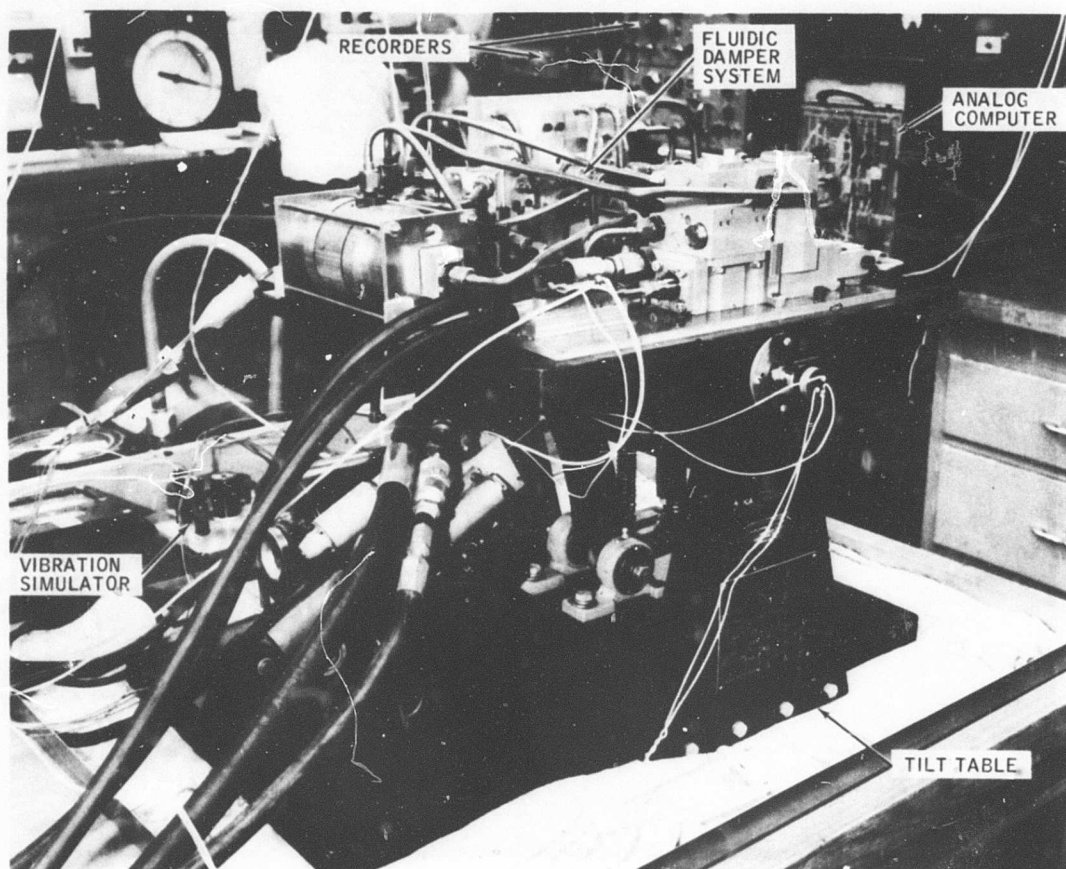


Figure 56. Tilt Table

Rate Sensor and System Operating Point Tests

The initial system operating condition was using 2.5 gpm rate sensor flow input with 2.0 gpm passing through the pickoff sink. The fluid amplifier network used a 10 psid supply pressure. It was found that considerable output noise in the form of actuator jitter resulted. The actuator jitter would increase with fluid temperature and eventually the rate sensor pickoff sink flow would change from laminar to turbulent. At this condition, servoactuator jitter was very violent. It appeared that the fluid noise spectrum contained a 3 to 7 cps random modulation of the high frequency "hash". Since the system passband extends to 10 cps, the 3 to 7 cps modulation shows up as noise. To prevent the sensor pickoff sink flow from becoming turbulent, it was decided to reduce the pickoff sink flow rate. The results of this initial investigation are shown in Table V.

TABLE V SYSTEM OUTPUT NOISE		
Sensor Pickoff Sensor Flow Rate	Fluid Temperature Range	Actuator Jitter- Equiv. Deg. of Tail Rotor Deflection
2.0 gpm	100° F - 115° F	±0.109
2.0 gpm	150° F - 152° F	±0.215
2.0 gpm	158° F	±0.91*
1.5 gpm	82° F - 89° F	±0.053

*Sink flow became turbulent due to fluid viscosity.

The system operating point investigation was continued. To obtain the best rate sensor and system operating point from a "noise" standpoint, the rate sensor pickoff sink flow was reduced from 2.0 gpm to 0.95 gpm and the fluid amplifier network power nozzle differential was reduced from 10 psid to 5 psid. Although a reduction in system loop gain and range was the tradeoff, a reduction in system noise was considered to be mandatory. Table VI shows the resulting system noise with the new operating point.

TABLE VI SYSTEM OUTPUT NOISE		
Sensor Pickoff Sink Flow Rate	Fluid Temperature	Actuator Jitter- Equiv. Deg. of Tail Rotor Deflection
0.95 gpm	75° F	±0.0265
0.95 gpm	120° F	±0.083
0.95 gpm	175° F	±0.165

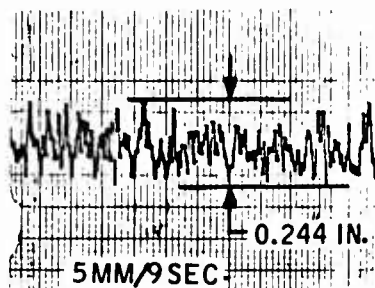
NOTE: 75° F to 175° F oil temperature range was limit of test hydraulic power source equipment.

Figure 57 shows recordings of the original output noise condition and the output noise conditions with the revised system operating point.

Fluid Amplifier Cascade Gain

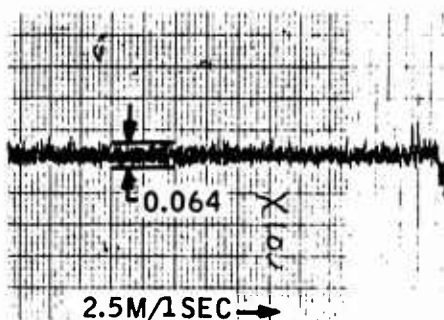
Since the fluid amplifier network power supply pressure differentials were reduced below the minimum recommended values, the gain and range were rechecked. Figures 58 and 59 show these results at a fluid temperature of 85° F. Comparing these results to Figures 42 and 43, it is seen that the gain has been reduced from 43 to 24 and the range from 7 psid to 2.5 psid. Additional gain checks at several operating conditions were made on the straight-through cascade to obtain a feel for the possible effect on network dynamic loop gain. These results are shown in Table VII.

TABLE VII STRAIGHT-THROUGH CASCADE GAIN TABULATION		
Gain	Supply Pressure Differential	Fluid Temperature
44	11.4	107° F
44	10	90° F
44	15	90° F
52	10	120° F
37	7	120° F
34	5	120° F
24	5	85° F



a. Original

PICK-OFF SINK FLOW = 2.0 GPM
 AMPL. SUPPLY PRESSURE = 10 PSID
 OIL TEMPERATURE = 158°F



b. Revised

PICK-OFF SINK FLOW = 0.95 GPM
 AMPL. SUPPLY PRESSURE = 5 PSID
 OIL TEMPERATURE = 175°F

Figure 57. Output (Noise)

STRAIGHT CASCADE GAIN

$P_a = 13 \text{ PSI}$ $P_b = 8 \text{ PSI}$

$t_f = 85^\circ\text{F}$ $\text{GAIN} = 24$

5-18-66

P_a = CASCADE POWER NOZZLE
SUPPLY PRESSURE

P_b = CASCADE RETURN LINE
PRESSURE

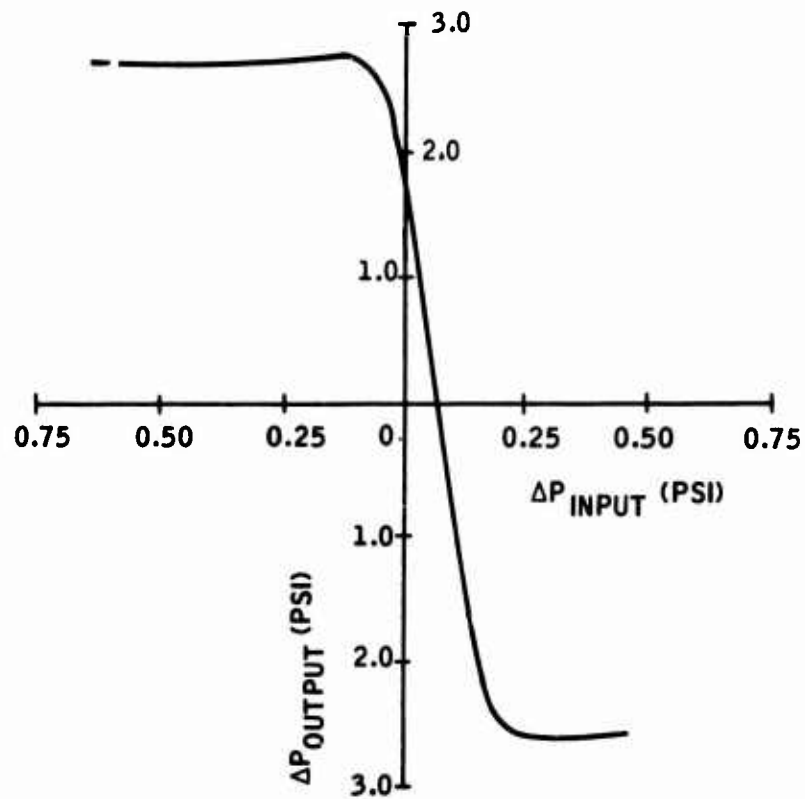


Figure 58. Straight Cascade Gain

LAG CASCADE GAIN

$P_a = 13$ psi $P_b = 8$ psi

$t_f = 85^\circ\text{F}$ GAIN = 24

5-18-66

P_a = CASCADE POWER NOZZLE
SUPPLY PRESSURE

P_b = CASCADE RETURN LINE
PRESSURE

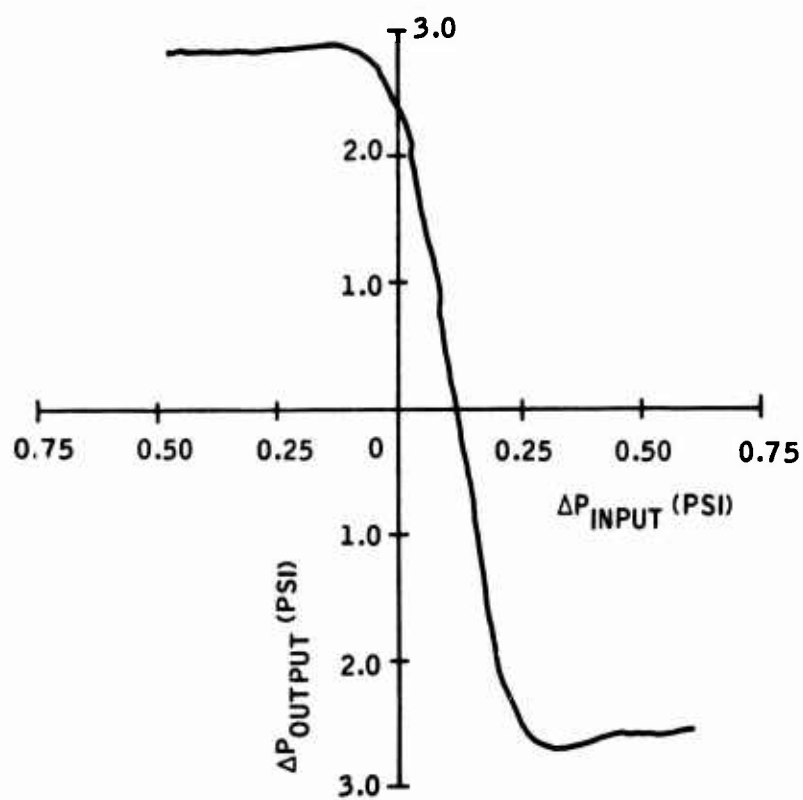


Figure 59. Lag Cascade Gain

It was concluded that the reduced cascade supply pressure would result in greater loop gain variations with fluid temperature change than would occur at the minimum recommended supply differential pressure (10 psid). It was also concluded that the effective range of the hi-pass would be reduced since less rate sensor temperature null shift could be cancelled out before using up the reduced range of the output amplifiers. This would be particularly true at the higher dynamic rate input signals.

Shorted Hi-Pass System Tests

Steady-State Gain

With the revised system operating point selected, system testing resumed. Figure 60 shows a schematic of the yaw damper system in the "as tested" condition. It should be noted that the output ports of the lagged cascade are blocked for the shorted hi-pass system configuration. This is necessary since the system d-c gain can be obtained only if the signal subtraction connections are removed.

The steady-state gain was determined by programming plus and minus short-duration steady-state rate inputs into the tilt table. The inputs were of sufficient duration to allow the servoactuator to achieve a steady-state position.

Figures 61, 62, and 63 show point-to-point plots of these results for three fluid temperature conditions. The steady-state gain test results as compared to design goals are shown in Table VIII.

TABLE VIII STEADY-STATE GAIN RESULTS TABULATION		
Parameter	Design Goal	Measured Result
Gain	0.15 ± 0.03 deg rotor/deg/sec	0.10 at 75°F fluid temp. 0.199 at 120°F fluid temp. 0.218 at 175°F fluid temp.
Linearity	20 percent	6.2% at 75°F fluid temp. 7.7% at 120°F fluid temp. 7.7% at 175°F fluid temp.
Range	± 16.7 deg/sec (nominal)	± 39 deg/sec (calculated since ± 20 deg/sec step rate was maximum used on tilt table) at 75°F fluid temp. ± 12.5 deg/sec at 120°F fluid temp. ± 10 deg/sec at 175°F fluid temp.

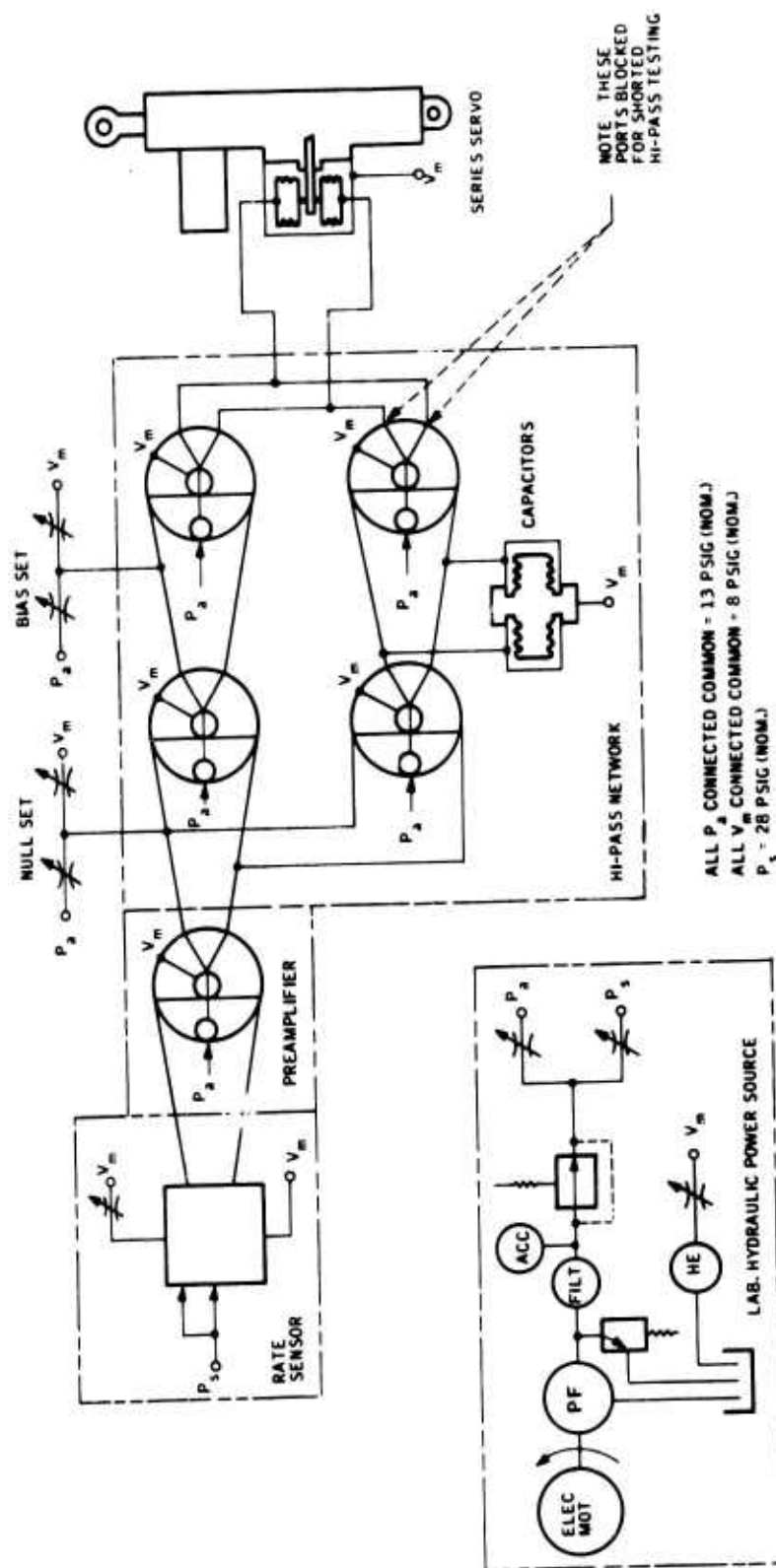


Figure 60 Hydraulic Schematic - UH-1B Yaw Damper (As-Tested Condition)

SHORTED HI-PASS SYSTEM GAIN

$t_f = 75^\circ\text{F}$ $P_b = 8\text{ PSI}$
 $P_a = 13\text{ PSI}$ $P_s = 28\text{ PSI}$
 $Q_b = 0.90\text{ GPM}$ $Q_t = 2.45\text{ GPM}$
 NULL NOISE = 0.008 IN. D.A.
 $\pm 0.0265\text{ DEG.}$

P_s = RATE SENSOR SUPPLY PRESSURE

P_a = CASCADE POWER NOZZLE SUPPLY PRESSURE

P_b = CASCADE RETURN LINE PRESSURE

Q_b = RATE SENSOR PICKOFF SINK FLOW RATE

Q_t = RATE SENSOR INPUT FLOW RATE

D. A. = DOUBLE AMPLITUDE

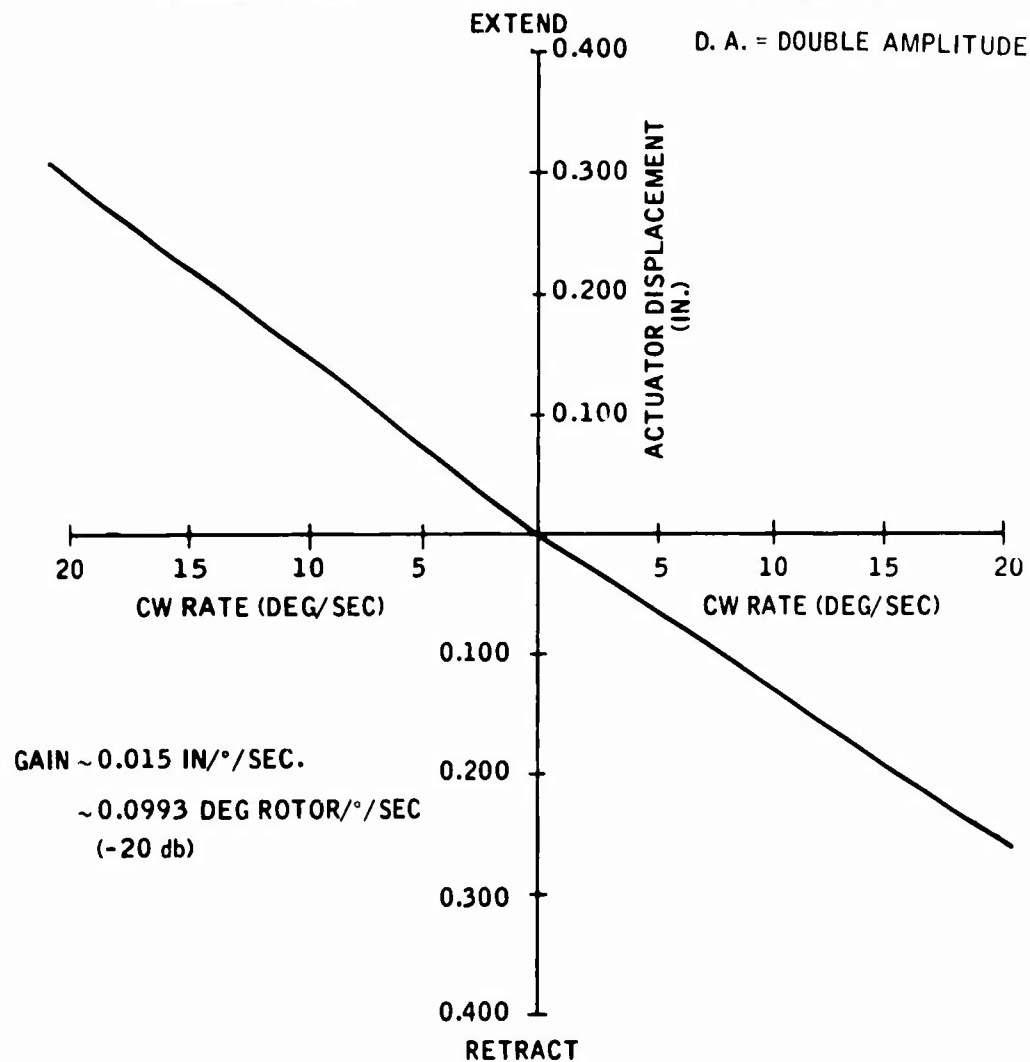


Figure 61. Shorted Hi-Pass System Gain

SHORTED HI-PASS SYSTEM GAIN

$t_f = 120^\circ\text{F}$ $P_b = 8 \text{ PSI}$

$P_a = 13 \text{ PSI}$ $P_s = 23 \text{ PSI}$

$Q_b = 0.95 \text{ GPM}$ $Q_t = 2.45 \text{ GPM}$

NULL NOISE = 0.025 IN. D.A.
 $\pm 0.083 \text{ DEG.}$

P_s = RATE SENSOR SUPPLY
PRESSURE

P_a = CASCADE POWER NOZZLE
SUPPLY PRESSURE

P_b = CASCADE RETURN LINE
PRESSURE

Q_b = RATE SENSOR PICKOFF
SINK FLOW RATE

Q_t = RATE SENSOR INPUT
FLOW RATE

D. A. = DOUBLE AMPLITUDE

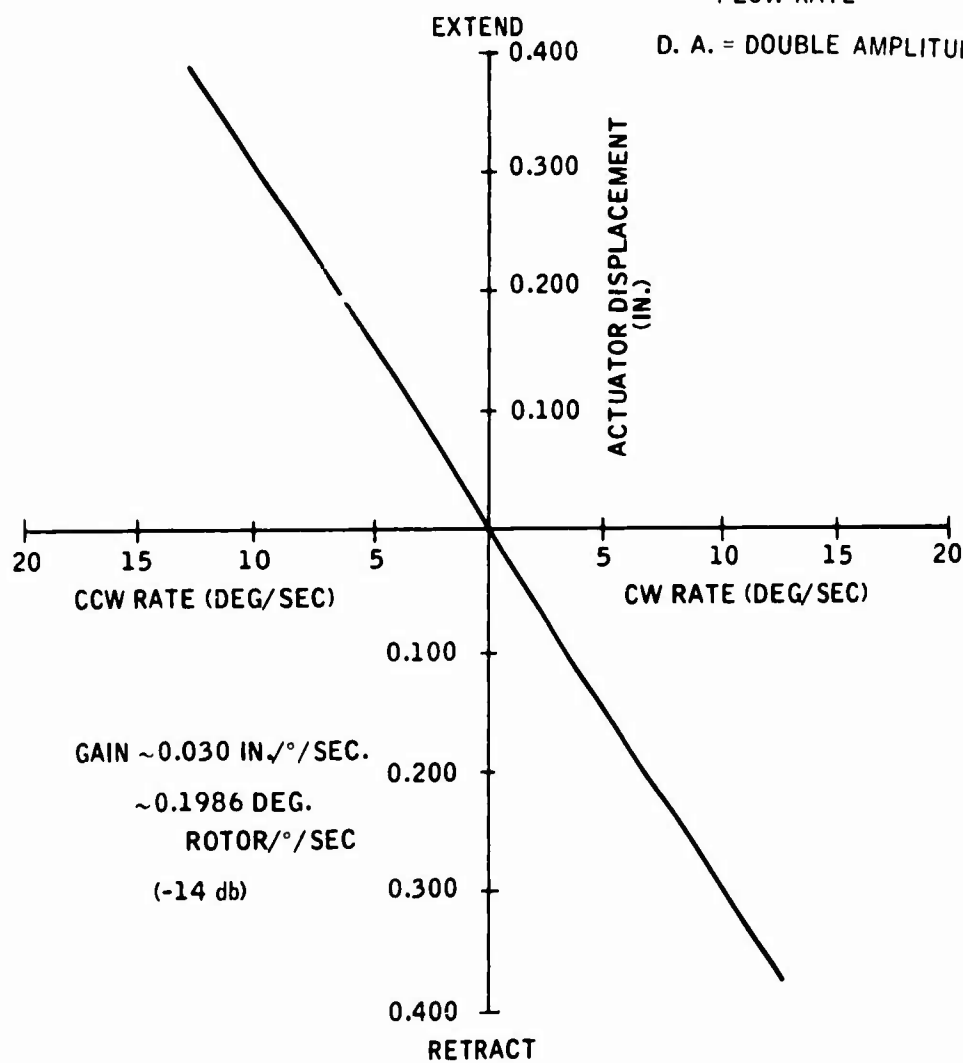


Figure 62. Shorted Hi-Pass System Gain

SHORTED HI-PASS SYSTEM GAIN

$t_f = 175^\circ\text{F}$ $P_b = 8 \text{ PSI}$
 $P_a = 13 \text{ PSI}$ $P_s = 5.1 \text{ PSI}$
 $Q_b = 0.95 \text{ GPM}$ $Q_t = 2.45 \text{ GPM}$
 NULL NOISE = 0.050 IN. D.A.
 $\pm 0.165 \text{ DEG.}$

P_a = CASCADE POWER NOZZLE
SUPPLY PRESSURE

P_b = CASCADE RETURN LINE
PRESSURE

Q_b = RATE SENSOR INPUT
SINK FLOW RATE

Q_t = RATE SENSOR INPUT
FLOW RATE

D. A. = DOUBLE AMPLITUDE

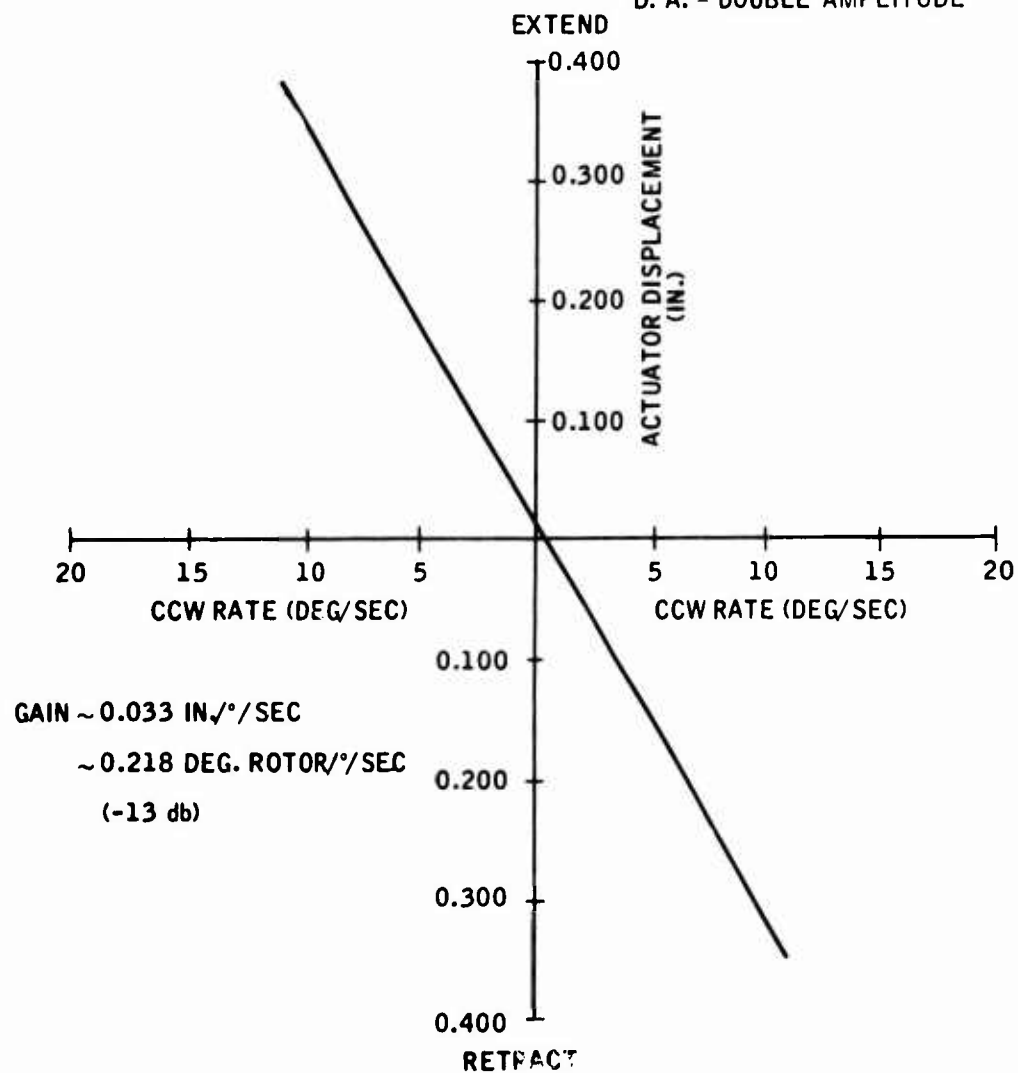


Figure 63. Shorted Hi-Pass System Gain

Dynamic Response

Frequency response tests were made on the system in the "shorted hi-pass" configuration to determine the effect, if any, of reduced pickoff sink flow rate on dynamic response. For these tests a sinusoidal input was programmed into the tilt table from the function generator. The results of these tests are shown in Figure 64. It should be noted that system loop gain is expressed in db for convenience. The test input signal was $\pm 2^\circ/\text{sec}$. Rates up to $\pm 10^\circ/\text{sec}$ were also applied in the frequency spectrum of 1.0 cps to 10 cps to cross check the $\pm 2^\circ/\text{sec}$ results. Good correlation was observed.

It is interesting to note that if the servoactuator phase from Figure 50 is subtracted from the phase results in Figure 64 at 5 cps, it is seen that the sensor contributes about 100 to 110 degrees of phase shift. The theoretical design of the rate sensor indicated 90 degrees of phase shift at 5 cps. This is considered to be satisfactory correlation between predicted and actual results. It also indicates that the estimated rate sensor transfer function for the analysis work was correct.

A tabulation of measured loop gain compared to design goal is shown in Table IX.

TABLE IX SHORTED HI-PASS SYSTEM LOOP GAIN		
Design Goal	Measured Result	Fluid Temperature (°F)
-16 ± 1.0 -1.5 db	- 20 db	75
	- 14 db	120
	- 13 db	175

Null Shift With Fluid Temperature Change

The system null shift was checked in the shorted hi-pass configuration. It was observed that negligible null shift would occur during a test period of several hours as long as the fluid temperature was stabilized. Whenever the fluid temperature was changed several degrees, the system null changed. Figure 65 illustrates this effect over a temperature range of 80°F to 125°F. The system was initially nulled at 120°F fluid temperature with the null adjust valve. It was noted, however, that since the fluid temperature changed slowly, there was no difficulty in re-nulling using the null adjust valve.

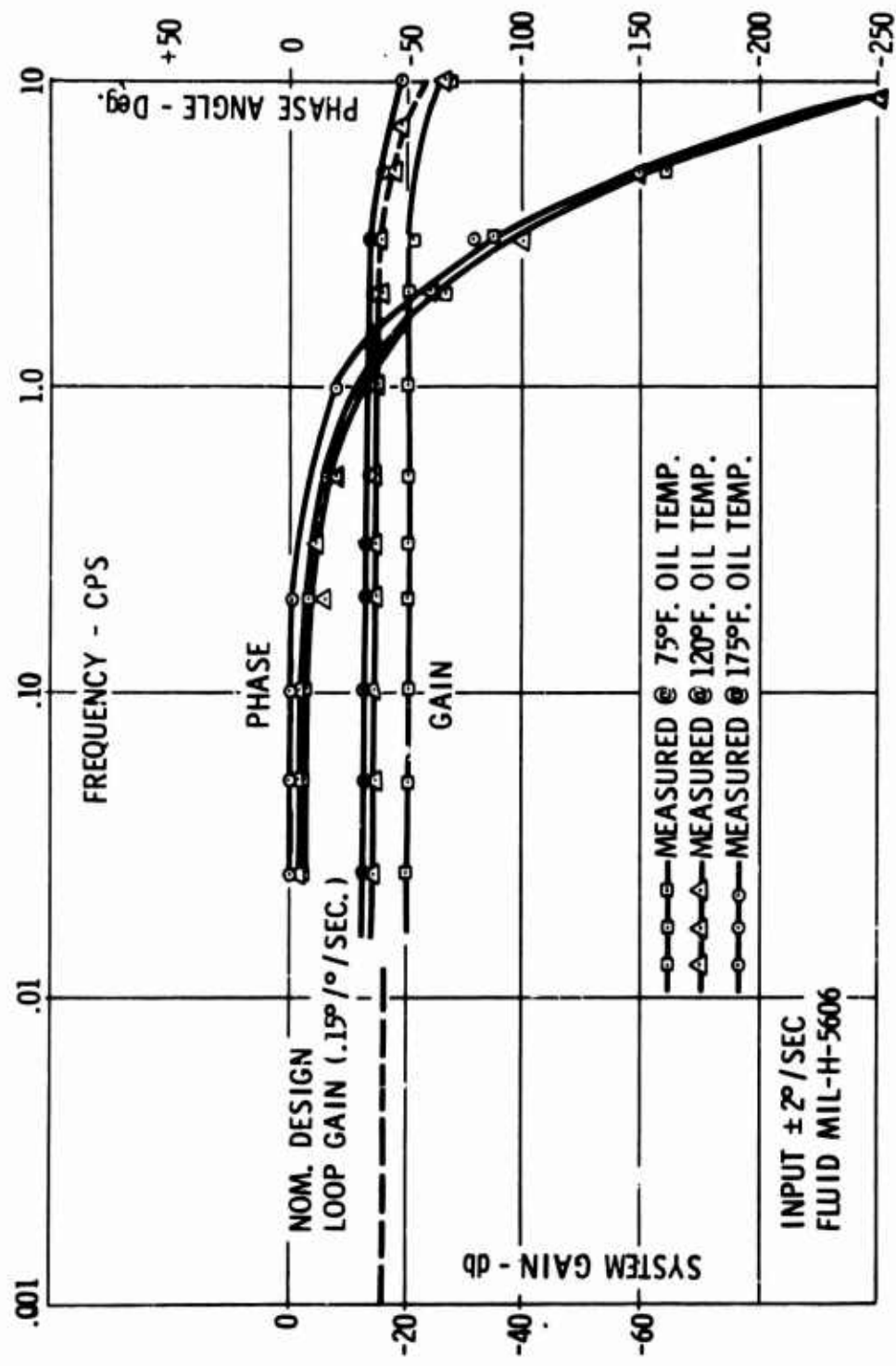


Figure 64. Shorted Hi-Pass Open Loop Frequency Response

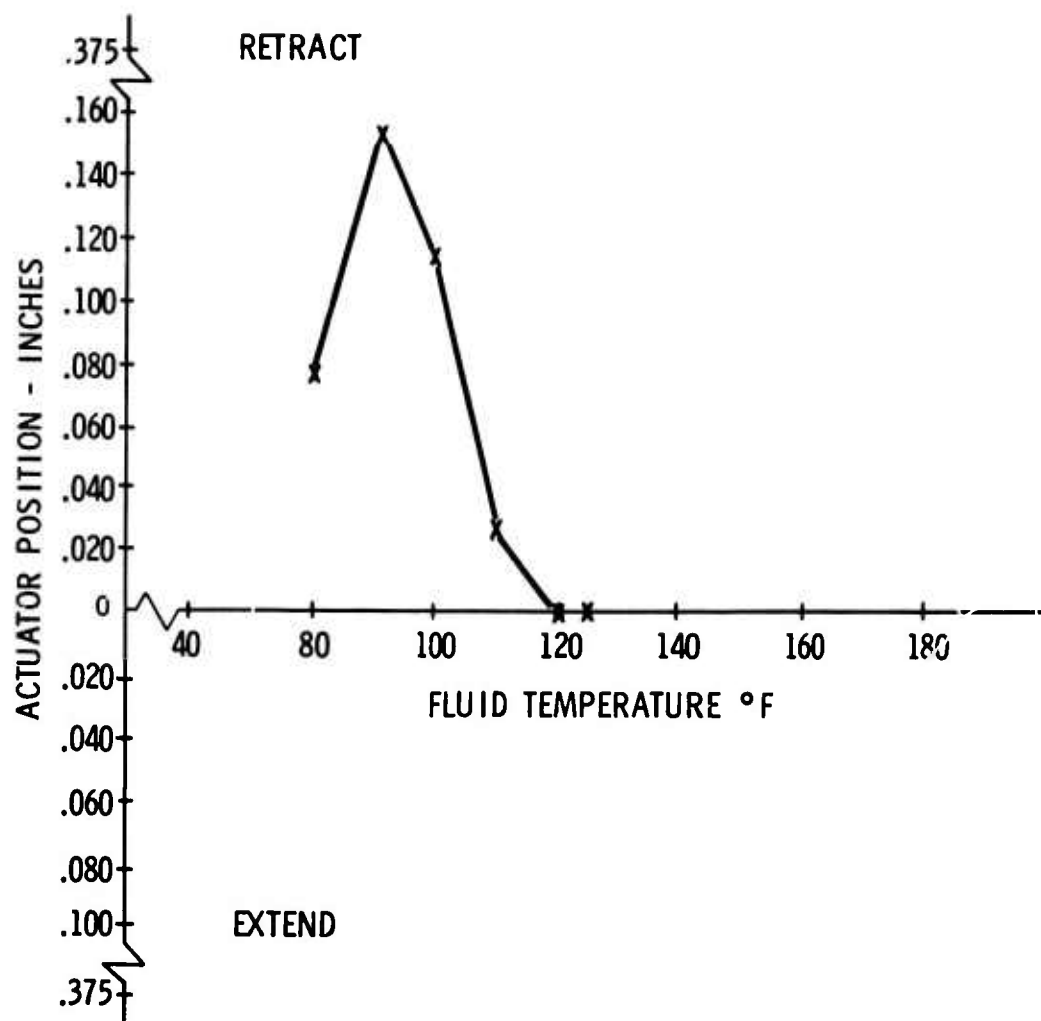


Figure 65. Shorted Hi-Pass System Null Shift Versus Fluid Temperature

It was concluded that for a straight-through gain cascade system, the pilot should be able to null periodically during the fluid temperature rise to equilibrium without difficulty.

Threshold

The system threshold test was conducted with the shorted hi-pass configuration. The threshold is defined in this case as the minimum signal necessary to produce the first controlled motion of the servo-actuator. This was observed at a rate input of 0.17 deg/sec, which was the low limit of the angular rate motion producing servo (tilt table). The servoactuator threshold at the test system loop gain was equivalent to 0.1 deg/sec input at the rate sensor. It is then seen that the rate sensor must equal approximately 0.07 deg/sec. It is believed that the rate sensor threshold is actually less than 0.05 deg/sec, but the low rate limit of the tilt table servo prevented precise measurement.

Since system threshold has been specified as an angular rate input, it should be recognized that the servoactuator's portion of the system threshold is dependent upon system gain.

Hi-Pass System Tests

The hi-pass system tests were conducted with the lag cascade connected parallel out-of-phase with the straight-thru cascade as shown in Figure 60. The same procedure used for the shorted hi-pass system testing was used during these tests.

Dynamic Response

Frequency response tests with a sinusoidal input were conducted at three different fluid temperatures. The results of these tests are shown in Figure 66. It should be noted that these responses are compared to the theoretical design goal as determined by the analog simulation. In a theoretical hi-pass system, the steady-state loop gain and dynamic loop gain (flat portion of gain response curve) are considered equal. In an actual case, this is true only if no difference in component loading occurs between the shorted hi-pass and hi-pass system configurations. Since the output amplifiers loaded each other somewhat during dynamic operation, the hi-pass system loop gain is lower than the shorted hi-pass system loop gain.

Table X shows a tabulation of loop gain compared to the design goal.

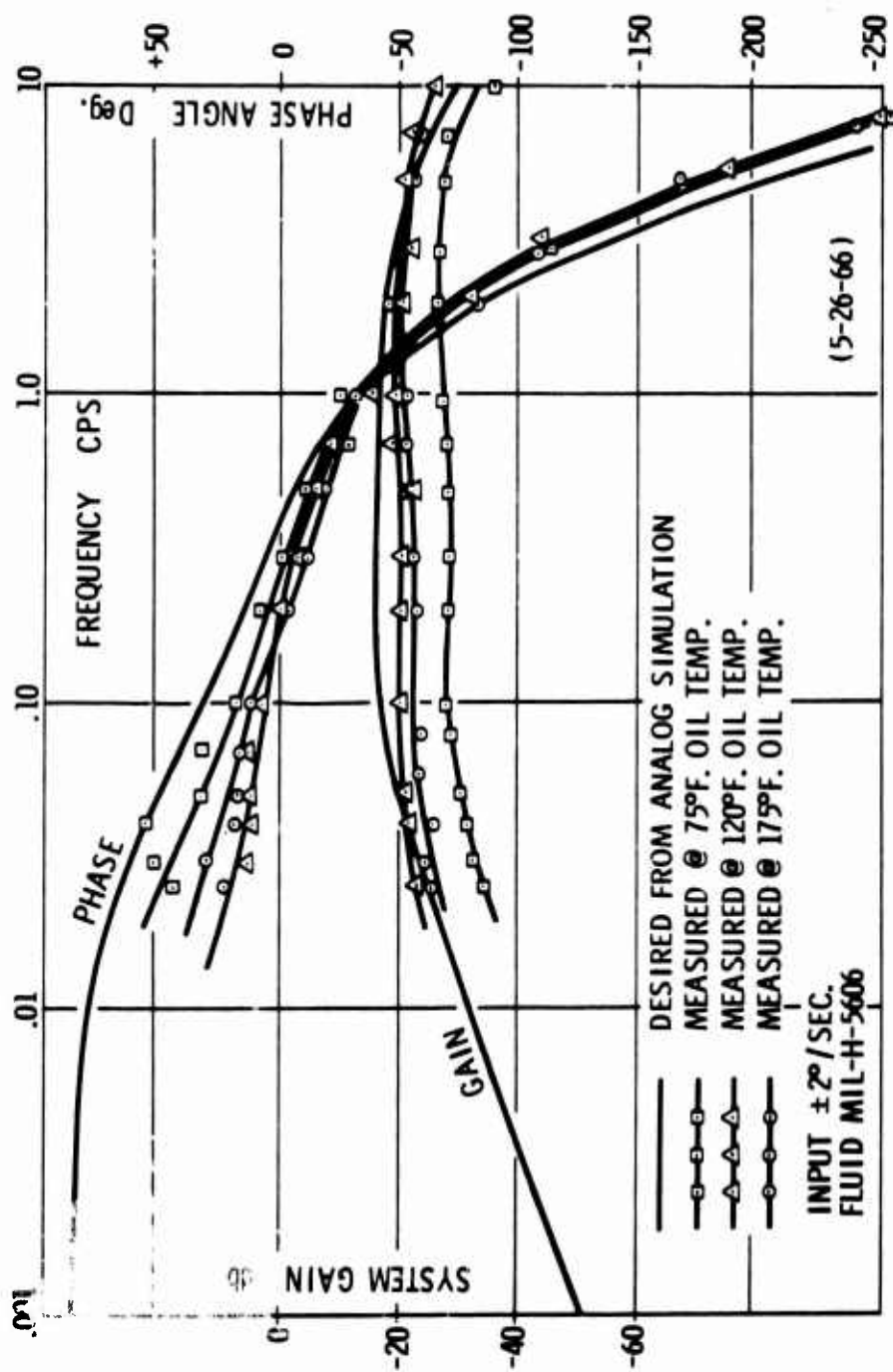


Figure 66. Hi-Pass Open Loop Frequency Response

TABLE X HI-PASS SYSTEM LOOP GAIN		
Design Goal	Gain at 1.0 cps	Fluid Temperature
-16 ^{+1.0} -1.5 db	-26 db	75° F.
	-19 db	120° F.
	-20 db	175° F.

It is noted that increasing the fluid temperature above 120° F. should have resulted in a slight increase in gain (120° F. fluid temperature point considered as nominal), as was seen during the shorted hi-pass configuration tests (Figure 64). The absence of loop gain increase is due to the fact that steady-state rate sensor output caused by temperature null shift was cancelled in the hi-pass, which used up hi-pass network linear range. The output amplifier was then shifted to a dynamic operating point in its non-linear region which washed out the effect of sensor gain increase from increased efficiency due to reduced oil viscosity.

The variation in loop gain resulting when the oil temperature is reduced from 120° F. is primarily due to the effect of increased oil viscosity on the component gains.

The dynamic responses shown in Figure 66 are considered to be quite good with respect to general curve shape as compared to theoretical requirements. It is noted that the nominal condition (120°F. oil temperature) gain is approximately 3 db below ideal theoretical gain. Considering that the hardware was designed using a mathematical design approach, a divergence of actual results and theoretical goal of 3 db would be considered as close agreement.

Although there was some scattering of points in the phase responses, no definite trend with respect to fluid temperature variation developed. The measured phase lag at frequencies above 1.0 cps was less than the theoretical phase lag because apparently the real system contains less hydraulic lags than those estimated for the theoretical system.

Null Shift with Fluid Temperature

Hi-pass system null shift with fluid temperature is illustrated in Figure 67. It is noted that the initial bias (120° F. temperature) was not adjusted out since it did not have any influence on the test. This bias or offset was only 0.064 inch out of a total actuator travel of 0.750 inch. Comparing the temperature null shift of the hi-pass system (Figure 67) with the temperature null shift of the shorted

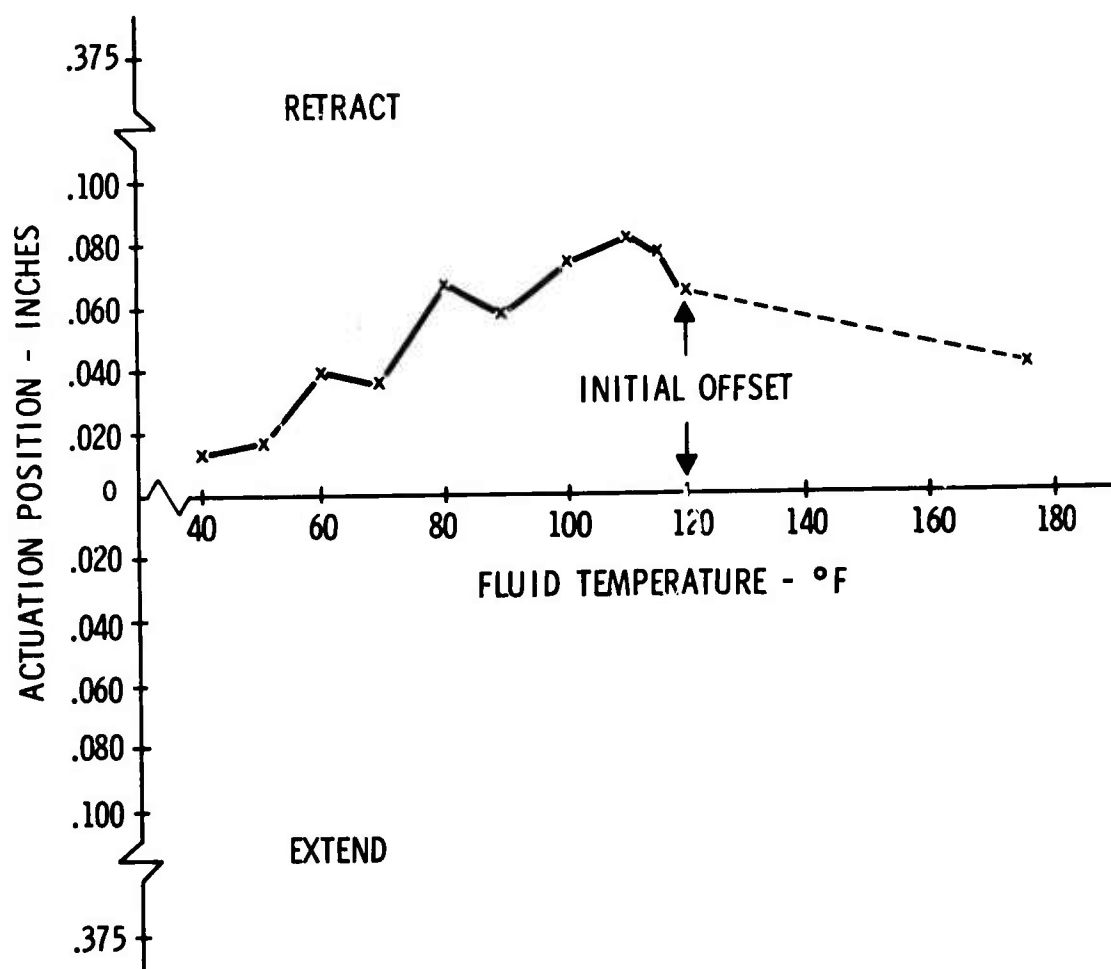


Figure 67. Hi-Pass System Null Shift Versus Fluid Temperature

hi-pass system (Figure 65), it is seen that the hi-pass network does a creditable job of cancelling rate sensor null shifts. Although no data was obtained on individual fluid amplifier temperature null shifts, it is believed that these must be quite small in order to obtain the system results shown in Figure 67.

The changes in actuator null are attributed to individual amplifier non-linearities (not readily noted on best straight-line gain plots), resulting in small output differences during subtraction of steady-state inputs.

CONCLUSIONS

Open-loop dynamic response was in reasonable agreement with the design goal at nominal conditions. The shape of the phase and amplitude response plots showed that the hi-pass function was achieved. The nominal condition loop gain was approximately 3 db below design goal due to unpredicted loading of the output amplifiers during dynamic operation.

Loop gain is affected by oil viscosity at oil temperatures below 100° F. This is primarily due to the viscosity temperature characteristic of the specified MIL-H-5606 fluid.

Fluid noise increased with fluid temperature although system loop gain did not necessarily increase. It is believed that the air content of the fluid may have a significant bearing on system noise.

The system threshold is believed to be less than 0.17 deg./sec. This could not be verified since the low rate limit of the test tilt table was approximately 0.17 deg./sec.

CLOSED-LOOP TESTING

SUMMARY

Closed-loop response testing at nominal conditions was conducted to determine damped aircraft response with the fluidic damper system engaged. The aircraft was simulated by an analog computer. A complete description of the test method and apparatus is presented.

Damped aircraft response recordings show that the fluidic damper met the design goal of improving the unaugmented aircraft damping ratio of approximately 0.35 to 0.60 when augmented.

DISCUSSION

The closed-loop testing was conducted using an analog computer to simulate the UH-1B helicopter. In this fashion the damper system performance in terms of damped aircraft response to disturbances could be evaluated.

Test Setup

Figure 68 shows a block diagram of the closed-loop test setup. The fluidic damper was mounted on a servo-driven tilt table. The vehicle equations of motion were programmed into the analog computer. The disturbance commands were a 10 ft/sec wind gust represented as a side-slip angle (β) and a 1-degree rudder step (θ_T). The β gust command was fed into the computer with initial conditions. The computer calculated the aircraft response to these inputs in terms of β (side-slip angle), $\dot{\psi}$ (yaw rate), ψ (yaw angle), and θ_T (tail rotor angle). The yaw rate signal ($\dot{\psi}$) was taken from the computer, modified to compensate for the tilt table dynamics, and then used to drive the table. The table drive servo was adjusted so that the table motions measured by a potentiometer and rate gyro were exact reproductions of the aircraft motions as calculated by the computer. Unaugmented aircraft performance was determined by opening up the electrical signal line from the fluidic damper to the computer (boost servo command). Augmented aircraft response was determined by feeding the fluidic damper servoactuator output electrically into the computer (boost servo command).

Photographs of the damper system and tilt table were presented previously on Figures 54, 55, and 56. Although the analog computer and recorders can be seen in the background on Figure 56, Figure 69 is a close-up view of the computer and recorders. Figure 70 is a block diagram of the analog computer setup. Table XI shows the potentiometer settings for the various flight conditions.

It should be noted that all tests were conducted with the roll axis fixed (pilot holding wings-level condition). To simulate this condition, the roll axis equations of motion were not applied to the analog computer.

Test Results

The system performance was measured at room ambient temperature with the oil temperature at 120° F. This was considered as nominal conditions. Aircraft response was measured at hover, 60 knots, 90 knots, and 120 knots. Since the hover condition is not meaningful

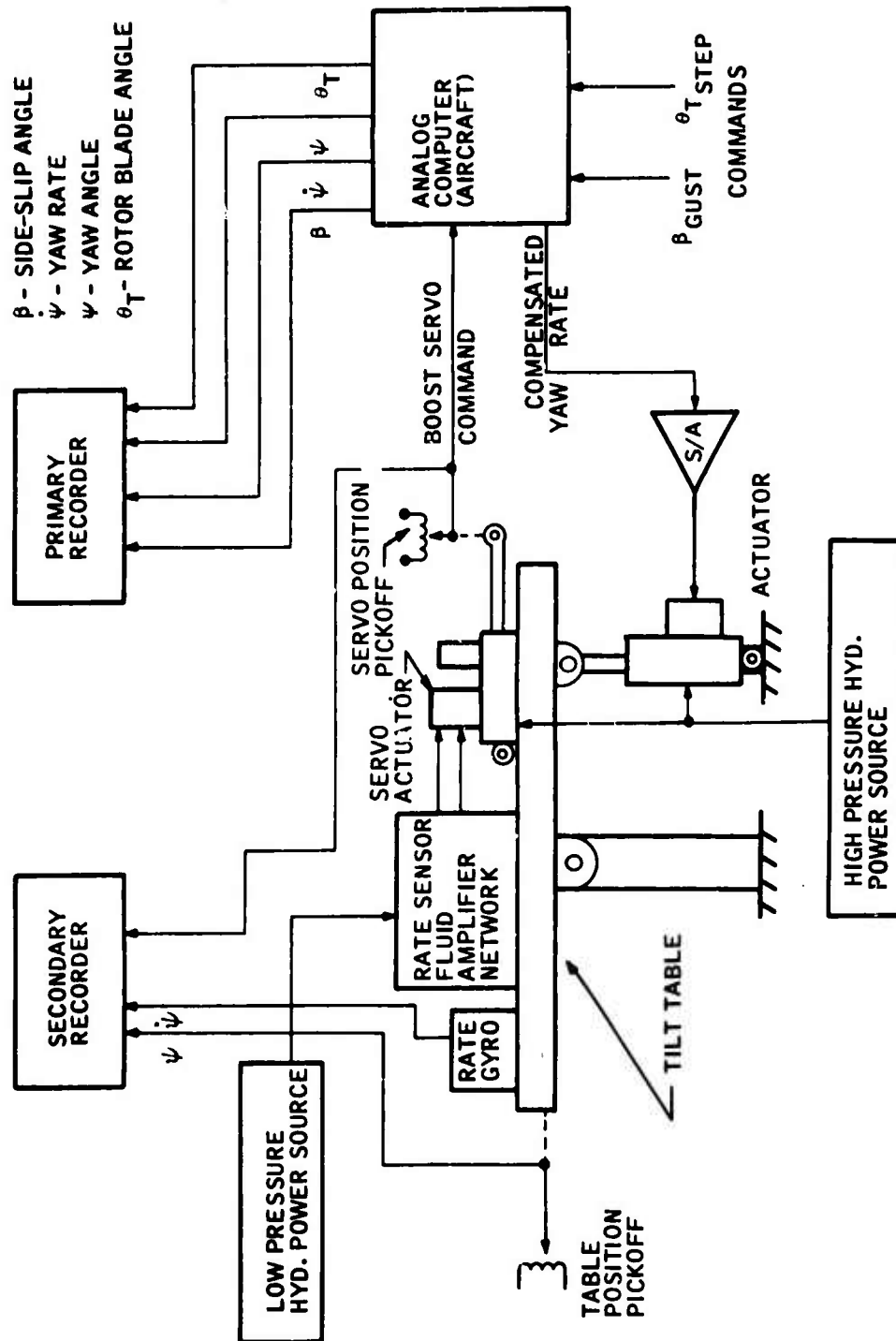


Figure 68. Closed Loop Test Setup



Figure 69. Analog Computer and Recorders

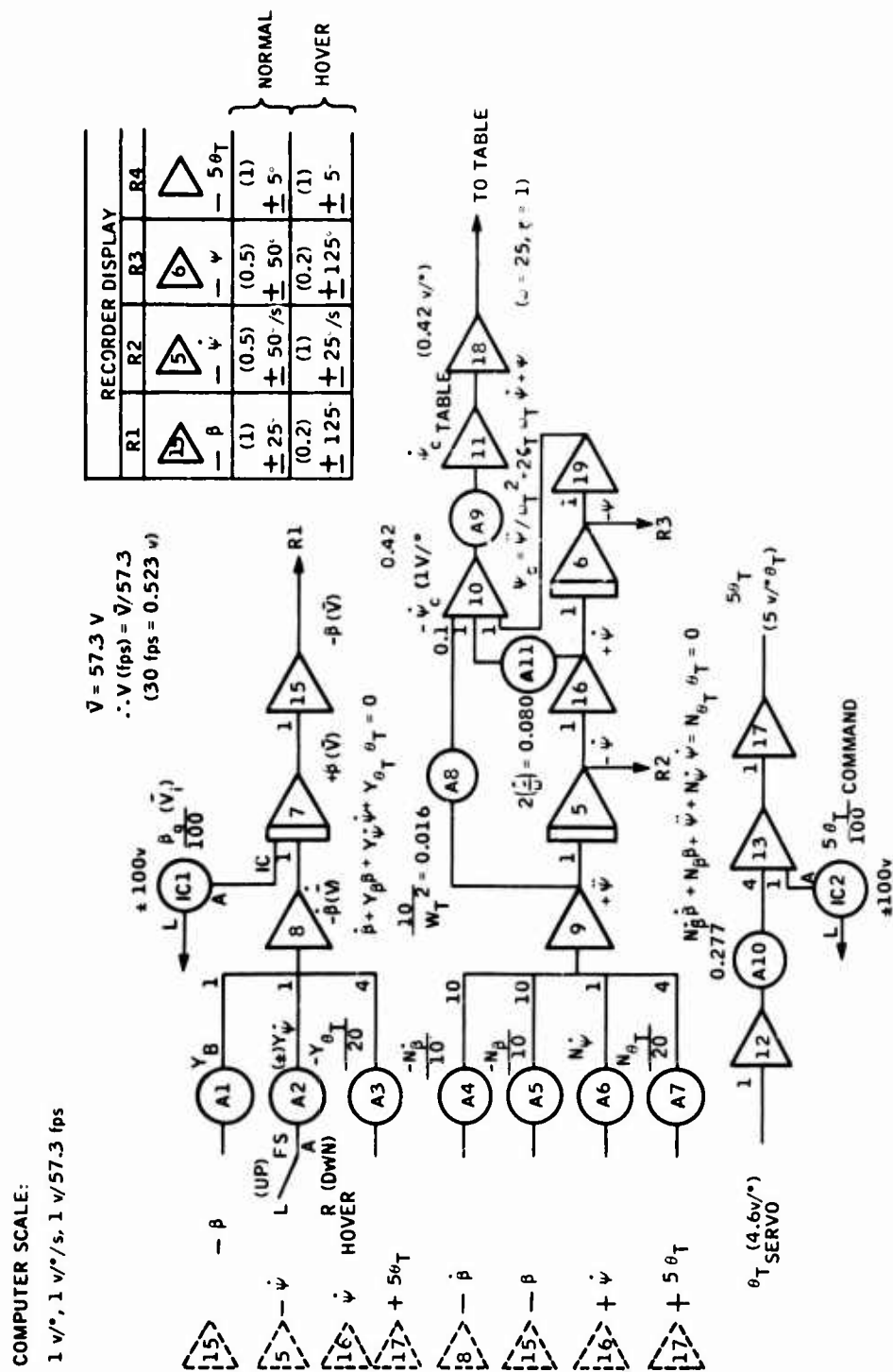


Figure 70. Block Diagram of Analog Computer Setup

TABLE XI POTENTIOMETER ASSIGNMENT SHEET ADM-1448									
Pot. No.	Parameter Description	Cond. Hover		Cond. 60 Kn.		Cond. 90 Kn.		Cond. 120 Kn.	
		GN	Set	GN	Set	GN	Set	GN	Set
A	1 $Y_{\beta} (C_{11}/b_{11})$	1	0.038		0.108		0.105		0.174
	2 $Y_{\psi} (C_{12}/b_{12})$	1	-0.775		0.990		0.990		0.993
	3 $-\frac{1}{20} Y_{\theta_T} (\frac{1}{20} C_{19}/b_{11})$	4	0.819		0.0102		0.0076		0.0068
	4 $-\frac{1}{10} N_{\beta} (\frac{1}{10} b_{21}/b_{22})$	10	0		0.129		0.155		0.173
	5 $-\frac{1}{10} N_{\beta} (\frac{1}{10} C_{21}/b_{22})$	10	0.0021		0.368		0.626		0.808
	6 $N_{\psi} (C_{22}/b_{22})$	1	0.684		0		0		0
	7 $\frac{1}{20} N_{\theta_T} (\frac{1}{20} C_{29}/b_{22})$	4	0.651		0.838		0.923		0.995
	8 $10/\omega_T^2 = 10/625$	1/10	0.016		0.016		0.016		0.016
	9 $(\psi_{TABLE}/\psi)_C$	1	0.42		0.42		0.42		0.42
	10 $(\theta_T/\theta_{SERVO}) \frac{1}{4} = 0.271$	4	0.277		0.277		0.277		0.277
	11 $Z(\zeta/\omega)_T = Z(0.9/25)$	1	0.080		0.080		0.080		0.080
B	12								
	1								
	2								
	3								
	4								
	5								
	6								
	7								
	8								
	9								
	10								
IC	1 $\beta_{9/100} (10 \text{ fps})$	1	0.173		0.162		0.108		0.081
	2 $\theta_{T \text{ command}} (10)$	1	0.05		0.05		0.05		0.05
	3								
	4								
	5								
	6								

in the absence of outer loop control, it has been omitted from this discussion. Only the three forward flight conditions are presented and discussed.

Figure 71 shows the augmented aircraft response compared to the un-augmented aircraft response for the 60-knot, 90-knot, and 120-knot forward flight conditions. The β response trace is used for evaluation of the equivalent second-order damping ratio.

In all three cases it can be seen that the augmented aircraft response has an equivalent second order damping ratio of approximately 0.60 or greater. Based on percent overshoot, the approximate damping ratios are tabulated in Table XII.

TABLE XII AIRCRAFT DAMPING RATIO TABULATION		
Vehicle Speed (knots)	Equivalent Second-Order Damping Ratio	
	Unaugmented Aircraft	Augmented Aircraft
60	0.35	0.62
90	0.32	0.60
120	0.38	0.70

*Design goal > 0.60 damping ratio

It is also seen from the rudder trace ($\theta_{T_{servo}}$) that the rudder noise is approximately 0.2 degree or less. It is noted that observation of the β and ψ traces indicates that the rudder noise appears to have little or no effect on the aircraft response.

CONCLUSIONS

The closed-loop response tests at nominal conditions show that the design goal of augmented aircraft damping of 0.60 or greater was achieved.

Rudder noise produced by the fluidic damper appears to have negligible effect on aircraft response.

BLANK PAGE

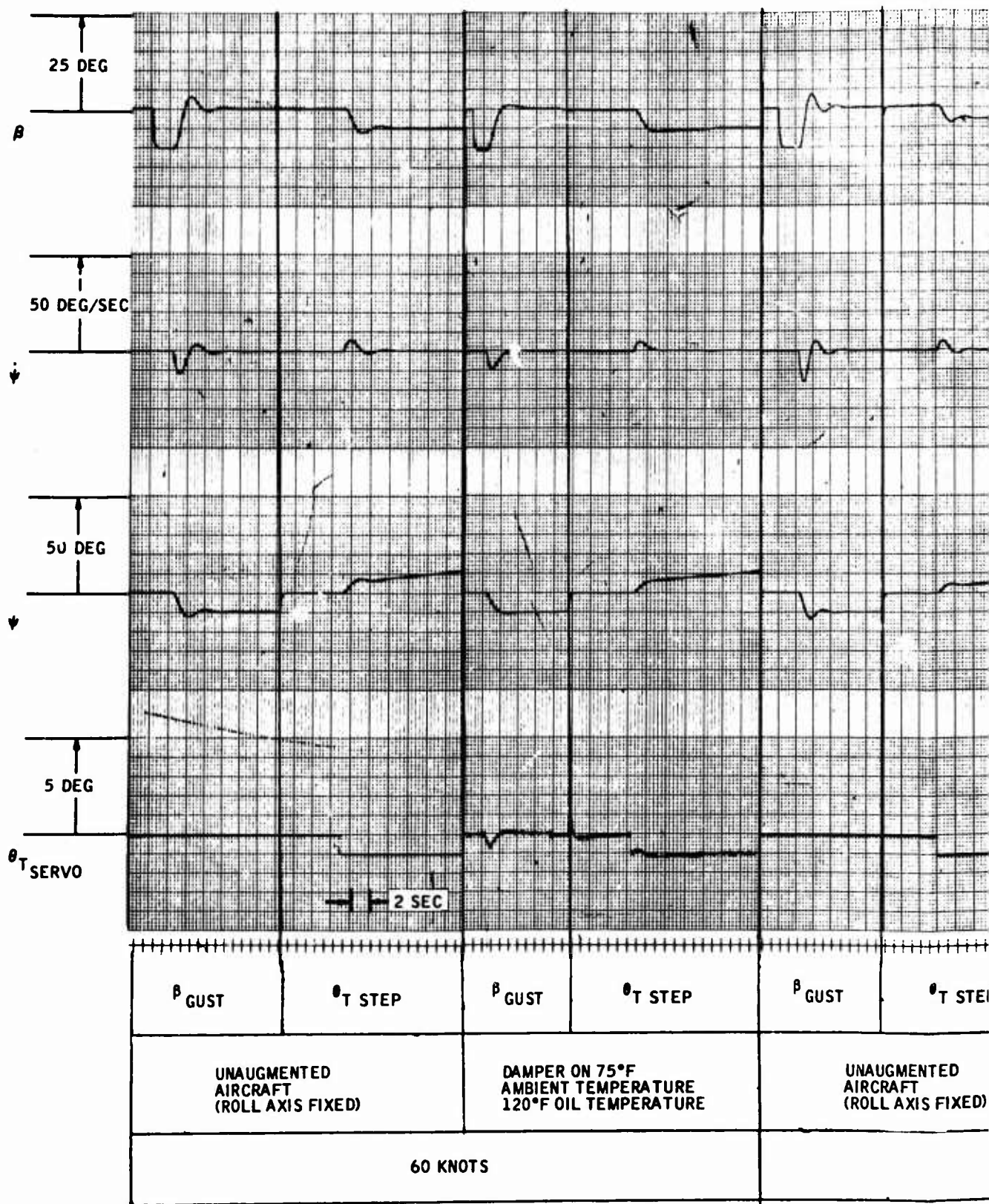
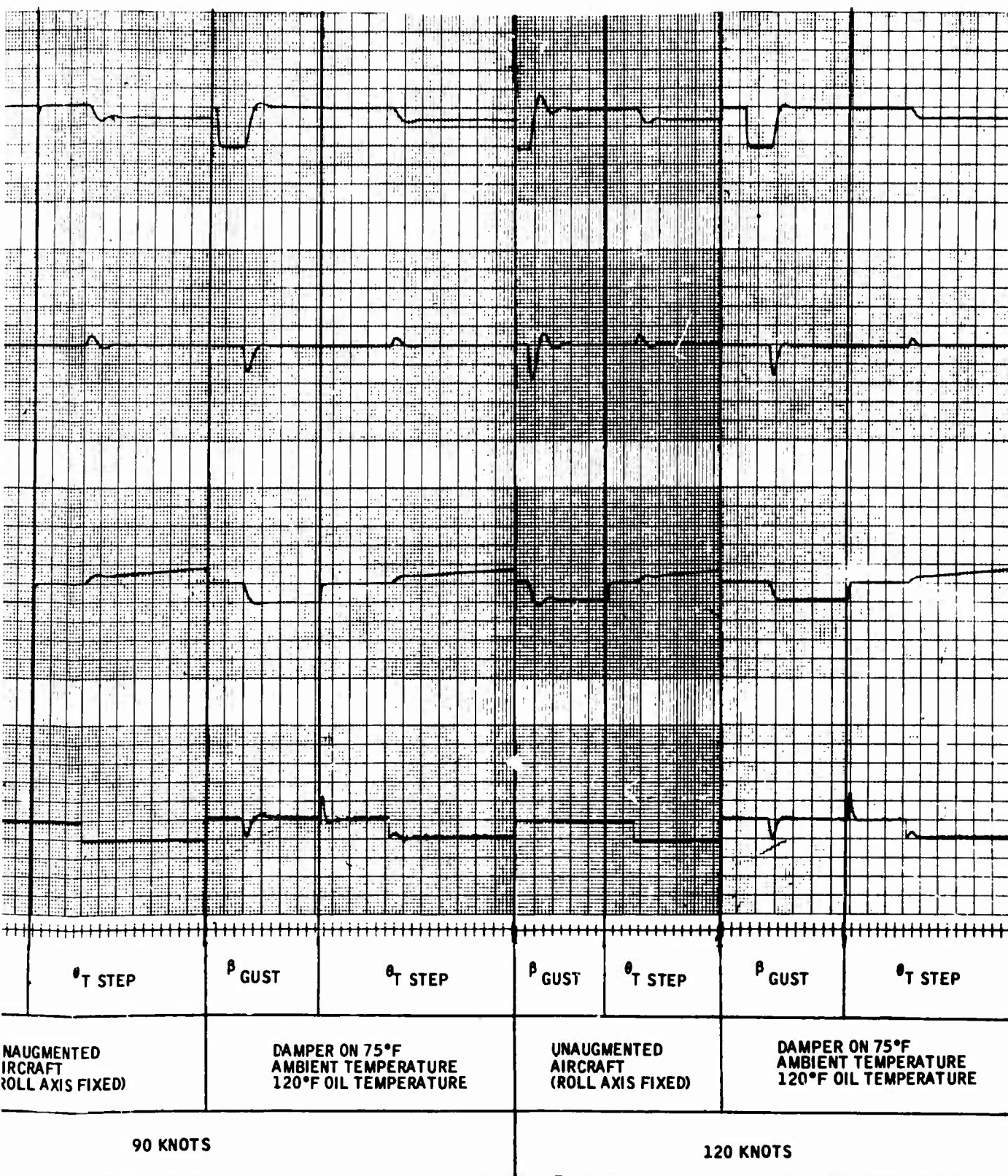


Figure 71. Closed Loop Res



ed Loop Response, Nominal Conditions

B

ENVIRONMENTAL TESTING

SUMMARY

Simulated -25°F flight day and 100°F flight day closed-loop performance testing was conducted. Augmented aircraft performance fell short of the design goal at the 60°F oil temperature condition, which represented the oil equilibrium temperature in the UH-1B on a -25°F day. Augmented performance met the design goal at oil temperatures above 80°F with a -25°F ambient. Design goal performance was achieved for the 100°F flight day.

Application of simulated aircraft vibration caused a 0.20-degree rotor offset but did not affect damped aircraft response.

Due to the breadboard nature of the damper system, the vibration scan results were inconclusive, other than that no damage resulted and system performance after vibration was the same as before the vibration.

DISCUSSION

The environmental testing consisted of the following items:

- Closed-loop response testing under simulated -25°F flight day conditions
- Closed-loop response testing under simulated 100°F flight day conditions
- Closed-loop response testing under nominal conditions with a simulated aircraft vibration applied to the fluidic damper apparatus
- Vibration scan at 0.1 inch double amplitude deflection from 0 to 20 cps and 2 g's acceleration from 20 to 500 cps in each of three mutually perpendicular axes.

Simulated -25°F Flight Day

The fluidic damper system mounted on the tilt table and the low pressure hydraulic power source were moved from the hydraulics laboratory to an environmental chamber. All other associated closed-loop test equipment, such as computer, recorders, etc., was moved to a location outside the chamber. The same procedure as used during nominal conditions closed-loop testing was employed.

The fluidic damper system and low-pressure hydraulic power source located in the environmental chamber were allowed to stabilize at a -25°F ambient temperature. The pump was started and closed-loop performance measured as the hydraulic oil heated up. The -25°F ambient temperature was maintained throughout the test.

Since the system hydraulic resistance varied as a result of viscosity changes, the input flow was controlled manually by a throttling valve between the pump discharge line and the fluidic system supply ports. During the course of the testing, this valve was adjusted only when the flow rate varied 4 percent off nominal. The flow was controlled manually since MS28886 aircraft hydraulic flow regulator valves could not be obtained to perform this function in time to maintain the program schedule.

Aircraft response was measured at various oil temperatures as the oil heated up. At oil temperatures below 60°F, there was no output from the fluidic damper due to negligible loop gain. This had been anticipated based on the open loop Bode plots at 75°F oil temperature.

Figure 72 shows the 60-knot flight condition with a comparison of unaugmented aircraft response and augmented aircraft response at oil temperatures of 60°F, 83°F, and 100°F.

Again using the gust response (β) for evaluation purposes, it is seen that at 60°F oil temperature, the augmented and unaugmented aircraft responses are virtually the same. It is noted from the rudder trace (θ_T) that there is only a very small rudder output with the damper on.

It is seen, however, as the oil temperature increases, that satisfactory augmented aircraft response occurs.

Table XIII shows a tabulation of approximate aircraft equivalent second order damping ratios based on percent overshoot.

The lack of augmentation at the 60°F oil temperature is attributed to insufficient loop gain. The low loop gain is due in part to increased oil viscosity reducing component gains plus the fact that the hi-pass network range has been used up in cancelling out rate sensor temperature null shifts. As hi-pass network range is used to cancel sensor null shifts, the dynamic operating points of the output amplifiers move out into their non-linear regions approaching saturation. When this occurs, dynamic loop gain becomes negligible. This situation could be corrected, however, by increasing the range of the hi-pass network.

Considering the boost system fluid temperature rise to equilibrium as a base, the 60°F oil temperature is equivalent to -25°F flight day operation. The 83°F oil temperature is equivalent to -2°F flight day operation, and the 100°F oil temperature is equivalent to 15°F flight day operation.

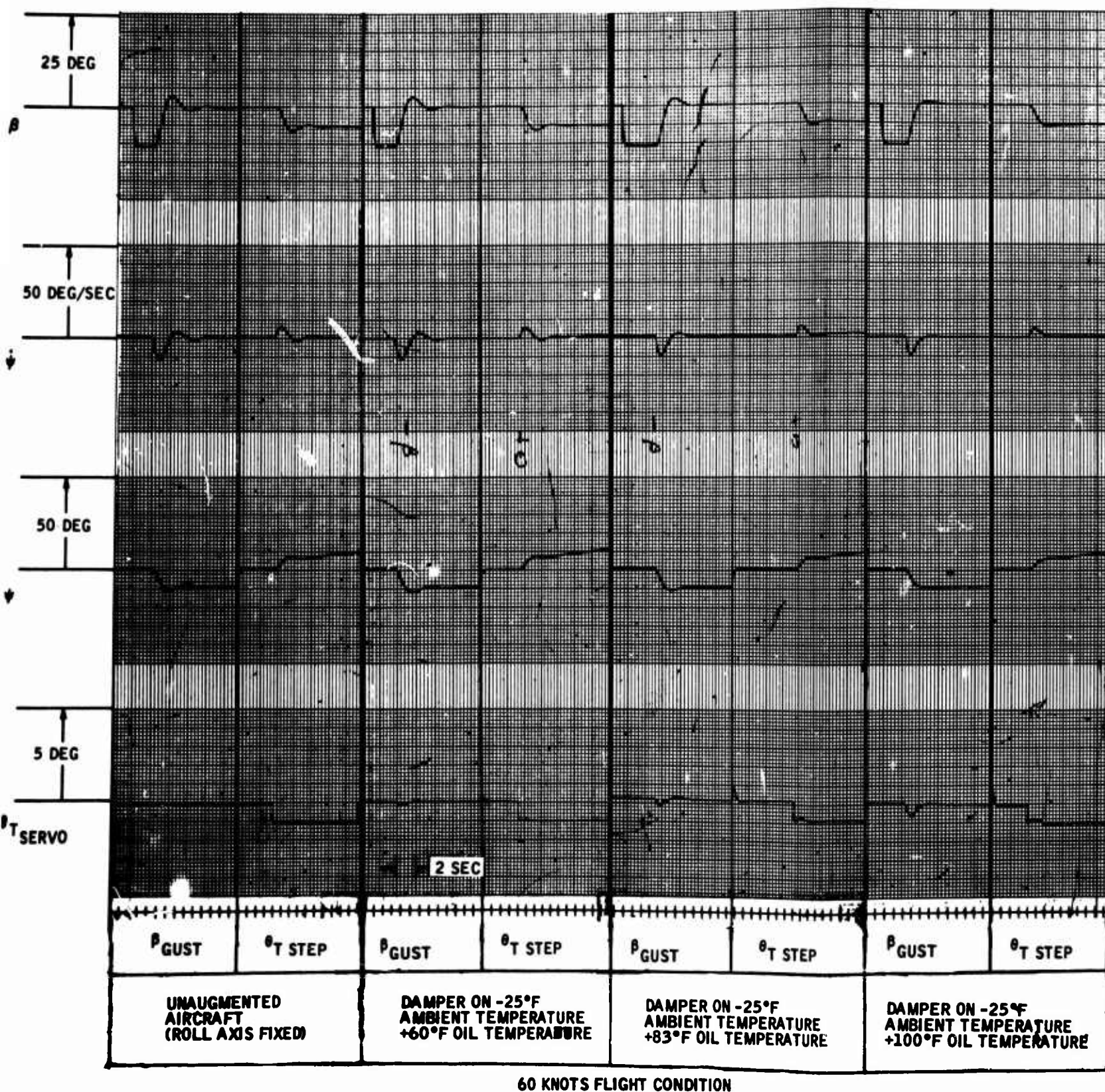


Figure 72. Closed Loop Response, -25°F Flight Day

TABLE XIII AIRCRAFT DAMPING RATIO TABULATION (-25°F Flight Day at 60 Knots)		
Oil Temperature (°F)	Equivalent Second-Order Damping Ratio	
	Unaugmented Aircraft	Augmented Aircraft
60	0.35	0.40
83	0.35	0.52
100	0.35	0.70

It is thus seen that the feasibility system with its current limitations can provide satisfactory performance down to a -2°F flight day condition.

The 90-knot and 120-knot conditions were also measured, and the responses were essentially the same as the 60-knot condition.

Simulated 100°F Flight Day

The same procedure as used for the -25°F flight day was used for this test except that the ambient temperature was held at 100°F and the input flow rate was permitted to vary up to 10 percent off nominal.

Figure 73 shows the damped aircraft response at oil temperatures of 125°F, 150°F and 180°F compared to the unaugmented aircraft. Using the gust response (β) for evaluation purposes, it is seen that the augmented aircraft equivalent second-order damping ratio is approximately 0.60 in all cases.

From the rudder trace (θ_T), it is seen that the noise varied from approximately something less than 0.10 degree to something more than 0.20 degree. It is noted that rudder noise appears to have little or no effect on damped aircraft response.

Table XIV shows a tabulation of aircraft damping ratios.

The oil temperature range from 100°F to 180°F is representative of UH-1B performance on the 100°F flight day. It is thus seen that the feasibility system provides satisfactory augmentation throughout this complete temperature range.

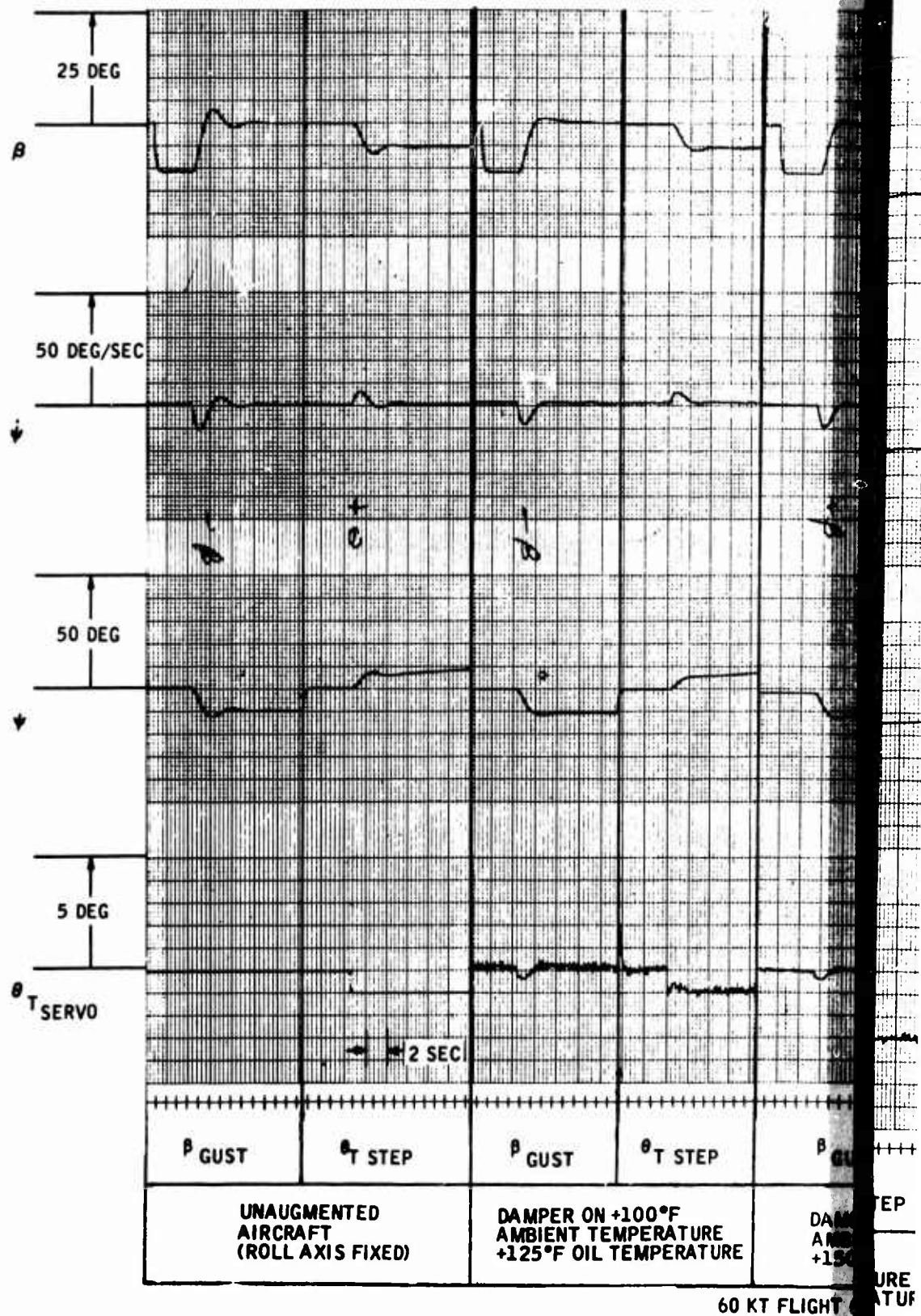
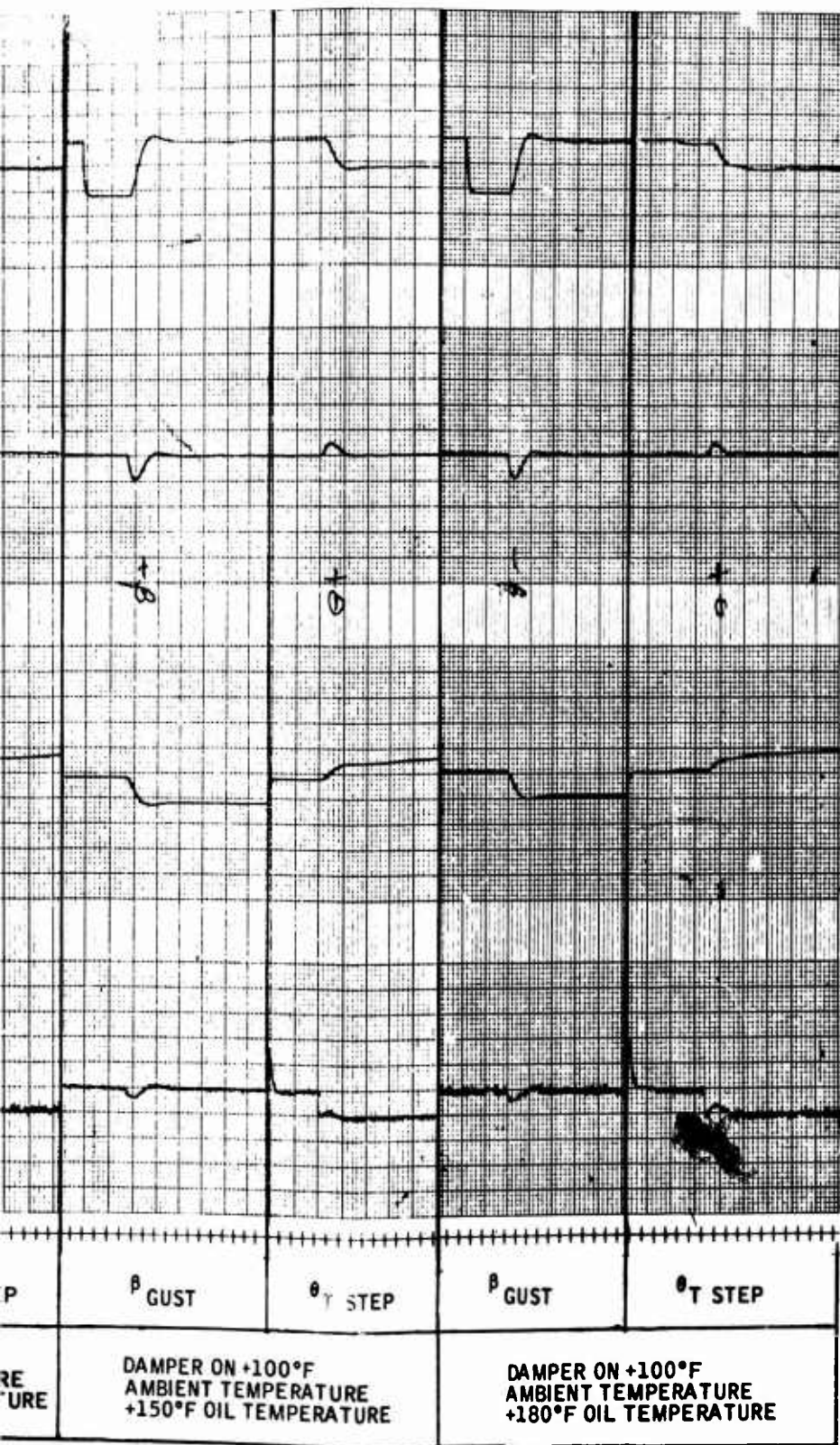


Figure 73. Closed Loop Response,

A



60 KT FLIGHT CONDITION

Response, 100 °F Flight Day

P

TABLE XIV AIRCRAFT DAMPING RATIO TABULATION (100°F FLIGHT DAY AT 60 KNOTS)		
Oil Temperature	Equivalent Second-Order Damping Ratio	
	Unaugmented Aircraft	Augmented Aircraft
125° F	0.35	0.60
150° F	0.35	0.60
180° F	0.35	0.60

It is also noted that by comparing the -25° F flight day performance with the 100° F flight day performance, it can be seen that the oil temperature is the controlling factor in obtaining satisfactory augmentation. Ambient temperature appears to have negligible effect on the system for similar oil temperatures.

Simulated Nominal Condition Flight with Simulated Aircraft Vibration

This test was performed in order to observe the effect of aircraft vibration on the fluidic damper performance. The same procedure as used for the nominal condition closed-loop response was employed except that an electric motor with an offset weight on its shaft was mounted to the stationary base of the tilt table. Operation of the motor applied a vibration perpendicular to the yaw axis of 0.25 g's at 29 cps. The motor can be seen behind the tilt table actuator in Figures 54 and 56. This level of vibration was considered representative of the measured vibration at the center of gravity on the UH-1B aircraft and was used for test purposes since it was anticipated that the fluidic damper would be near this location in the aircraft.

Figure 74 shows measured UH-1B vibration levels in the vertical mode. This data was provided by the Bell Helicopter Company, and it was stated that the vertical vibration was predominant in the aircraft.

A 120-knot flight condition was arbitrarily chosen for test purposes. Figure 75 shows the aircraft augmented response with and without vibration, compared to the unaugmented aircraft response. Here, again, it is seen that the augmented aircraft damping ratio is approximately 0.60 as compared to approximately 0.35 for the unaugmented aircraft. It is seen from the two augmented response traces that the vibration produced an offset of the tail rotor (θ_T) of about 0.20 degree. There also was a slight increase in tail rotor noise. Removal of the vibration removed the 0.20-degree tail rotor offset. Other than the tail rotor offset which could be trimmed out, the aircraft damped response appeared to be unaffected by the vibration.

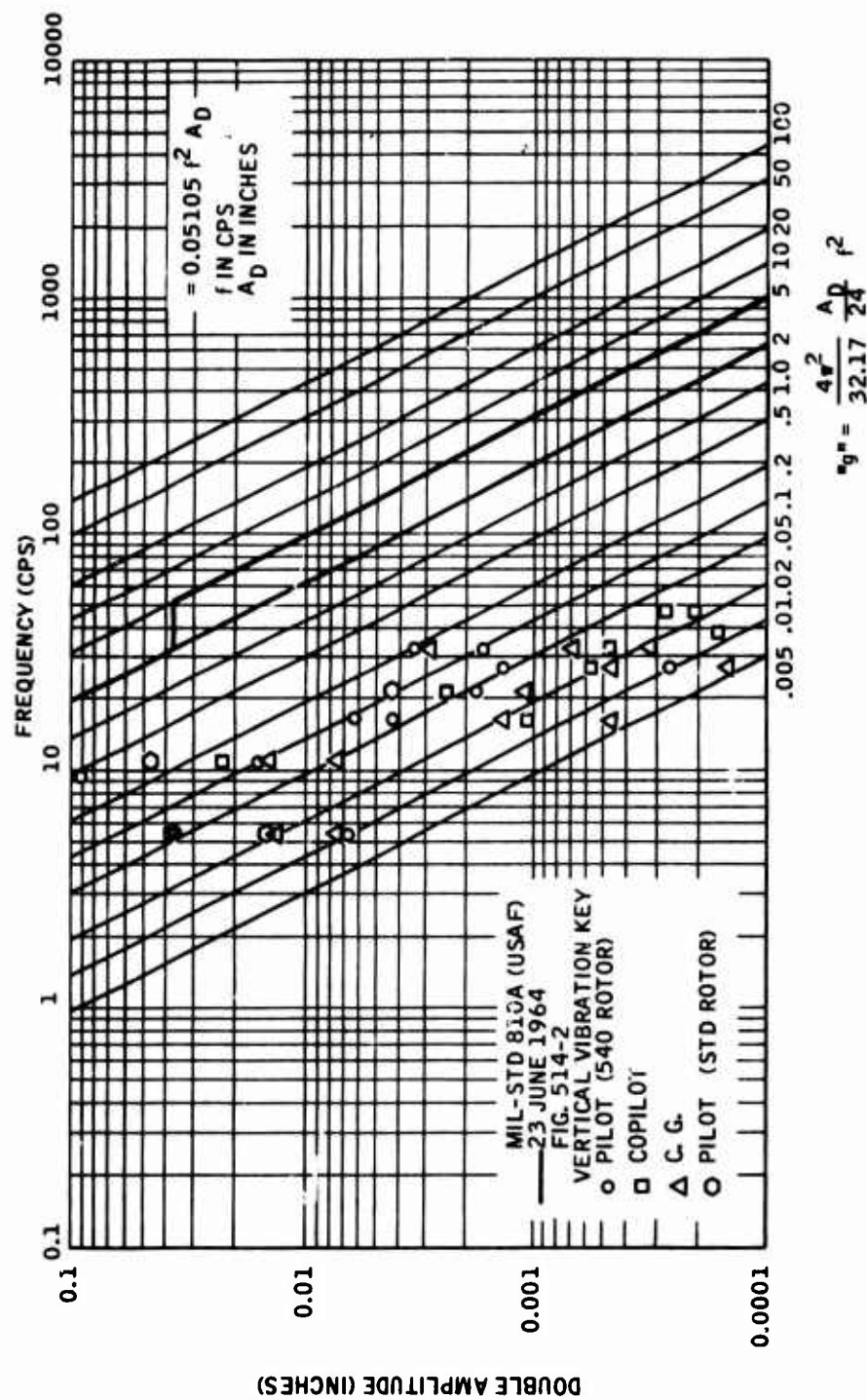


Figure 74. Measured UH-1B Vibration Levels

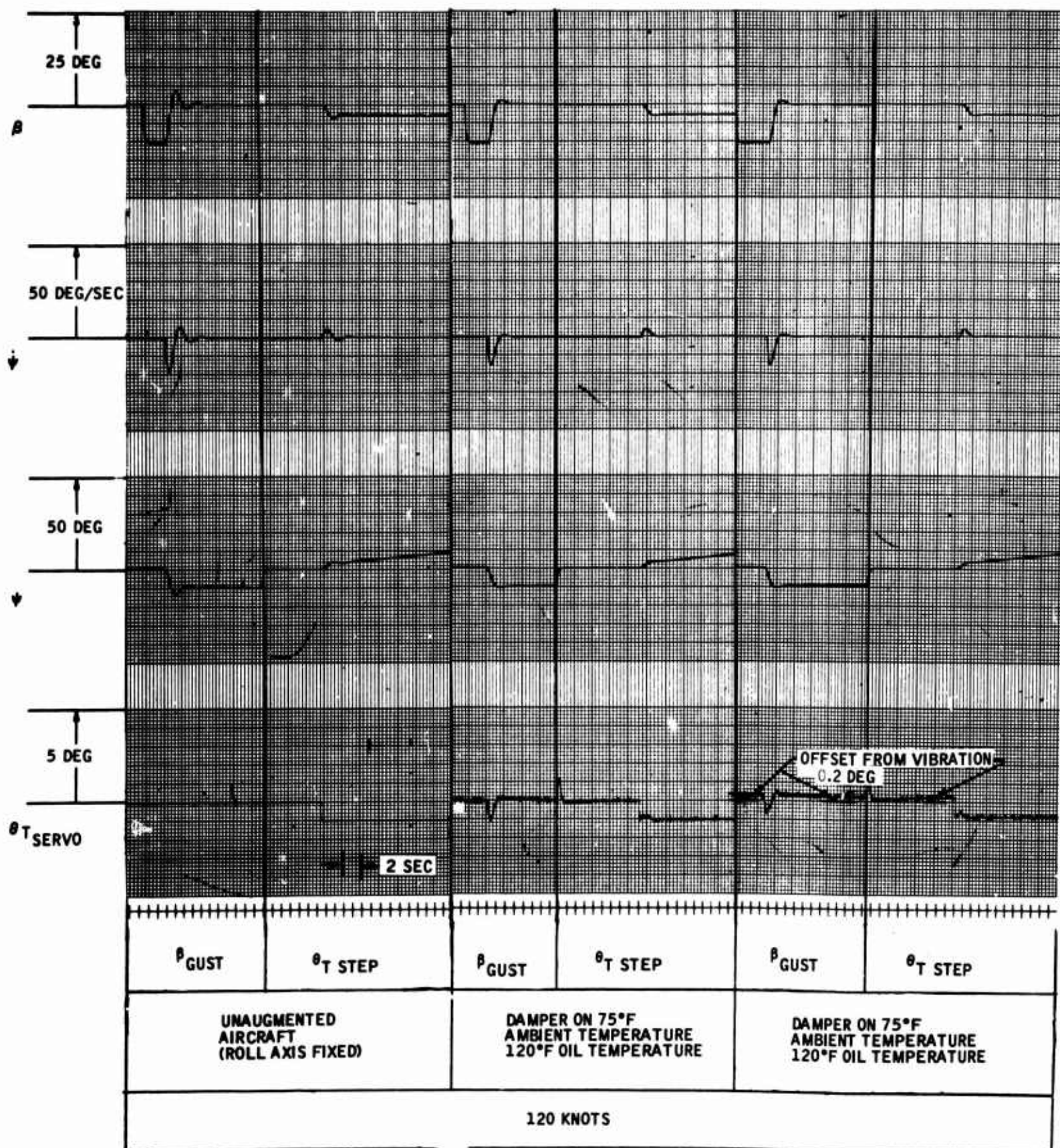


Figure 75. Aircraft Augmented Response With and Without Vibration Compared to Unaugmented Aircraft Response

It should be noted that this test was performed with the system exactly as shown in the photographs (Figures 54 and 55). No attempts were made to anchor any of the tubing. Since the pump unit was remote from the tilt table, the applied vibration caused vibrations of the damper main fluid supply and return lines. Since this was a breadboard arrangement and not representative of an aircraft installation, the cause of the 0.20-degree rotor offset could not be determined.

It was concluded, however, that the test results were encouraging in that as only the rotor offset occurred, it could be trimmed out, and damped aircraft response was essentially unaffected.

Vibration Scan

The fluidic damper was removed from the tilt table and mounted on a vibration fixture. The servoactuator was not vibrated and was mounted to a table adjacent to the vibration machine. Rubber hoses, approximately four feet long, connected the servoactuator to the fluidic apparatus. The tubing associated with the fluidic device was anchored to the mounted fixture with clamps and supports. The hoses from the pump discharge, system return, and servoactuator were not anchored due to the nature of the test setup. Here, again, it must be recognized that this was a breadboard system configuration and in no way is representative of an actual aircraft installation.

Fluid pressure was applied to the system and the servoactuator output was monitored. A vibration scan at 0.1 double amplitude deflection from 0 to 20 cps and 2 g's acceleration from 20 to 500 cps in each of three mutually perpendicular axes was applied. Referring to Figure 74, it is seen that the scan vibrations are significantly more severe than those occurring in the helicopter according to the Bell Helicopter Company data.

The results in all three axes were generally the same. At frequencies up to 20 cps, the vibration produced substantial motions of the hoses between the stationary-mounted servoactuator and the fluidic apparatus. Abnormal actuator piston excursions resulted when hose whipping occurred. Restraining the hose movement by hand substantially reduced actuator movement. As the scan progressed, abnormal actuator motion or offsetting was observed at frequencies of approximately 30 cps, 60 cps, 120 cps, 180 cps, 300 cps, and 500 cps. The maximum actuator movement incurred either by offsetting or wandering was equivalent to approximately 0.70 degree of rotor displacement. In all cases, the actuator returned to its original null when the vibration was removed. No physical damage was noted. System performance when tested after the vibration scan was the same as before the vibration scan.

No conclusions can be drawn as to the cause of actuator excursions during the test other than those caused by hose movements, since the system was in breadboard configuration to facilitate experimental feasibility testing and was in no way representative of an actual aircraft installation.

It can only be concluded that the breadboard system was not damaged by the vibration test. Also, meaningful performance data, when subjected to the vibration scan, can only be obtained with a system configuration and mounting that would duplicate the actual aircraft installation.

CONCLUSIONS

As a result of the environmental tests, the following conclusions are drawn:

- The -25° F flight day augmented performance was limited by the effects of oil viscosity and using up hi-pass network range in cancelling rate sensor temperature null shifts. This performance could be improved to be satisfactory down to 40° F oil temperature by providing increased range in the hi-pass network.
- The 100° F flight day performance was satisfactory.
- The 0.20-degree rotor offset incurred when simulated UH-1B aircraft vibration was applied could be trimmed out and did not appear to affect aircraft damped performance. Cause of the offset could not be determined due to the breadboard nature of the system.
- The results of the vibration scan are inconclusive other than that no physical damage resulted and system performance after the test was the same as prior to the test.
- Overall environmental test results were encouraging considering that this was a feasibility breadboard model system. The overall results show that the mechanization is feasible for helicopter flight control and that the problem areas uncovered should be solvable with further development effort.

CHAPTER 6

HYDRAULIC POWER SOURCE SYSTEM STUDY

SUMMARY

The fluidic damper system requires a low-pressure, constant-flow-type hydraulic power source due to its inherent "constant current" type operating characteristics. A power source of this type can be obtained using a constant displacement pump and standard AN or MS components connected as shown in Figure 76. This power source results in minimum vehicle engine loading. Utilization of the boost system hydraulic fluid provides equilibrium fluid operating temperatures within the design temperature range of the fluidic damper.

Overall installed system bulk and weight will be determined predominantly by existing MIL specifications covering aircraft hydraulic systems.

DISCUSSION

The UH-1B helicopter is equipped with two constant-pressure, variable-volume, high-pressure pumps. These pumps supply fluid to the dual boost hydraulic flight control system.

This type of hydraulic power source is not compatible with the fluidic damper system (except series servo), which requires a constant-volume, low-pressure hydraulic power source. Fluidic systems are basically "constant current" type systems (similar to open-center hydraulic systems), wherein the system pressure drop varies with the system hydraulic resistance as the input flow rate is held constant. Since the system hydraulic resistance varies with fluid viscosity, a constant-pressure hydraulic power source can be rarely used except in cases where the system hydraulic resistance can be held constant.

From the preceding discussion, it is seen that to operate over a broad fluid temperature range, the hydraulic power source system for the fluidic damper must be a low-pressure, constant-flow-type system.

DESCRIPTION OF HYDRAULIC POWER SOURCE SYSTEM

The constant-flow power source system is shown in schematic form in Figure 76. The power source consists of the following components:

1. Engine-driven dual-element pump
2. Safety relief valve
3. 10-micron filter

4. Supply line check valve
5. Accumulator
6. Rate sensor supply flow control valve
7. Fluid amplifier network supply flow control valve
8. Return line check valve
9. Three-way solenoid valve

The fixed displacement pump delivers supply fluid to the fluidic portion of the damper system. This pump is the second element of a dual-element pump (item 1). The primary or variable displacement element of the pump is the same as that currently used on the UH-1B helicopter. One of the current UH-1B pump suppliers has indicated that its UH-1B pump could be modified to include a fixed-displacement gear pump element on a common drive shaft with the mounting pad the same as the single-element UH-1B pump. This configuration would offer the cleanest installation, although a separate pump could be used if an additional drive quill was available.

The safety relief valve (item 2) is provided to limit the pump discharge pressure and to bypass pump flow not required by the system as the engine speed varies. The need to bypass excess pump flow results from having to size the fixed-displacement pump to provide adequate system flow at the minimum operational engine rpm.

The 10-micron filter provides contamination protection.

The check valves (items 4 and 8) provide a means of keeping the fluidic system full of fluid when the pump is not operating. The check valves also prevent fluid from draining out of the power source and/or rate sensor amplifier assembly during hydraulic maintenance or servicing operations.

The accumulator (item 5) is used to smooth out flow pulsations due to sudden changes in engine speed, if they occur. The hydraulic resistance of the 10-micron filter plus the inlet line check valve in conjunction with the accumulator makes up an RC type flow filter.

The flow control valve (item 6) provides a constant flow rate to the rate sensor regardless of changes in sensor internal hydraulic resistance and/or changes in upstream or downstream pressure.

The flow control valve (item 7) provides a constant flow to the fluid amplifier network regardless of changes in upstream or downstream pressure. The flow control valve can be used with this fluid amplifier network since all amplifiers use a common inlet pressure.

Figure 76 indicates the rate sensor-amplifier assembly to be a completely closed conduit system. With this configuration, the assembly can be checked and serviced as an end item and readily installed in

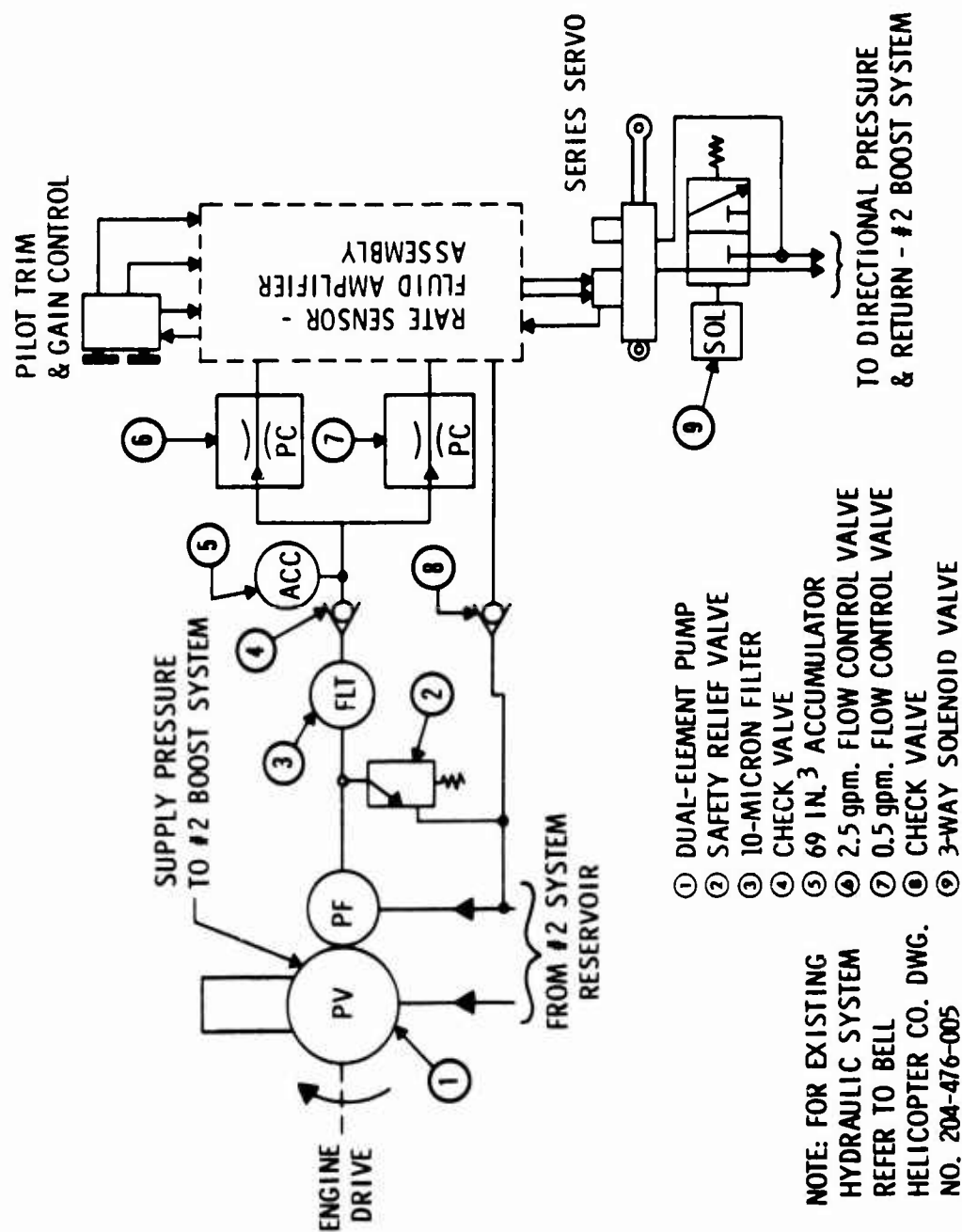


Figure 76. Proposed Hydraulic Circuit Yaw Damper System

the aircraft, as opposed to a previously contemplated configuration of having the assembly in a fluid-filled container.

The three-way solenoid valve (item 9) provides a means of engaging and disengaging the damper system. When the valve is energized, high-pressure fluid from the No. 2 boost system (directional control) is applied to the servoactuator which unlocks and is ready to operate in response to fluidic signals. With the valve in the de-energized position, the high-pressure fluid is blocked and the servoactuator pressure port is shorted to the return port. The loss of high pressure mechanically locks the servoactuator in its mid-position.

It should be noted that components such as check valves, relief valve, accumulator, flow control valves, etc., can be obtained as standard MS or AN hardware. The use of standard MS or AN hardware, wherever possible, will simplify the logistic support of the fluidic damper system since these items exist in the military inventories.

ESTIMATED POWER DEMAND

Since the fluidic system is a constant-flow type system, the power demand is continuous. The power demand for the system is calculated as follows:

$$\text{Power Demand} = \frac{\text{gpm} \times \text{pump } \Delta P}{\text{eff.} \times 1714} = \text{H. P.} \quad (3)$$

The following conditions are assumed:

- a. Flow rate = 3.0 gpm
- b. Efficiency = 85%
- c. Pump ΔP = 100 psi

The power demand is calculated to be:

$$\text{Power Demand} = \frac{3 \times 100}{0.85 \times 1714} = 0.206 \text{ H. P.} \sim 154 \text{ watts} \quad (4)$$

The 100-psi pump pressure is based on the sum of the anticipated component pressure drops from the pump outlet port to inlet port. These are 25 psid for the flow control valve, 2 psid for the 10-micron filter, 10 psid for the inlet and return check valves, 10 psid for hydraulic line loss, and 53 psid (at reduced temperature) for the rate sensor.

The series servo power demand is not included since it is the same for any augmentation system, whether it be electrohydraulic or fluidic.

FLUID TEMPERATURE CONSIDERATIONS

Data received from Bell Helicopter Company indicates that the hydraulic boost system reservoir fluid temperature stabilizes at +60° F. after 40 minutes of operation on a -25° F. flight day and at +185° F. after 40 minutes on a +100° F. flight day. Since the damper system draws fluid from the No. 2 boost system reservoir, it will be operating at these fluid temperatures which are within the damper system design goal fluid temperature range.

Performance degradation in the form of reduced loop gain, resulting in a lesser degree of augmentation, would be anticipated on the -25° F. flight day during the fluid warm-up period.

The standard hydraulic components of the system would not be materially affected by the fluid temperature range, as they would be qualified Type II (-65° F. to +275° F.) hydraulic system hardware.

ESTIMATE OF COMPONENT SIZES AND WEIGHTS FOR HYDRAULIC POWER SOURCE AND FLUIDIC DAMPER SYSTEM

In order to obtain a general overall view regarding the component sizes and weights for the installation of the fluidic damper in a UH-1B helicopter, an estimate of component sizes and weights is presented. It must be recognized that the fluidic damper installed in the aircraft would fall under the requirements of MIL-H-5440A, Hydraulic Systems, Aircraft; Design, Installation and Test Of. This specification and other specifications contained therein govern such things as fittings, hoses, tubing, type of connections, pumps, valves, filters, accumulators, etc. It is the general compliance with all these existing regulations that will primarily determine the complete damper system bulk and weight. For example, although the rate sensor and fluid amplifier network apparatus is small in size, with low weight, the package assembly size and weight will be determined largely by the input and output manifolds necessary to contain the required fittings (AN, MS, or NAS) and allow for proper connecting of hoses or tubing. Another factor controlling system bulk and weight is the hydraulic tubing required in cases where the servos are remote from the power source and also when pilot manual input controls (trim) are located remotely from the servo.

It should also be recognized that the system bulk and weight resulting from an actual installation may be significantly less than estimated since it may be possible to reduce tubing and number of fittings over that estimated, due to actual conditions permitting a more optimum installation than that assumed.

With this background in mind, Table XV shows a tabulation of system component estimated sizes and weights.

TABLE XV ESTIMATED COMPONENT SIZES AND WEIGHTS TABULATION		
Component	Estimated Size Envelope (dimen- sions in inches)	Estimated Weight (pounds)
Dual-Element Pump (this is approximately 3 lb. greater and 2 inches longer than current pump)	5 x 5 x 7	12.0
Safety Relief Valve (similar to MS 28893)	1 3/16 dia. x 5	1.0
Filter (MS 28720)	1 7/8 x 1 7/8 x 5	1.0
Accumulator (AN bladder type)	5 1/2 sphere	3.5
Flow Control Valve (similar to MS 28886-2.5)	1 1/8 dia. x 3 13/16	0.4
Flow Control Valve (similar to MS 28886-0.5)	1 1/8 dia. x 3 13/16	0.4
Check Valve (MS 28890)	1 1/8 dia. x 3	0.3
Check Valve (MS 28890)	1 1/8 dia. x 3	0.3
Solenoid Valve (Tactair series 600 per MIL-V-5529A)	1 13/16 x 2 3/8 x 5 17/32	1.5
Rate Sensor and Amplifier Assembly	8 x 5 x 4 (estimated repackaged design with input and output manifolding)	4.5
Servoactuator (HRM no. 85111200)	2 5/8 x 4 1/2 x 9 3/4	3.9
Pilot Trim Control	2 x 2 1/2 x 3	1.0
Trim Indicator	2 x 2 1/2 x 3	0.7
Hoses	15 feet of 3/8 dia. (power source to fluidic damper)	3.0
	40 feet of 1/4 dia. (rate sensor-amplifier package to servo plus cockpit trim control to fluidic system)	4.8
Fittings (AN, MS, and NAS)	----	6.0

With respect to additional hydraulic fluid requirements, the estimated fill volume for the fluidic damper system including lines is approximately 0.25 gallon. This would be about 2 pounds of additional weight. Assuming that the fluidic damper draws its fluid from the No. 2 boost system reservoir, this amount of fluid should be added to the reservoir after the fluidic damper fill procedure has been completed. This would then bring the No. 2 boost system reservoir back to its prescribed operational level. Since the fluidic damper system oil volume is essentially the same in the operative or non-operative condition, no additional reservoir capacity over and above the No. 2 boost system reservoir would be anticipated.

CONCLUSIONS

The hydraulic power source system described herein satisfies the "constant flow" type requirement. The hydraulic pump can be a single unit or incorporated as an element of the boost pump, if desired. Use of the constant-flow, low-pressure power source results in an estimated vehicle engine loading of about 0.20 hp as compared to about 2.9 hp if high-pressure boost fluid were to be reduced in pressure and used. The total damper system bulk and weight will be determined predominantly by compliance with the requirements of MIL-H-5440A, Hydraulic Systems, Aircraft; Design, Installation and Test Of.

CHAPTER 7

CONCLUSIONS

The following conclusions are drawn based on the data and results obtained during conduction of the program:

- A fluidic rate damper system, utilizing hydraulic oil, is feasible for helicopter flight control system mechanization.
- Gain variations of this fluidic damper system are primarily a function of the MIL-H-5606 oil viscosity-temperature characteristic, particularly at oil temperatures of less than 100° F.
- An increase in the hi-pass network linear range is necessary in order to achieve satisfactory aircraft augmented response in the oil temperature range of 40° F. to 70° F., without resorting to external oil temperature control means. Modifying the present system to hi-pass directly from the rate sensor without prior amplification and then building the required loop gain with downstream amplification should result in the desired performance improvement. This will allow the hi-pass to cancel rate sensor temperature null shifts without shifting the hi-pass output amplifiers into the non-linear portion of their gain curves.
- The simulated UH-1B aircraft appeared to be tolerant of the fluid noise encountered in this fluidic damper system. Causes of the fluid noise were not specifically defined during the program, although aeration of the hydraulic fluid in the laboratory low-pressure pump unit is suggested as a prime contributor.
- A low-pressure, constant-flow hydraulic power system can be added to the current vehicles using primarily standard AN and MS hydraulic components. The low-pressure pump could be incorporated into the high-pressure boost pump to form a dual-element unit to supply both boost oil and fluidic system oil, if modification of the engine transmission accessory drive pad to provide an extra pump quill was considered undesirable.
- The hydraulic rate sensor overall performance was considered to be very satisfactory. Temperature null shift (oil viscosity change) appears to be the primary problem. Although this situation could be accommodated with

increased hi-pass network range, further investigation to reduce temperature null shift would be desirable.

- The performance of hydraulic fluidic systems, using hardware of the same type as used in this system, can be predicted in advance of fabrication with reasonable correlation between actual performance and predicted performance.
- Fluidic control systems using hydraulic oil should be considered for other aircraft flight control applications and auxiliary control applications such as helicopter gunship armament pod control.

CHAPTER 8

RECOMMENDATIONS

The following recommendations for further work are submitted for consideration:

- Conduct a flight test program using the present breadboard fluidic damper system reconfigured to reduce gain variations with oil viscosity changes and repackaged to permit suitable aircraft installation.

A flight test program is required in order to evaluate system performance under actual operating conditions. Bench tests and simulated flights are certainly important in the development process but there is no substitute for actual flight test. This is due to the fact that simulations do not and cannot include all effects of actual vehicle operation, since many of these effects defy mathematical description.

- Conduct further investigation of fluid amplifier and rate sensor gain variations with oil viscosity change. This will yield data to permit refining the design performance prediction process to include these effects in a precise manner. Refinement of the performance prediction process will serve to further shorten the development process in that valid performance predictions will cover a wider range of environments than is now possible.
- Conduct investigations to determine the practical low limit of fluid noises in the hydraulic fluidic damper system.
- Conduct investigations to reduce temperature null shift in the hydraulic vortex rate sensor. Significantly improved performance in pneumatic rate sensors has resulted from investigations into fabrication techniques. It is believed that these same fabrication techniques could provide equivalent performance improvements in the hydraulic rate sensor.

APPENDIX I
FLUID STATE HYDRAULIC DAMPER

1.0 SCOPE

This specification defines the design requirements for a fluid state hydraulic damper. These requirements reflect the findings of design studies conducted under the U. S. Army Aviation Materiel Laboratories Contract DA 44-177-AMC-294(T) dated 24 June 1965. Necessary engineering records, drawings, tests, etc., shall be initiated to provide one breadboard system for delivery to the customer.

2.0 APPLICABLE SPECIFICATIONS AND REFERENCES

2.1 The following documents and the applicable specifications referenced therein shall apply to the Fluid State Hydraulic Damper to the extent specified herein:

2.1.1 Honeywell Document 5F-E-54, Fluid State Hydraulic Damper.

2.1.2 MIL-H-8501A, Helicopter Flying and Ground Handling Qualities, General Requirements For.

2.1.3 MIL-H-5606, Hydraulic Fluid, Petroleum Base, Aircraft, Missile, and Ordnance.

2.2 The Fluid State Hydraulic Damper shall be capable of satisfactory operation when exposed to the following environmental conditions:

2.2.1 Vibration - Per MIL-STD-810A, Helicopter Test Curve B.

2.2.2 Temperature - The system shall be able to start at -25°F ambient temperature with the fluid at -25°F and then operate satisfactorily with the temperatures ranging from -25°F ambient with the fluid at +40°F to +100°F ambient with the fluid at +240°F.

2.2.3 Supply Pressure Variations - The fluid state components of the system, excluding the power section of the augmentation servoactuator, will be subjected to a supply pressure variation of ± 10 percent from nominal. The augmentation servoactuator will be subjected to supply pressure variations normally occurring in the aircraft directional hydraulic power boost control system.

3.0 DESIGN REQUIREMENTS

3.1 General

- 3.1.1 The fluid state hydraulic damper shall be designed to demonstrate performance potential of a fluid-amplification stability augmentation system, utilizing hydraulic fluid, for Army V, STOL and rotary wing aircraft. The yaw axis of the UH-1B Helicopter shall be considered as the application for demonstration of performance potential.
- 3.1.2 The fluid state hydraulic damper shall consist of the following functional units:
 - 3.1.2.1 Yaw Rate Sensor - The yaw rate sensor provides differential pressure outputs which are proportional to the yaw angular rate of the aircraft.
 - 3.1.2.2 Preamplifier - The preamplifier accepts and amplifies the yaw rate sensor differential pressure output.
 - 3.1.2.3 Shaping Network - The shaping network accepts the output of the preamplifier, amplifies it, and shapes it according to the transfer function $\frac{TS}{1+TS}$.
 - 3.1.2.4 The trim control permits the pilot to supply a differential pressure signal to the servoactuator for cancelling out any null offsets introduced by the shaping network. A trim indicator in the cockpit will be required to sense and indicate steady-state pressure differentials at the input to the servoactuator.
 - 3.1.2.5 The servoactuator, mounted in series with the aircraft directional power boost servo, accepts differential pressure signals from the shaping network and trim control, and converts them to displacements of the power boost servo pilot valve.
- 3.1.3 Weight, bulk, and power consumption shall be optimized to the extent possible without compromising reliable and demonstrable functioning. Inter-unit connections shall be accomplished in a manner that will permit replacement of individual functional components.
- 3.2 Power Supply
 - 3.2.1 The input power to the system (except augmentation servoactuator) shall be a continuous flow of hydraulic fluid per MIL-H-5606 which is subjected to 10-micron (nom.) filtration. The power flow rate shall be 3.25 gpm (nom.) at a pressure of 40 psig (nom.) above the system return pressure.

3.2.2 The input power to the augmentation servoactuator shall be hydraulic fluid per MIL-H-5606 at a pressure of 1000 psig (nom.) which is obtained from the aircraft directional hydraulic power boost system.

3.3 Performance

3.3.1 All performance requirements in this section pertain to normal operating conditions. Normal operating conditions are defined as:

Ambient Temperature - $70^{\circ} \pm 2^{\circ}\text{F}$

Hydraulic Fluid Temperature - $100^{\circ} \pm 10^{\circ}\text{F}$

Hydraulic Fluid Pressure - Inlet, nominal per component spec., Return - atmos.

3.3.2 The yaw rate sensor shall meet the following performance requirements when supplied with a uniform flow rate of 2.5 gpm and connected to the specified load:

Load	One set of nozzles 0.025 inch square x 0.0375 inch long
Inlet Pressure	≤ 40 psig
Scale Factor	≥ 0.003 psid/ $^{\circ}$ /sec
Linearity	5% of full scale
Range	$\pm 60^{\circ}$ /sec
Threshold	$\leq 0.05^{\circ}$ /sec
Null Shift	$\leq 1\%$ of full scale
Response	Phase lag shall be no more than ϕ (deg) = $18 \times$ frequency (cycles per second), no amplitude amplification, and no more than 3 db attenuation below 3 cycles per second.

3.3.3 The preamplifier shall meet the following performance requirements when supplied with a uniform power flow rate at pressure of 11.4 psig and connected to the specified load:

Load	Two sets of nozzles 0.025 inch square x 0.0375 long connected in parallel
Power Flow	0.10 gpm (nom.)
Pressure Gain	≥ 2.18 psi/psi
Linear Range	± 0.30 psid
Saturation	≥ 2.50 psid

Bias $\leq 5\%$ of full signal

Response Phase lag $\sim 45^\circ$ at not less than 5 cps, Amplitude $\sim -3\text{db}$ at not less than 5 cps.

3.3.4 The shaping network shall meet the following performance requirements when supplied with a uniform power flow rate at a pressure of 11.4 psig and connected to the specified load:

Load	Deadhead
Power Flow	0.53 gpm (nom.)
Straight-Through Gain	≥ 16.5 psi/psi
Linear Range	± 2 psid
Null Output Pressure	$4.0 \begin{smallmatrix} +2.0 \\ -0.0 \end{smallmatrix}$ psig above return pressure
Saturation	$7.0 \begin{smallmatrix} +2.0 \\ -0.0 \end{smallmatrix}$ psid
Bias	$\leq 15\%$ of full signal
Response	$\frac{T_H S}{1 + T_H S}$
	$2 \text{ sec.} < T_H < 3 \text{ sec.}$

3.3.5 The trim control shall meet the following performance requirements:

Sensitivity	0.012 psi/ $^\circ$ dial
Resolution	≤ 0.1 psi
Linear Range	± 2 psi
Power Flow	0.15 gpm (nom.)

3.3.6 The servoactuator shall meet the following performance requirements:

Transfer Stage

P_c Quiescent Level (above R_c)	4 psig
ΔP_c (full control signal range)	± 2 psid
P_c Max. (above R_c)	10 psig
R_c Max.	50 psi

Actuator Stage

System Pressure	1000 psi
Stroke	± 0.38 in.
Piston Area	0.38 sq. in.
Output Force	380 lb (max.)
Centering Force	≥ 25 lb.
Threshold	0.4% max.
Rated Velocity	15 in/sec. no load
Dynamic Response	90° phase lag at 10 cps (min.) at 25% rated input
Hysteresis	2% of full stroke
Supply Proof Pressure	4500 psi
Burst Pressure	7500 psi
Return Proof Pressure	1000 psi
Neutral Leakage	0.12 gpm

- 3.3.7 The Fluid State Hydraulic Damper shall meet the following performance requirements:

Nominal Steady-State Gain (Shorted Hi-Pass)	<u>0.023 in. actuator defl. °/sec.</u>
Response	See Figure 77
Dynamic Range	25°/sec.
Linearity	20%

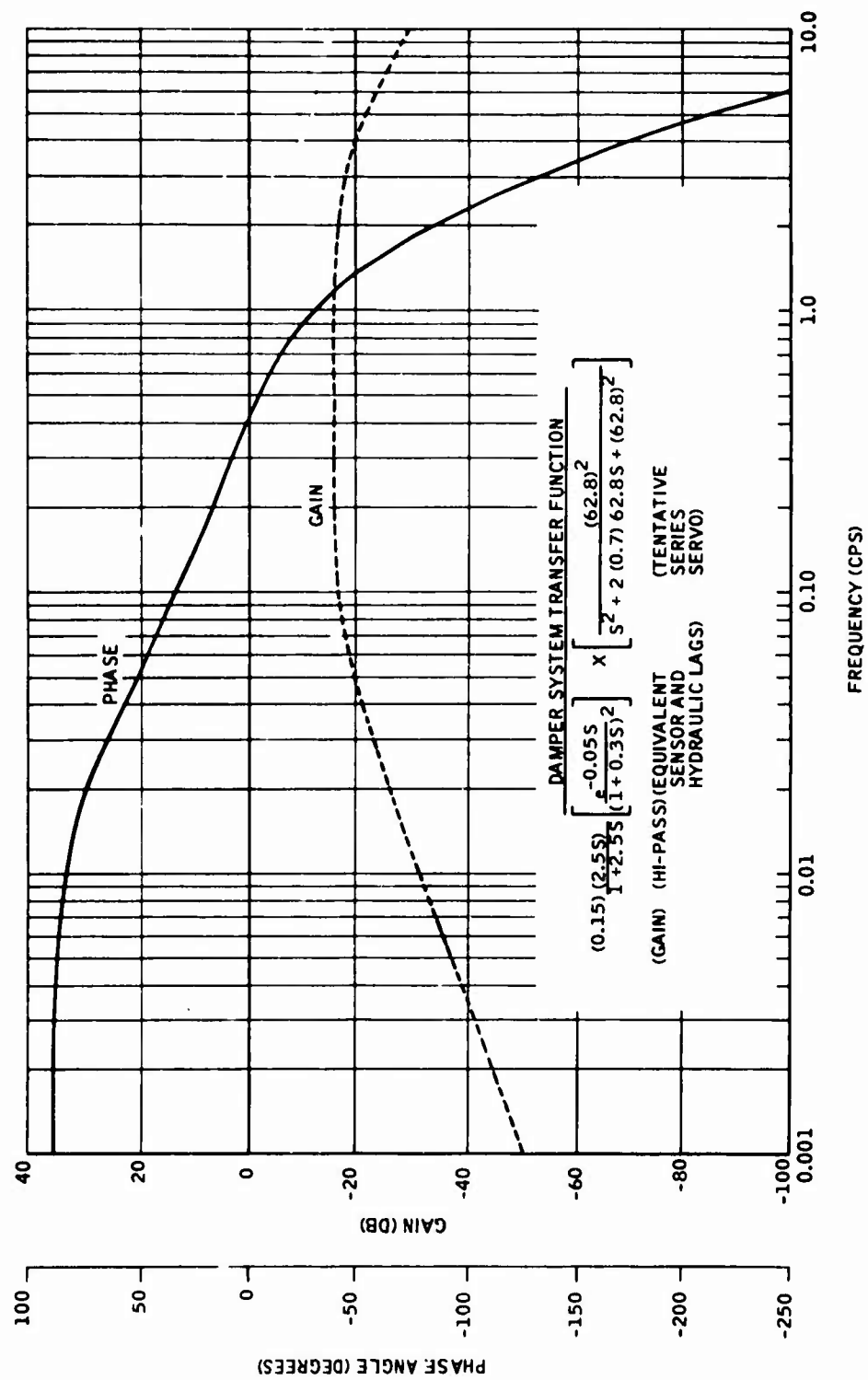


Figure 77. Damper System Response

Threshold	0.10°/sec
Aircraft Damping	≥ 0.6

3.4 Performance Under Environmental Test Conditions

The fluid state hydraulic damper and the individual functional units shall meet the performance requirements of Paragraph 3.3 when subjected to the environmental requirements of Paragraph 2.2, with the following exceptions:

3.4.1 Yaw Rate Sensor

3.4.1.1 During temperature tests, the null shift shall not exceed 10 percent of full scale output and the scale factor shall not vary from that obtained under normal conditions by more than ± 20 percent.

3.4.1.2 During pressure test, the null shift shall not exceed 2.0 percent of full scale output.

3.4.2 Preamplifiers

3.4.2.1 During temperature tests, the linear range shall not be less than ± 0.25 psid.

3.4.2.2 During pressure test, the bias shall be no greater than 6 percent of full signal.

3.4.3 Shaping Network

3.4.3.1 During the temperature test, the linear range shall not be less than ± 1.8 psid.

3.4.3.2 During pressure test, the bias shall not exceed 18 percent of full signal.

APPENDIX II

SYSTEM TEST REQUIREMENTS

1.0 OPEN LOOP, SHORTED HI-PASS TESTS

This set of test requirements is designed to measure the steady-state performance of the PFHD without the shaping network.

The pure fluid hydraulic damper (PFHD) shall be mounted on a tilt table as shown in Figure 78 with the output of the lag section of the shaping network disconnected from the system and blocked off. The system supply pressure, supply flow rate, tilt table angular displacement and/or rate, and augmentation actuator position shall be monitored and continuously recorded while performing the following tests:

1.1 Gain, Range, and Linearity

The system shall be trimmed to null prior to starting the test run. Uniform angular rates (of sufficient duration to secure accurate measurements) varying from 0°/sec to +20°/sec. shall be applied to the tilt table. Angular rates shall be applied in 2°/sec increments. The plot of actuator displacement versus table angular rate shall be compared with the Technical Development Specification (TDS) requirements.

1.2 Threshold

Angular rates varying sinusoidally at a frequency of not more than 0.01 cps shall be applied to the tilt table and the minimum angular rate amplitude which produces a detectable displacement of the actuator shall be noted and compared to the requirements of paragraph 3.3.7 of the TDS.

1.3 Null Drift

The purpose of this test is to determine the long-term drift characteristics of the system with the hi-pass network (shaping) shorted and when operating at nominal conditions.

With the system initially adjusted to null and zero angular rate applied to the tilt table, the servo-actuator displacement shall be continuously recorded during a one-hour-duration test period.

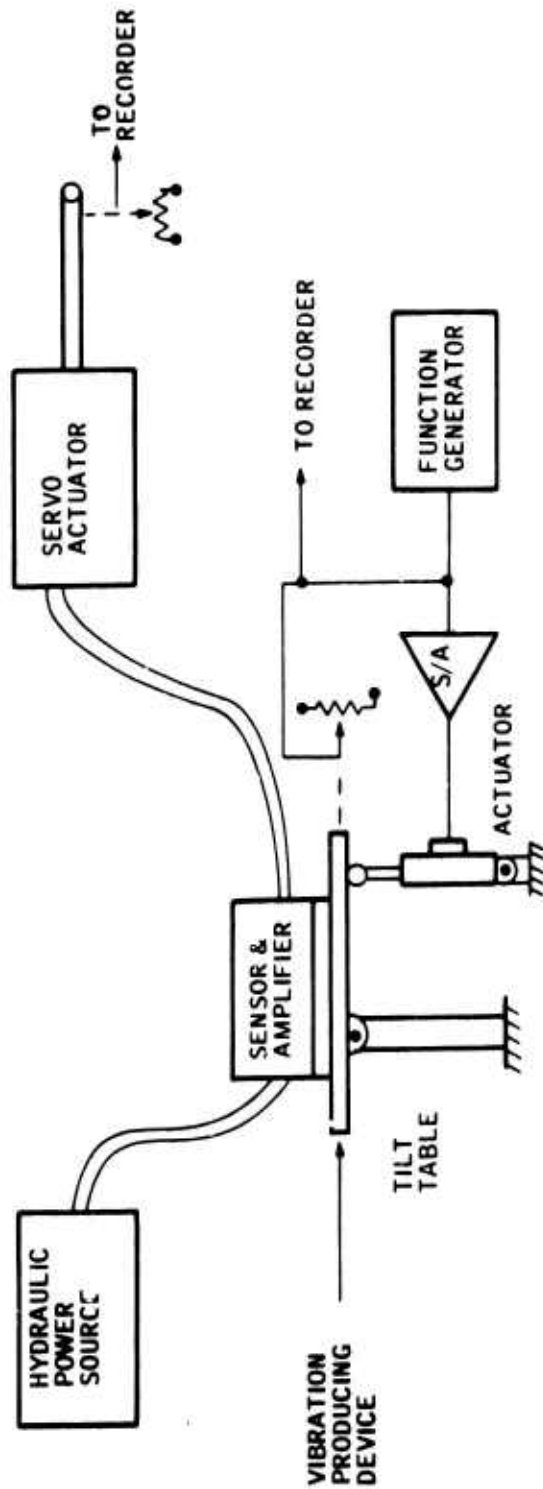


Figure 78 Open Loop Test Setup

The test record shall be examined and the maximum deviation from initial null shall be noted. The frequency character, if any, of the changing null shall also be noted.

2.0 OPEN-LOOP SYSTEM TESTS

This set of test requirements is designed to verify system performance characteristics on system output to input basis. The PFHD test setup is the same as shown on Figure 78 except that the output of the lag section of the shaping network is connected to the system.

2.1 Dynamic Response

A sinusoidal varying angular rate of $1^\circ/\text{sec}$ constant amplitude shall be applied to the tilt table throughout the frequency spectrum of 0.01 cps to 10 cps. The phase angle and amplitude ratio shall be measured at the following frequencies: 0.010, 0.02, 0.03, 0.04, 0.05, 0.10, 0.20, 0.30, 0.50, 1.0, 2.0, 3.0, 5.0, and 10.0 cps. Repeat test at $5^\circ/\text{sec}$ amplitude. The plots of phase angle and amplitude ratio shall be compared with Figure 77 of the TDS.

2.2 Null Drift

The purpose of this test is to determine the long-term drift characteristics of the complete PFHD and to evaluate the ability of the shaping network to reduce the drift as determined by the procedure of paragraph 1.3. The test procedure as stated in paragraph 1.3 shall be repeated.

The test record shall be examined and the maximum deviation from initial null shall be noted. The frequency character, if any, of the changing null shall also be noted.

3.0 CLOSED-LOOP SYSTEM TESTS

The PFHD is mounted on a test setup as shown in Figure 79. The loop is closed through an analog computer which simulates the aircraft aerodynamic characteristics as well as the aircraft power boost servo characteristics and control linkage non-linearities. Step input commands of a lateral gust (β) corresponding to a 15 ft/sec cross-wind and a rudder pedal input corresponding to 1° tail rotor blade deflection shall be inserted into the computer. The tilt table motion shall be recorded and compared with system analog simulation results to determine compliance with TDS aircraft performance requirements.

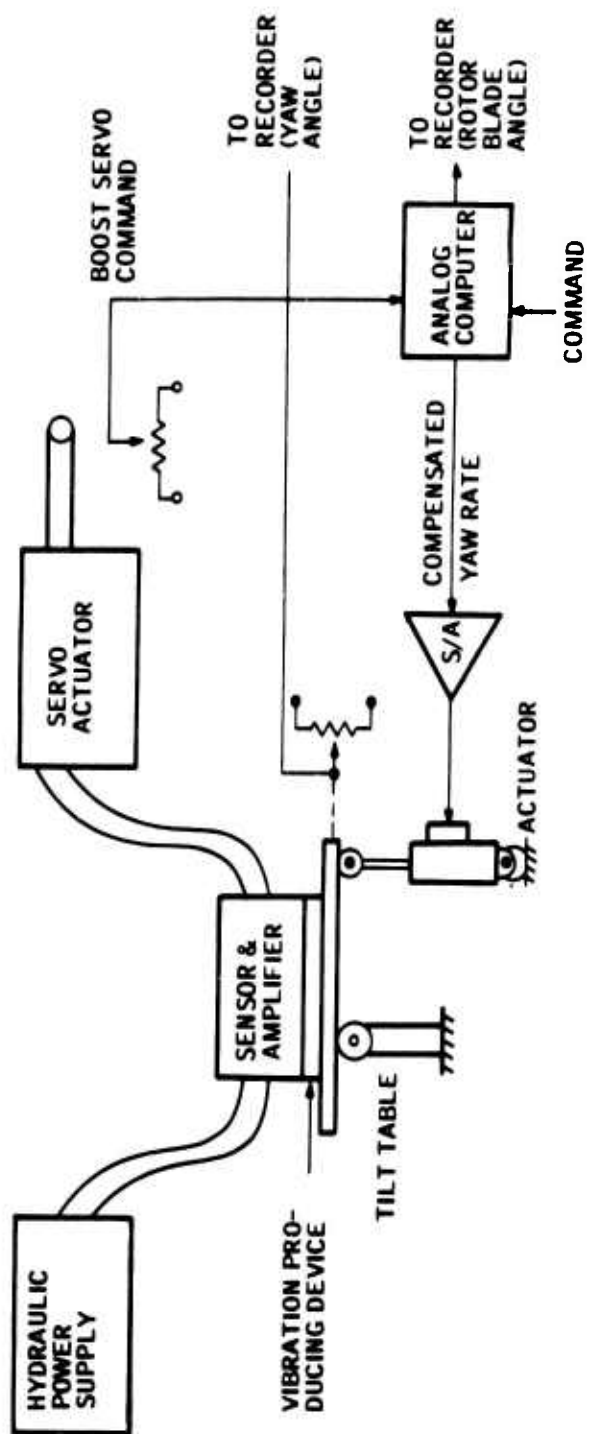


Figure 79. Closed Loop Test Setup

4.0 ENVIRONMENTAL TESTS

The following series of environmental tests is designed to determine the PFHD closed-loop performance when the PFHD is subjected to simulated conditions which may be encountered in the aircraft.

The PFHD shall be mounted on the closed-loop test setup (Figure 79). The test setup shall be equipped with a device to produce vibration in the vertical direction simulating the dominant vertical vibration mode encountered in the UH-1B aircraft (0.2 g at 30 cps).

4.1 Temperature Tests

4.1.1 Cold Start Test

The PFHD shall be subjected to an ambient temperature soak of sufficient duration to stabilize the system hardware at -25°F. The fluid shall also be stabilized at -25°F.

The system shall be activated; after a period of one minute, a rudder pedal step command equivalent to a 1° tail rotor blade deflection shall be inserted into the computer. The output of the servoactuator shall be recorded and compared to the performance obtained under nominal operating conditions.

4.1.2 Fluid Warm-Up Tests

Immediately following the completion of the cold start test, the fluid temperature shall be increased at a rate sufficient to reach a stabilized fluid temperature of +40°F in 20 minutes - +2 minutes, -0 minutes.

During this period of increasing fluid temperature, the rudder pedal step command shall be applied at 5-minute intervals and the PFHD system performance noted and compared to the nominal conditions performance.

4.1.3 +40°F Fluid Temperature Tests

Immediately following completion of the fluid warm-up test, with the fluid temperature stabilized at +40°F, a sinusoidal response test shall be conducted as described in paragraph 2.1. The phase and amplitude ratio plots shall be compared with those obtained at nominal operating conditions.

Upon completion of the sinusoidal response test, rudder pedal steps and lateral wind gust steps as described in paragraph 3.0 shall be applied. The resulting performance shall be compared to the performance under nominal operating conditions.

The vibration-producing device shall be activated and the rudder pedal steps and lateral wind gust steps shall be re-applied. The resulting performance shall be compared with the performance obtained without the vibration.

4.1.4 Increased Fluid Temperature Tests

The PFHD shall be stabilized at an ambient temperature of +100° F with the fluid temperature at +100° F. The fluid temperature shall be raised to 185° F in 40 minutes \pm 4 minutes and stabilized.

A sinusoidal response test shall be conducted as described in paragraph 4.1.3.

Rudder pedal and lateral wind gust step test shall be conducted as described in paragraph 4.1.3.

The vibration-producing device shall be activated and the rudder pedal and lateral wind gust test repeated.

4.2 Supply Pressure Variation Tests

The system supply pressure shall be varied from nominal by \pm 10 percent and the simulated aircraft performance shall be recorded and compared to TDS requirements.

4.3 Vibration Tests

With the PFHD mounted on the closed-loop test setup (Figure 79), the vibration-producing device shall be activated. The actuator displacement shall be continuously monitored and recorded. After observation of the effect of vibration on the system null, rudder pedal steps and lateral wind gust steps as described in paragraph 3.0 shall be applied. The resulting performance shall be compared with the nominal operating conditions performance.

Upon completion of this test, the PFHD shall be mounted on a vibration machine and tested per MIL-STD-810A, Helicopter Test Curve B. The PFHD shall be energized and the actuator displacement continuously monitored and recorded.

Upon completion of the test, the PFHD shall be examined for evidence of damage and then subjected to the closed-loop test as described in paragraph 3.0.

Unclassified

Security Classification

DOCUMENT CONTROL DATA - R&D		
(Security classification of title, body of abstract and indexing annotation must be entered when the overall report is classified)		
1. ORIGINATING ACTIVITY (Corporate author) Honeywell Inc. 2600 Ridgway Road Minneapolis, Minnesota		2a. REPORT SECURITY CLASSIFICATION Unclassified
		2b. GROUP
3. REPORT TITLE Fluid State Hydraulic Damper - UH-1B		
4. DESCRIPTIVE NOTES (Type of report and inclusive dates) Final Report		
5. AUTHOR(S) (Last name, first name, initial) Burton, Robert V. Heinecke, Richard L. Carlson, Donald N. St. John, Robert R.		
6. REPORT DATE February 1967	7a. TOTAL NO. OF PAGES 178	7b. NO. OF REFS 0
8a. CONTRACT OR GRANT NO. DA44-177-AMC-294(T) b. PROJECT NO. IP121401A14186 c. d.	9a. ORIGINATOR'S REPORT NUMBER(S) USAAVLABS Technical Report 66-87 9b. OTHER REPORT NO(S) (Any other numbers that may be assigned this report) 15-003R	
10. AVAILABILITY/LIMITATION NOTICES Distribution of this document is unlimited.		
11. SUPPLEMENTARY NOTES		12. SPONSORING MILITARY ACTIVITY U. S. Army Aviation Materiel Lab Fort Eustis, Virginia 23604
13. ABSTRACT <p>This report covers the developmental work accomplished on a program to demonstrate the feasibility of using fluidic sensing amplification and signal shaping techniques to mechanize a single-axis, rate feedback damper system for V/STOL aircraft. The specific design goal was to increase the yaw axis damping ratio of the UH-1B helicopter from 0.30 unaugmented to 0.60 augmented.</p> <p>The control problem was analyzed and the damper system mechanization defined through the use of analog and digital computer simulation techniques. The component hardware was designed, fabricated, and bench tested.</p> <p>Closed-loop system bench testing, using an analog computer to simulate the UH-1B helicopter, showed that the fluidic damper system was feasible for helicopter control system mechanization. The addition of the damper system to the simulated aircraft raised the yaw axis damping ratio from 0.30 unaugmented to 0.60 augmented.</p> <p>Recommendations for further work are presented.</p>		

DD FORM 1473
1 JAN 64

Unclassified

Security Classification

Unclassified
Security Classification

14. KEY WORDS	LINK A		LINK B		LINK C	
	ROLE	WT	ROLE	WT	ROLE	WT
Rate Sensor Fluid Amplifier Shaping Network Series Servo Hi-Pass Open Loop Closed Loop Fluidic Damper						

INSTRUCTIONS

1. ORIGINATING ACTIVITY: Enter the name and address of the contractor, subcontractor, grantee, Department of Defense activity or other organization (*corporate author*) issuing the report.

2a. REPORT SECURITY CLASSIFICATION: Enter the overall security classification of the report. Indicate whether "Restricted Data" is included. Marking is to be in accordance with appropriate security regulations.

2b. GROUP: Automatic downgrading is specified in DoD Directive 5200.10 and Armed Forces Industrial Manual. Enter the group number. Also, when applicable, show that optional markings have been used for Group 3 and Group 4 as authorized.

3. REPORT TITLE: Enter the complete report title in all capital letters. Titles in all cases should be unclassified. If a meaningful title cannot be selected without classification, show title classification in all capitals in parenthesis immediately following the title.

4. DESCRIPTIVE NOTES: If appropriate, enter the type of report, e.g., interim, progress, summary, annual, or final. Give the inclusive dates when a specific reporting period is covered.

5. AUTHOR(S): Enter the name(s) of author(s) as shown on or in the report. Enter last name, first name, middle initial. If military, show rank and branch of service. The name of the principal author is an absolute minimum requirement.

6. REPORT DATE: Enter the date of the report as day, month, year, or month, year. If more than one date appears on the report, use date of publication.

7a. TOTAL NUMBER OF PAGES: The total page count should follow normal pagination procedures, i.e., enter the number of pages containing information.

7b. NUMBER OF REFERENCES: Enter the total number of references cited in the report.

8a. CONTRACT OR GRANT NUMBER: If appropriate, enter the applicable number of the contract or grant under which the report was written.

8b, 8c, & 8d. PROJECT NUMBER: Enter the appropriate military department identification, such as project number, subproject number, system numbers, task number, etc.

9a. ORIGINATOR'S REPORT NUMBER(S): Enter the official report number by which the document will be identified and controlled by the originating activity. This number must be unique to this report.

9b. OTHER REPORT NUMBER(S): If the report has been assigned any other report numbers (*either by the originator or by the sponsor*), also enter this number(s).

10. AVAILABILITY/LIMITATION NOTICES: Enter any limitations on further dissemination of the report, other than those imposed by security classification, using standard statements such as:

- (1) "Qualified requesters may obtain copies of this report from DDC."
- (2) "Foreign announcement and dissemination of this report by DDC is not authorized."
- (3) "U. S. Government agencies may obtain copies of this report directly from DDC. Other qualified DDC users shall request through _____."
- (4) "U. S. military agencies may obtain copies of this report directly from DDC. Other qualified users shall request through _____."
- (5) "All distribution of this report is controlled. Qualified DDC users shall request through _____."

If the report has been furnished to the Office of Technical Services, Department of Commerce, for sale to the public, indicate this fact and enter the price, if known.

11. SUPPLEMENTARY NOTES: Use for additional explanatory notes.

12. SPONSORING MILITARY ACTIVITY: Enter the name of the departmental project office or laboratory sponsoring (*paying for*) the research and development. Include address.

13. ABSTRACT: Enter an abstract giving a brief and factual summary of the document indicative of the report, even though it may also appear elsewhere in the body of the technical report. If additional space is required, a continuation sheet shall be attached.

It is highly desirable that the abstract of classified reports be unclassified. Each paragraph of the abstract shall end with an indication of the military security classification of the information in the paragraph, represented as (TS), (S), (C), or (U).

There is no limitation on the length of the abstract. However, the suggested length is from 150 to 225 words.

14. KEY WORDS: Key words are technically meaningful terms or short phrases that characterize a report and may be used as index entries for cataloging the report. Key words must be selected so that no security classification is required. Identifiers, such as equipment model designation, trade name, military project code name, geographic location, may be used as key words but will be followed by an indication of technical context. The assignment of links, rules, and weights is optional.

Unclassified
Security Classification